# Fabrication of Carbon Nanotube Structures Using Dielectrophoresis

by

Ali Kashefian Naieni

B.Sc., Shiraz University, 2005

M.Sc., Sharif University of Technology, 2007

A THESIS SUBMITTED IN PARTIAL FULFILLMENT OF

THE REQUIREMENTS FOR THE DEGREE OF

DOCTOR OF PHILOSOPHY

in

The Faculty of Graduate and Postdoctoral Studies

(Electrical and Computer Engineering)

THE UNIVERSITY OF BRITISH COLUMBIA

(Vancouver)

February 2014

© Ali Kashefian Naieni

## Abstract

Carbon nanotubes (CNTs) are promising materials for many applications due to their attractive electronic, optical, mechanical and thermal properties. Currently, the main challenge facing their widespread usage is the inability to fabricate nanotube devices reproducibly.

Dielectrophoresis (DEP) is a versatile method for the fabrication of nanostructures from a solution. However, while this method offers advantages such as overall control over the positioning of the nanotubes and the possibility of pre-selecting the types of CNTs, there are many unknowns about how the process works, leading to unreliability and irreproducibility. Although there have been reports on different parameters affecting DEP results, some important factors such as the movement of the solution and the interactions among nanotubes during the process have often been neglected.

This thesis presents a combination of experimental and modeling efforts to investigate the mechanisms at work during DEP. Experiments were performed to evaluate the influence of the conductivity of the solution. A framework based on finite-element method simulations was developed to unveil the mechanisms involved. The results showed that variations in the conductivity of the solution, leading to changes in electrothermal movements, could lead to substantial differences in the outcome. Higher levels of repeatability were achieved by using low-conductivity solutions.

The mutual interactions of nanotubes during DEP were also investigated using both experiments and simulations; it was shown that these could lead to the formation of periodic patterns in the deposited nanotubes.

Finally, a particle tracing simulation formalism was developed, allowing one to follow the CNTs in their journey from the solution to the substrate, taking into account several influential factors: the DEP force, the movement of the solution itself, and the Brownian movement of the CNTs. Metallic and semiconducting nanotubes were traced in various scenarios and the effective forces were explored every step of the way.

The work reported in this thesis thus leads to a better understanding of the DEP process and the mechanisms involved in the deposition of nanotubes, and potentially that of other nano-objects, taking us a step closer to engineering reproducible processes for nano-device fabrication.

## Preface

The contributions reported in this thesis have resulted in the following publications and presentations:

**Journal papers:**

- A. Kashefian Naieni, A. Nojeh, "Effect of solution conductivity and electrode shape on the deposition of carbon nanotubes from solution using dielectrophoresis," Nanotechnology, 23, 495606, 2012. (Part of Chapter 3)
- A. Kashefian Naieni, A. Nojeh, "The role of field frequency and its dependence on solution conductivity in dielectrophoretic deposition of carbon nanotubes," accepted for publication in Microelectronic Engineering. (Part of Chapter 4)
- A. Kashefian Naieni, A. Nojeh, "The mutual interactions of carbon nanotubes during dielectrophoresis," accepted for publication in IEEE Transactions on Nanotechnology. (Part of Chapter 5)
- A. Kashefian Naieni, A. Nojeh, "A numerical study of the forces affecting the movement of carbon nanotubes in the solution during dielectrophoresis," submitted. (Part of Chapter 6)

**Conference papers:**

- A. Kashefian Naieni, A. Nojeh, "Investigation of the dynamics of carbon nanotube deposition in dielectrophoresis," Proceeding of the 5th IEEE International Nanoelectronics Conference, 2013. (Part of Chapter 5)

**Conference presentations:**

- A. Kashefian Naieni, A. Nojeh, "Investigation of the effect of various parameters in deposition of carbon nanotubes using dielectrophoresis," Eleventh international conference on the science and application of nanotubes, Montreal, Canada, Jun-Jul 2010.
- A. Kashefian Naieni, A. Nojeh, "The effect of field frequency and solution conductivity on dielectrophoretic deposition of carbon nanotubes," 56th international conference on electron, ion, and photon beam technology and nanofabrication, Hawaii, United States, May 2012.
- A. Kashefian Naieni, A. Nojeh, "Dynamics of carbon nanotube deposition in dielectrophoresis," 5th IEEE International Nanoelectronics Conference, Singapore, January 2013.
- A. Kashefian Naieni, A. Nojeh, "Tracking the movement of carbon nanotubes during dielectrophoretic deposition," 57th international conference on electron, ion, and photon beam technology and nanofabrication, Nashville, United States, May 2013.

The author was the main researcher of all of the publications. The experiments and simulations were designed and performed by the author, under the supervision of Prof. Alireza Nojeh. The manuscripts were written by the author with the assistance of Prof. Alireza Nojeh.

The author's work at UBC has also led to additional publications, although they are not included in this thesis. A list of these publications is presented in Appendix A.

# Table of Contents

## List of Tables

## List of Figures

## Acknowledgements

I would like to express my deepest gratitude and appreciation to my advisor, Prof. Alireza Nojeh, for his continuous support, encouragement, and guidance. I consider myself fortunate for having the opportunity to work with him. I have enormously benefited from and was constantly amazed by his enthusiasm, dedication and deep knowledge.

I would like to convey my gratitude to the members of my doctoral qualifying and final examination committees: Prof. David Pulfrey, Prof. John Madden, Prof. Boris Stoeber, Prof. Shahriar Mirabbasi, Prof. Edmund Cretu, and Prof. Victor C.M. Leung.

I would like to thank my colleagues and friends at the Nanostructure Lab for their help and support during the past few years.

I am indebted to all my friends in Vancouver for the unforgettable memories and sincere friendships.

Lastly, and most importantly, I wish to express my genuine gratitude to my family. I could always feel the warmth of their everlasting love despite the cold oceans between us.

To my family,

for their endless love and support.

# Chapter 1: **Introduction**

The remarkable properties of Carbon nanotubes (CNTs) have placed them under the spotlight for the past two decades. Many of their properties are rooted in their very high aspect ratio, small diameter which practically makes them a one-dimensional structure, and the strong and robust $sp^2$ carbon-carbon bond. These characteristics have made nanotubes potential candidates for a wide variety of applications: from the space elevator to ultra-fast electronic devices.

Despite the high hopes for CNTs and the significant amount of research dedicated to examining their use in numerous applications, there are challenges on the way of producing commercial products based on nanotubes that are yet to be resolved. The reproducible fabrication of devices based on certain types of nanotubes is the missing piece of the puzzle toward their widespread usage, in particular for electronics applications.

## 1.1 CNT's structure

CNTs are tubes made of carbon atoms with a diameter in the nanometer scale. A nanotube can be thought of as a rolled graphene sheet. Since there are infinite ways to roll up a sheet with a periodic structure like graphene into a cylinder, CNTs represent a collection of carbon tubes with different diameters and properties. Each nanotube can be uniquely described by a chiral vector which is basically a vector in the honeycomb lattice of the graphene sheet. It is a multiple of the basis vectors that can be written as $\vec{c} = n\overrightarrow{a_1} + m\overrightarrow{a_2}$ and is often written as a pair of integers (n,m). The chiral vector determines the pitch and circumference of the nanotube (Fig. 1-1) [1], [2].

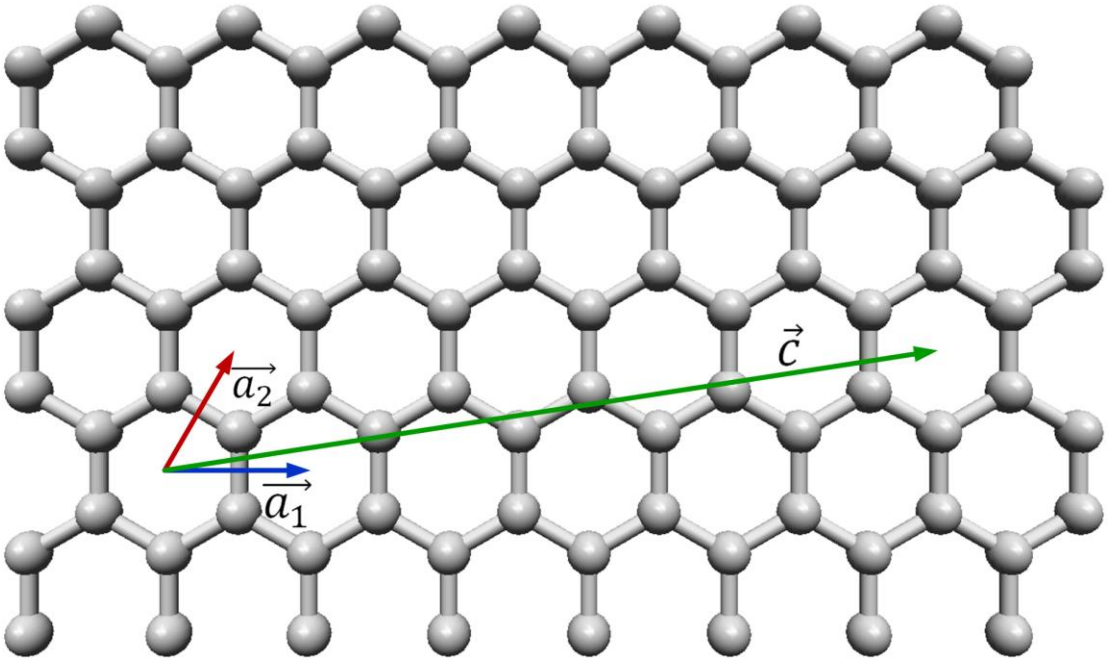


Fig. 1-1. Basis vectors (red and blue) and a chiral vector (green) in the graphene lattice.

CNTs can be either single-walled or multi-walled (Fig. 1-2). Single-walled carbon nanotubes (SWNTs) are made of just one cylinder. The diameter of an SWNT can range from less than a nanometer to a few nanometers. These nanotubes can be either metallic or semiconducting depending on their chirality. If the resulting value from the subtraction of the two indices is divisible by 3, the nanotube is metallic; otherwise it is semiconducting. The band gap of semiconducting nanotubes behaves approximately in proportion with the inverse of their diameter [3].

MWNTs are made of several concentric nanotubes. This type of CNTs have a more rigid structure because of their multiple layers and are usually considered metallic due to the high

chance of existence of at least one metallic tube among the tubes which create the MWNTs, as well as the large diameter of the outer tubes which means small band gap for the outer shells.

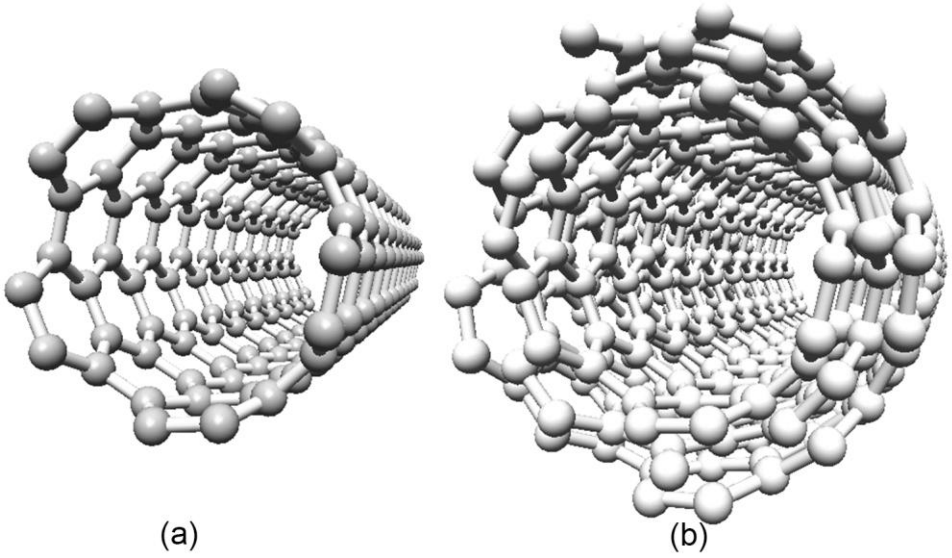


Fig. 1-2. Schematics of (a) single-walled and (b) multi-walled CNTs.

## 1.2 Fabrication of CNT based devices

In order to be able to exploit the promising characteristics of nanotubes, there is a need for a reliable method for depositing one or more CNTs between at least two electrodes. An adjacent third electrode is required for making three-port devices such as a transistor.

There are different methods for creating two- and three-port devices on the surface using CNTs. Chemical vapor deposition (CVD) is one of these methods in which the CNTs grow from decomposition of a carbon source gas in the presence of catalyst materials [4], [5]. The position of the catalysts can be determined using normal lithography methods. Vertical and horizontal growth of nanotubes is possible with this method. For the horizontal ones, the nanotubes can be directed using electric field, gas flow, patterned surface or substrate surface morphology [6]–[10]. Growth of CNTs with an almost defect-free structure and the ability to make SWNTs as

well as MWNTs are two of the advantages of this method. The disadvantages are difficult process control for achieving repeatable results and the high-temperature nature of the process.

Another technique for creating CNT-based electronic devices starts by dispersing nanotubes suspended in a solution onto a substrate. Nanotubes will be found in random positions after the solution evaporates. The electrodes are then patterned and deposited using electron beam lithography, where the nanotubes are [11]. Despite the low contact resistance of the devices made by this method, the elaborate process makes this technique not usable in many cases.

Dielectrophoresis (DEP) is another method for deposition of nanotubes from solution. In this method, an alternating voltage is applied to pre-patterned electrodes immersed in a solution of suspended CNTs. The CNTs are either attracted or repelled by the field gradient depending on their physical properties. If the force is attraction, the nanotubes go toward the maximum electric field gradient, which is between the two electrodes, and deposit there on the surface due to the Van der Waals force [12]–[14]. The low-temperature nature, relatively good control over the position of the deposited nanotubes, simplicity of the required equipment and availability of solutions containing particular types of CNTs are some of the advantages of DEP over other methods. Nonetheless, in absolute terms, DEP still lacks sufficient control and repeatability. This method is at the core of the work presented in this thesis, and is described in detail in the next section.

### 1.3 Dielectrophoresis

When a polarizable particle is placed in an electric field, positive and negative charges are induced on the opposite sides of the particle, which can establish an electric dipole. The magnitude of the charge depends on factors such as the magnitude of the applied electric field,

the frequency of the electric field (polarizability is frequency-dependent), and the morphology of the particle [13]. The interaction between the electric field and the dipole cannot generate any net force if the field is uniform since the Coulomb forces on the two sides of the particle are equal in magnitude and opposite in direction and cancel out. However, in a non-uniform electric field, there will be a net force, which can affect the particle's motion. Fig. 1-3 illustrates the difference between uniform and non-uniform fields affecting a particle.

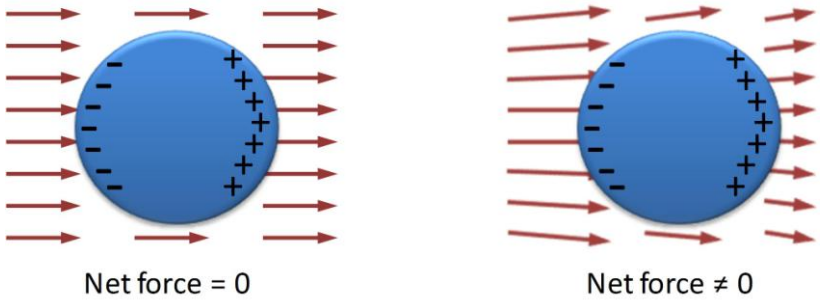


Fig. 1-3. Polarizable objects in uniform and non-uniform electric fields.

If the particle is floating in a medium, the DEP force can be toward/against the direction of the electric field gradient. If the particle has a polarizability higher than that of the medium, the DEP force pushes it toward the region of maximum electric field (positive DEP), whereas if it has a lower polarizability, it is pushed away from that region (negative DEP). Considering the dependence of the DEP force on the physical properties of the particles in the medium, this method can be used for the separation of different particles.

DEP has been used in various research areas for capturing and sorting a wide variety of particles. Applications include manipulation of cells and other biological particles [15], [16], nanoparticles sorting and manipulation [17]–[19], and improvement of atomic force microscopy probes (by placing a CNT at the very tip to increase the probe resolution) [20].

## 1.4 DEP of CNTs

DEP is one of the popular methods for the deposition of nanotubes. The process usually starts by pouring a few drops of a CNT-containing solution on the sample with previously fabricated electrodes. Alternatively, the sample can be immersed in the solution to achieve a higher level of consistency from experiment to experiment. Once an alternating voltage is applied to a pair of electrodes, the CNTs align themselves with the electric field lines and approach the gap between the two electrodes and eventually deposit.

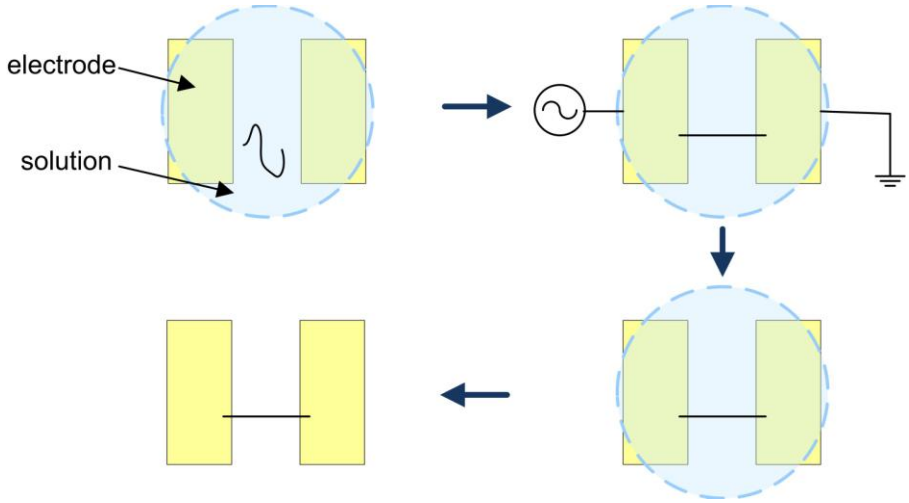


Fig. 1-4. DEP deposition process: a solution drop is placed on the electrodes. Once the voltage is applied CNTs align themselves with the field and move toward the electrodes. Electrodes can be used to connect to CNTs after the experiment.

While the basics of this process seem to be straightforward, there are many parameters that can affect the results, and the mechanisms arising because of different phenomena that are involved in moving the particles toward their final destination. Moreover, having a wide range of physical

properties among CNTs, from a semiconductor with considerable band gap to a perfect conductor, makes the final result of DEP deposition more complex.

Various parameters such as the amplitude and frequency of the applied voltage, the duration of application of the voltage, electrodes geometry and design, substrate properties, CNT concentration in the solution, and also physical properties of the solution can have an effect on the deposition in the DEP method.

Since the DEP force depends on the electric field, a higher applied voltage is expected to attract more nanotubes. Different reports have experimentally confirmed this in various solutions such as water, ethanol, and dichloroethylene [21]–[23]. Arun *et al.* determined a minimum required field for deposition in the case of aqueous solutions with added surfactants [22]. However, the reported level of increase in the density of deposited nanotubes because of increased voltage is not the same in all these works.

The duration of the application of the potential difference to the electrodes is another effective parameter. The movement of nanotubes under the influence of the electric field can be divided into two categories: rotational and translational. Li *et al.* and Peng *et al.* investigated the time needed for these movements [24], [25]. They concluded that, because of the magnitude of the torque exerted due to the interaction between the induced dipole in the CNT and the field, the time needed for the rotation of nanotubes to the direction of the field is in the sub-millisecond range, and is typically much smaller than their translation time toward the electrodes. Once aligned with the field, a longer manipulation time gives CNTs a higher chance for moving toward the electrodes and depositing on or near them. Therefore, a higher density of deposited nanotubes was achieved as the duration of application of the voltage was increased [22], [24]. For electrodes with a gap much larger than the maximum length of suspended nanotubes, CNTs

gradually cover the gap starting from the edges of the electrodes and filling it up layer-by-layer as time goes by (see Fig. 2 in [26]).

The DEP force is altered with the change in the magnitude of the dipole moment of the particle, which itself is a function of its polarizability. The polarization depends on the frequency. Therefore, DEP force on a particle can have different values and directions as the frequency of the applied voltage changes. Dimaki and Boggild observed better alignment in the network of nanotubes as they increased the frequency from 10 kHz to 10 MHz [27]. An aqueous solution with surfactant was used in their work. Moscatello *et al.* also reported better alignment of multi-walled nanotubes at higher frequencies [23]. They observed a higher density of deposited nanotubes as they increased the frequency from 50 Hz. The density decreased again for frequencies above 10 MHz. Sarkar *et al.* performed DEP using a 99% semiconducting nanotube aqueous solution at frequencies from 50 kHz to 5 MHz [28]. While the CNTs did not make a bridge between 2-μm-apart electrodes at 50 kHz, the density and bridging of the nanotubes increased at higher frequencies with a maximum at 1 MHz. Above 1 MHz, although the CNTs were aligned well with the field, their density was considerably lower compared to the maximum value.

The morphology of the network of nanotubes is not the only outcome that is affected by the change in the frequency of the applied voltage. The percentage of the metallic and semiconducting nanotubes, which make the network, is also a function of the frequency. This is due to the difference in the polarizability of the two CNT types. While metallic nanotubes experience positive DEP in a very wide range of frequencies due to their very high conductivity and permittivity, semiconducting nanotubes only experience a positive force at lower frequencies [29]. The threshold frequency depends on the properties of the medium. This phenomenon was

used to separate metallic and semiconducting nanotubes and create networks of mostly metallic CNTs [17]. Considering the low polarizability of the semiconducting nanotubes, their deposition even at low frequencies was attributed to either their surface conductance due to the presence of surfactant materials [30] or to their dielectric anisotropy [31].

The motion of CNTs because of the DEP force is influenced by the electric field strength and pattern. The geometry of the sample used for the experiment directly determines the electric field distribution. Thus, parameters such as shape of the electrodes, existence of a conductive layer underneath the substrate oxide layer, and the oxide thickness can affect the DEP results. Xu *et al.* used simulations and experiments to compare round-shape electrodes with rectangular (sharp angled) electrodes [32]. They demonstrated that, in the case of round electrodes with smooth curved edges, CNTs are mostly attracted toward the protruding point of the semicircle. On the other hand, the DEP force is strongest around the angles when the electrodes have sharp corners. Single nanotubes were captured using very sharp triangular-shape electrodes made by electron beam lithography [33]. Other effective parameters such as voltage, time and solution concentration were proven very important for making these devices.

The presence of a conductive layer underneath the isolating layer of the substrate can influence the final morphology of the deposited CNTs. This is often the case when a doped silicon wafer with oxide on the top is used as the substrate. Marquardt *et al.* used short metallic nanotubes to probe the electric field in two types of samples: insulating substrate, and oxidized conducting substrate [34]. While the nanotubes filled the gap for the insulating substrate, they covered mostly the edges of the electrodes in the second case. The authors attributed this to the change in the DEP force direction very close to the substrate due to the differences in the electric field patterns. The degree of influence of the conductive substrate on the DEP results depends directly

on the thickness of the oxide layer. For a thin oxide layer of 200 nm, a high percentage of the nanotubes cover the edges of the electrodes rather than bridging the two electrodes, but for thicknesses above 500 nm most of the nanotubes actually bridge the two electrodes [35].

Preparing a suitable solution that contains well-separated CNTs with a low concentration of aggregates and impurity particles is an important step for the successful deposition of nanotubes using DEP. The appropriate solution should be stable at room temperature, non-toxic, with a very low concentration of aggregates and impurity particles. Some of the solutions used for nanotube dispersion such as dimethylformamide and dichloroethane evaporate very fast, which makes them hard to use for the DEP experiment [36].

The concentration of CNTs in the solution is an important factor as well. It was shown that there is an almost linear relation between the number of deposited nanotubes from a surfactant-free aqueous solution and the initial concentration of nanotubes in the solution [37]. This is true for the case of solutions containing only semiconducting nanotubes [28] and is independent of the shape of the electrodes [38].

### 1.5 Hydrodynamic motion of the solution during DEP

DEP is not the only force affecting the nanotubes during deposition. The particles suspended in a solution are subject to a drag force from the solution, which is proportional to and in the direction of the relative fluid flow velocity. Therefore, any phenomena that can induce a movement in the solution will affect the CNTs as well [39].

To investigate the movement of the CNTs during a DEP experiment, an electrokinetic framework must be developed (Electrokinetics is the study of movement of particles in suspensions subject to an electric field). Forces such as electrothermal and AC electroosmosis

can create agitation in the solution. Moreover, the Brownian force can also disrupt the movement of nanotubes due to its non-deterministic nature.

The potential difference applied between the two electrodes for DEP has secondary effects such as generating a current, which passes through the solution. The magnitude of the current is a function of the conductivity of the solution. The power generated due to Joule heating increases the temperature of the fluid surrounding the electrodes. Even a small alteration in the absolute value of temperature can create a significant temperature gradient due to the small size of the device. This gradient results in gradients in permittivity and conductivity in the fluid. The electric field acting on the inhomogeneities of permittivity and conductivity generates a body force on the solution known as the electrothermal force [40], [41]. It was shown that the electrothermal force induces a semicircular pattern of movement in the solution above the two opposing electrodes as shown in Fig. 1-5. The direction of motion depends on the frequency of the applied electric field. For frequencies below the so-called cross-over frequency, the solution moves from above the gap toward it and then moves away, tangential to the electrodes as shown in the figure. Otherwise, the direction of motion in the solution is the opposite. The cross-over frequency itself can be written as a function of the charge relaxation time. The charge relaxation time of the liquid is the ratio between the permittivity and conductivity of the solution [40]. The details will be discussed in the following chapters.

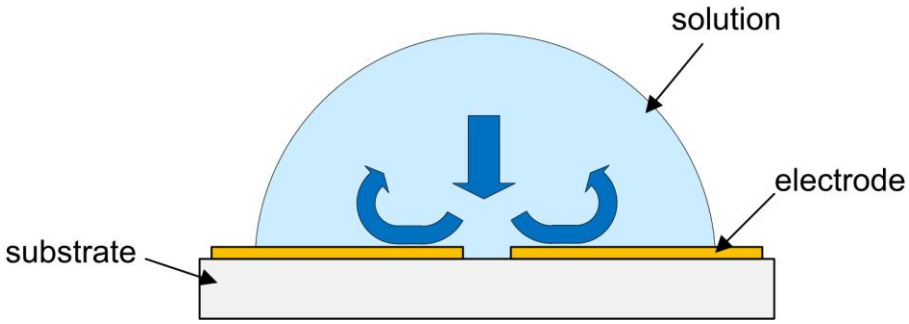


Fig. 1-5. Electrothermal movement of the solution

AC electroosmotic flow in a solution originates from the action of the tangential electric field on the ions in the double layer formed on the electrodes [39]. A double layer refers to two layers of charge on the surface of a solid immersed in an electrolyte. The movement of the charges due to the tangential field creates a flow very close to the surface of the electrodes because of the drag which exists between the ions and the solution. In an AC electric field, since both the sign of the charges on the electrodes and the direction of the electric field change in each half cycle, the direction of the AC electroosmotic flow remains the same. Fig. 1-6 shows the forces which are at the root of AC electroosmosis and also the movement of the solution due to them.

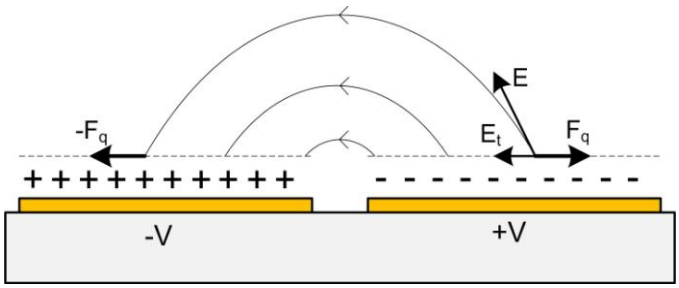


(a)

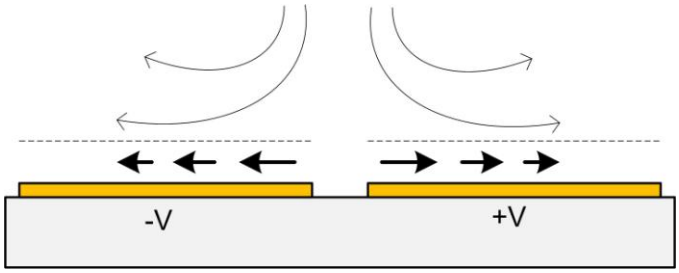


(b)

Fig. 1-6. (a) The forces on the double layer ions, (b) flow movement due to electroosmosis. E, $E_t$, $F_q$, and V denote the electric field, tangential component of the field, Coulombic force on the charges and the applied voltage, respectively.

Studies concerned with estimating the order of magnitude of various hydrodynamic forces showed that, for systems with a characteristic length in the micrometer scale, the two dominant forces are electrothermal and AC electroosmosis [40], [42]. Obviously, the exact value of the velocity at different points in the solution depends on many parameters such as the conductivity and permittivity of the solution.

AC electroosmosis is mainly effective for the lower frequency range, in which the electric double layer has sufficient time to form (up to a few tens of kHz); it drastically decreases at higher frequencies. For most of the frequency spectrum, the electrothermal force is the dominant force on the solution and can agitate it [42].

Although the hydrodynamic forces on the fluid were proven to be effective on the final results of DEP of particles, they are rarely taken into account. In the case of deposition of nanotubes using DEP, researchers usually neglect them or mention them as negligible in their reports, which does not seem to be correct in many cases.

Lin *et al.* simulated the effect of the electrothermal force by adding a force term in solving the Navier-Stokes equation in a two-dimensional plane [43]. They did not consider the electroosmosis movement in the solution; they gave the reason as the frequencies where this force is influential being well below the frequency of the applied potential in their experiments. It was shown that the electrothermal agitation can carry the semiconducting CNTs with it and affect their motion due to the weakness of the DEP force on them. They mentioned that they do not expect the metallic nanotubes to be influenced as much due to the strength of the DEP force affecting them. It was shown that the direction and magnitude of the electrothermal force can change with the frequency depending on the physical properties of the solution.

In their insightful work, Burg *et al.* developed a two-dimensional framework for evaluating the extent of effectiveness of various electrokinetic forces during the DEP of CNTs [44]. They showed that in the solutions made using surfactants, the electrothermal force can be the dominant factor in the long-range movement of nanotubes. The DEP force is mainly effective around the electrodes, and its domain of influence depends on the type of the nanotube. Moreover, they showed that the magnitude, direction and general pattern of electrothermal motion can change with the frequency.

## 1.6 Research objectives

As mentioned in the previous subsections, there have been multiple scientific studies performed on examining the final results of DEP of CNTs as a function of DEP parameters. Significant inconsistencies exist among these reports, which could be attributed to the use of different solvents and procedures for preparing the solution. The effect of these differences was often not taken into account, leading to apparent contradictions. Moreover, the lack of repeatability, reproducibility and reliability in the resulting CNT devices from DEP, has limited the use of this method to research labs. Unveiling the effect of the neglected parameters can possibly lead to a higher yield in creating devices with DEP.

Important questions thus remain, which are the focus of the investigations reported in this thesis. Prior to this work, the relation between the final morphology of the nanotubes on the surface and the solution movements, specifically because of the electrothermal force, was not clear. This is important because different methods for the preparation of nanotubes result in solutions with different conductivities. The electrothermal force is a function of the conductivity of the solution; therefore, the degree of influence of this force can change for different solutions. To tackle this problem experimentally, preparation of solutions with a range of conductivities but similar in every other aspect is necessary. This is a challenge considering that there is a relation between the number of nanotubes suspended and the amount of surfactant in the solution, which is also the main reason behind the change in conductivity [45].

Both the DEP force and the electrothermal force depend on frequency. An important question here is how the effects of these two main forces evolve with respect to each other as the frequency of the applied voltage is varied.

Another key phenomenon that can be responsible for the deposition patterns resulting from DEP deposition is the mutual interaction between nanotubes. Once a CNT is connected to one of the electrodes during the experiment, its electric potential and also the potential profile around it change, in turn affecting the forces on other nanotubes and also on the solution. Vijayaraghaven *et al.* considered the change in the DEP force and stated that the deposition of a CNT on sharp electrodes results in a change in the DEP force around the electrodes from attraction to repulsion during the rest of the process [46]. While this may be the case for sharp electrodes, it cannot explain the patterns forming during experiments using electrodes having other shapes.

The magnitude of the DEP force on the nanotubes depends directly on their physical properties and is therefore orders of magnitude different for metallic and semiconducting nanotubes. This opens up the floor for the non-deterministic Brownian motion to be of importance in some cases. To be able to find out how effective each of the forces are in the journey of semiconducting or metallic nanotubes from the solution to the surface, a framework is required which can handle not only the force on the nanotubes (DEP) and on the solution (electrothermal), but also the random Brownian movement.

The main research questions can be summarized as follows:

1. What is the effect of the electrothermal force on the morphology of nanotubes deposited using DEP from solutions with different conductivities?
2. How do electrothermal and DEP forces evolve with respect to each other as the applied frequency changes, and how does the final deposition pattern change?
3. What are the mutual effects of CNTs on each other and on the solution motion during DEP?

4. What are the dominant forces affecting the semiconducting and metallic nanotubes during each stage of DEP deposition?

## 1.7 Methodology

The research described in this thesis includes both experiments and numerical modeling, emphasized almost equally. The experiments were performed using various solutions and DEP settings. The experimental results show the dependence of the final morphology of nanotube deposition on the settings used, but cannot directly reveal the mechanisms involved in forming those results. For this reason, a framework based on finite-element simulations was developed and used to quantify the forces and mechanisms competing in each particular case. The results of these simulations were extracted and used in a particle tracing formalism in order to track the movement of the nanotubes in an environment containing deterministic as well as random forces.

## 1.8 Thesis overview

This thesis has seven chapters. The overview, related works and the research questions are described in the current chapter. The second chapter is dedicated to explaining the methodology and theoretical background used in the experiments and simulations in general. Each of the subsequent four chapters addresses one of the four research questions posed above. The last chapter presents a summary of the findings, contributions made, and also suggests some directions for future research.

# Chapter 2: **Methodology**

The methods that were used in this thesis can be divided into two major categories: the experimental ones and those used in numerical simulations. The techniques used for preparing, performing and evaluating the results of the experiments will be discussed first. The second section of this chapter is dedicated to describing the framework used for the simulations and its theoretical background.

## 2.1 DEP experiments

The necessary elements for performing a DEP experiment are the solution containing the particles (here the CNTs) and also the substrate containing pre-patterned electrodes. The solution should be stable, inert in the ambient environment, and contain well dispersed individual SWNTs. The substrate should have electrodes in desired shapes. The electrodes are usually made using microfabrication techniques. The small gap between the electrodes makes the creation of large electric fields by applying relatively small voltages possible. The electrodes are designed to have large flat-pad extensions so that microprobes can connect them to the external circuitry.

### 2.1.1 Solution preparation

Water is one of the most popular solvents for preparing particle solutions due to its inert and stable nature. CNTs are inherently hydrophobic and therefore insoluble in water. Preparing CNT aqueous solutions[1] requires modifying the interaction between water molecules and the CNT surface. The methods available for doing so can be divided into chemical (covalent bonds are

[1] It might be debatable whether to call these nanotubes solutions or suspensions; however, in keeping with the existing literature on nanotube DEP, we will use the word "solution".

made to the CNT surface) or physical (the agents interact with the CNT through Van der Waals forces) techniques [47].

Chemical methods functionalize the surface of the CNTs (adding chemical groups covalently attached to the nanotube surface) to enhance the solubility of the CNT in the medium. The aggressive nature of these methods, which are typically performed by using concentrated acids at high temperatures, can introduce defects into the structure of CNTs [47]. In general, CNTs can be functionalized by oxidation using materials such as peroxyacids or metal oxidants, or reduction with thiols, carbenes, etc [48]. The advantage of this method is that there is no need for any other agent for dispersion of nanotubes, and no material other than CNTs would be added to the solvent.

The surfactant-free solutions used in this research were prepared from a SWNT solution commercially available from Nano-Lab Inc. [49], in which the nanotubes were carboxylated prior to suspension in water. The nanotubes had lengths in the range of 1-5 μm and an average diameter of 1.5 nm. The initial concentration of the solution was 1 g/l. The nanotube solution was diluted to the desired concentration for each experiment.

Using the noncovalent (physical) method has the advantage of not interfering significantly with the $\pi$ electrons of the CNTs and therefore preserving their electrical properties. A wide range of dispersive agents can be used to help the CNTs disperse in water. These materials include surfactants, polymers, single-stranded DNA, etc. [45]. The surfactant molecules have hydrophobic and hydrophilic ends. They interact with the nanotubes through their hydrophobic head and with water using the hydrophilic one. In general, ionic surfactants are preferred for preparing CNT-water solutions, whereas non-ionic surfactants are mostly used for organic

solvents [47]. The electrostatic repulsion of ionic surfactants is believed to help in the stabilization of the solution [45].

The process for making CNT solutions usually starts with mixing the surfactant (most typically sodium dodecyl sulfate (SDS) (Fisher BioReagents, catalog No. BP 166-100) or sodium dodecylbenzene sulfonate (SDBS) (American Chemicals LTS, catalog No. S2853-1100) for CNT aqueous solutions) with the appropriate weight percentage with CNT powder and water. This mixture is ultrasonicated to break the CNT bundles and disperse the individual CNTs. The solution is then centrifuged and the supernatant is extracted to separate the individual nanotubes from the remaining aggregates and other impurities such as metal catalyst particles. Fig. 2-1 shows the process schematically.

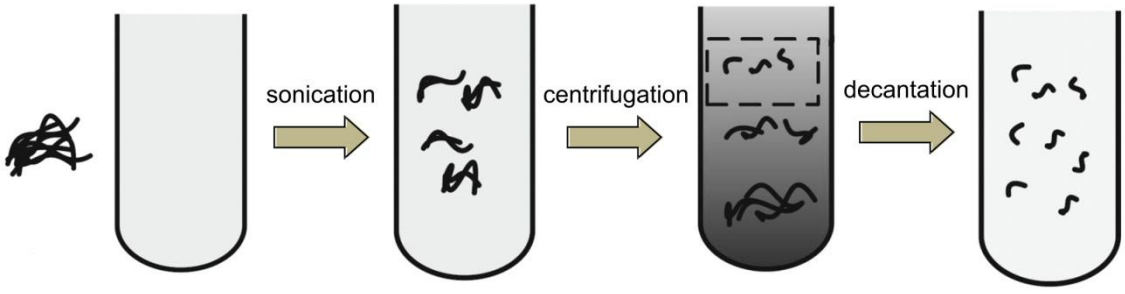


Fig. 2-1. Steps in making a CNT solution using surfactants (from [29], with modifications).

To obtain a stable solution with optimum value of surfactant concentration and surfactant time, various solutions with different material concentrations and process times were made and tested using experiments such as dry-out (pouring a drop of solution on the substrate and letting in dry). Table 2-1shows the specifications of these solutions and Fig. 2-2 is a photograph demonstrating their relative darkness, which is an indication of the concentration of the suspended nanotubes.

Table 2-1. CNT Solutions with various surfactant concentrations and sonication times.

| | SDS concentration (wt%) | sonication time (min) |
|---|---|---|
| S1 | 0.3 | 10 |
| S2 | 1 | 10 |
| S3 | 3 | 10 |
| S4 | 1 | 30 |
| S5 | 1 | 3 |

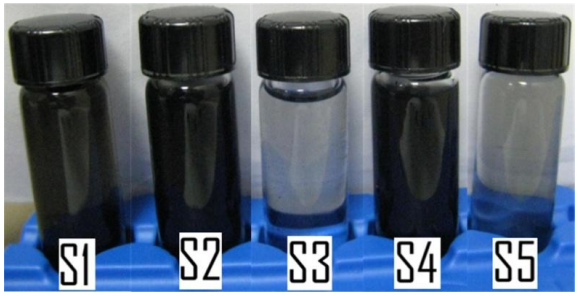


Fig. 2-2. Solutions with various surfactant concentrations and sonication times.

The results of dry-out experiments of these samples showed that increasing the surfactant concentration over the critical micelle concentration (CMC), which is the concentration of surfactants above which micelles are spontaneously formed, reduces the amount of dispersed nanotubes in the solution. The osmotic pressure of micelles around the nanotubes close to each other creates an effective attraction between the nanotubes, which ultimately results in re-bundling of CNTs. This phenomenon is known as depletion attraction in colloidal suspensions [45], [50], [51]. Lower amounts of surfactant reduce the number of CNTs as well but not as drastically as in the previous case. The optimum level seems to be around the CMC value. Increasing the sonication time not only does not help in increasing the concentration of CNTs in the solution but also can increase the number of defects in the CNT structures and shorten their lengths [52].

Adding the centrifugation step for multiple hours at speeds such as 10,000 rpm resulted in homogeneous, well dispersed solutions which were stable for several months (Fig. 2-3).

Fig. 2-3. From left to right: 0.1 wt% CNT with SDS, 0.1 wt% CNT with SDBS, 0.025wt% CNT with SDS, and 0.025wt% CNT with SDBS.

Although the final concentration of CNTs in the prepared solutions is different from its initial value due to decantation of the solution after centrifugation, it is apparent from the color of the solutions after centrifugation that there is a close relationship between initial and final concentrations (compare the two samples on the left side of Fig. 2-3 with the two samples on the right side).

### 2.1.2 Design and fabrication of electrodes

**Photolithography**

Microfabrication technology has made creating large fields with relatively low voltages possible. This is particularly important in DEP because of the dependence of the DEP force on the magnitude of the electric field. To be able to move sub-micrometer particles, a field of $10^4$-$10^5$ V/m is required [40]. If electrodes with just a few micrometers of distance in-between are used, a potential difference on the order of a few volts can create a large enough electric field.

Although various substrates have been used, doped silicon wafers with an oxide layer on top are very common in DEP deposition of nanotubes. The doped silicon underneath the oxide can be used as a back gate once the CNTs are deposited [53], [54]. Moreover, in some reports, the capacitive coupling between the conductive substrate and one of the electrodes was used for applying the voltage for DEP, substituting the direct contact to one of the electrodes [46], [55]. As it was mentioned in the Introduction chapter, the conductive base can also affect the electric field lines during DEP and therefore the oxide needs to have sufficient thickness to avoid excessive modification of the field.

Different designs for the electrodes were examined. Here, the ones which were used for the results presented in this thesis are described in detail.

The first approach for creating the chips was using photolithography. A mask was designed and outsourced for fabrication at Simon Fraser University's (SFU) 4D Labs [56]. The mask was made on a quartz plate and the patterns were created using read right chrome down standard (the text would read correctly on the wafer and mask should be facing down during the lithography). Fig. 2-4 shows the entire mask and Fig. 2-5 shows two of the main types of devices on the mask.

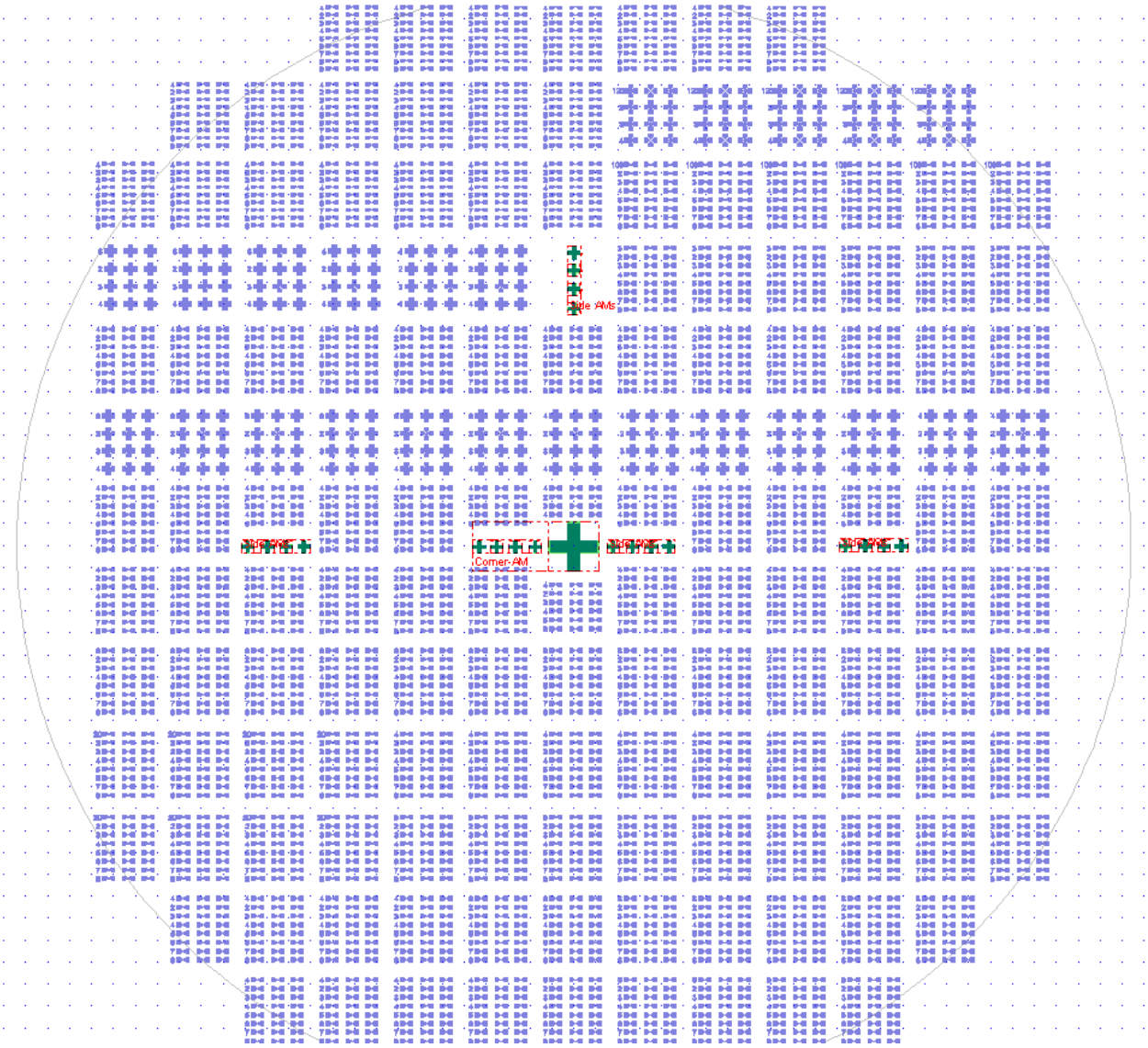


Fig. 2-4. The designed 5-inch mask.

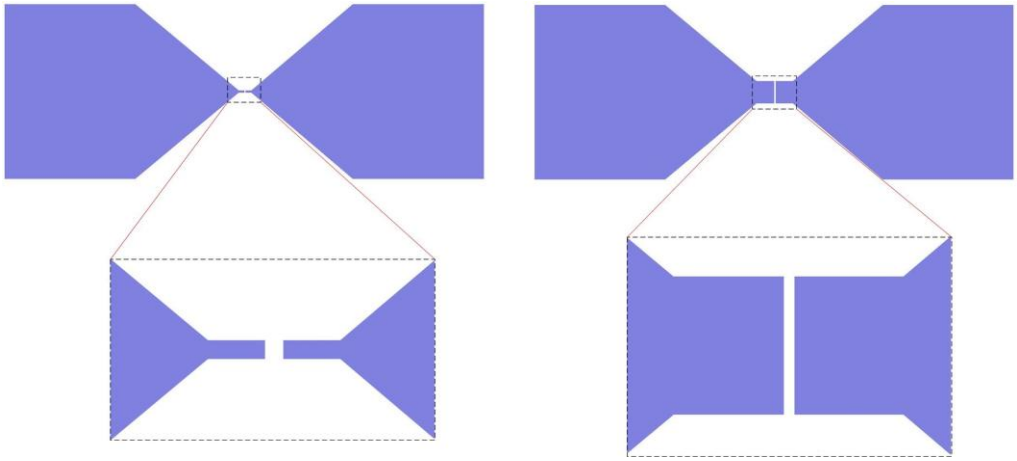

Fig. 2-5. Two of the main types of devices on the mask.

The devices shown in Fig. 2-5 will be called narrow and wide electrodes, respectively. The devices were made of two parts: a large pad for connection to external circuitry through the use of microprobes and a narrow/wide area between the opposing electrodes for capturing the nanotubes. The width of the electrodes of the narrow device close to the gap region was 4 µm. The same part in the wide electrodes had a width of 50 µm. Devices with gaps of 4, 6, 8, and 20 µm were placed on the mask.

The narrow electrode design was intended for making devices with single or a few carbon nanotubes while the wide electrodes provided enough area for depositing multiple nanotubes or CNT matt devices. The mask included 24 similar devices on each chip with an area of 8x8 $mm^2$.

The final goal of the fabrication process of this design was to create electrodes made with a 40-50-nm-thick palladium layer over a 5-20-nm-thick layer of chromium. It was shown that palladium creates an almost ohmic contact with nanotubes due to its high work function [57].

The fabrication process was performed at UBC's AMPEL Nanofabrication Facility [58] and SFU's 4D Labs [56]. The overall processes performed in these two facilities were the same,

although different equipment models were used. The process started by cleaning a 4-inch wafer with acetone (sometimes boiling acetone for better cleaning) and then alcohols such as methanol or isopropanol and subsequently de-ionized (DI) water. The wafer was dried under a stream of nitrogen gas after. To ensure that no water remained on the surface, the wafer was baked at about 100ºC for 10 minutes. After letting the sample cool down, a layer of HMDS primer was deposited on the surface using either spin coating or a vacuum dessicator. HMDS is an adhesion promoter, which improves the bonding between the photoresist and surface by replacing the –OH groups on the surface [59]. The next step was to spin coat the positive photoresist on the wafer (AZ P4110 or AZ MiR 703). The wafer was first placed on the spinner (if the HMDS priming step was performed using spinning, the wafer was left in the air for at least one minute). The photoresist was poured on the wafer using a disposable pipette. Bubbles and small drops of photoresist on the wafer were avoided as they tend to affect the quality of the resist layer after spinning. The spinner was programmed to gradually reach the maximum speed. The cycle included a spread time for the resist at low speeds so the resist covers the entire wafer. The appropriate maximum speed and the duration of spinning depend on the photoresist material and on the spinner. The typical values used were 30-60s for the time and 4000-6000 rpm for the maximum speed. The thickness uniformity and photoresist homogeneity across the wafer are key for a successful lithography process.

Once the surface was uniformly covered by the resist, it was prebaked on a hotplate to evaporate the remaining solvent in the resist and create a stable resist film. A mask aligner (Canon PLA-501F or OAI MBA 800) was used for transferring the patterns on the mask to the wafer by UV exposure. The exposed areas become more soluble in the developer. The duration of exposure depends on the power of the UV lamp (which can change over time) and the parameters used for

preparing the photoresist layer. Therefore, the optimum values were found by systematic experimentation which usually fell in the range of 4 to 6 s. The wafer was then developed in resist developers.

After development, the clear areas on the mask were free of photoresist on the wafer. For the deposition of metals, a two-step electron-beam physical vapor deposition method was used. In this method the accelerated electron beam hits the anode, which is the metal source. High vacuum is necessary for the free passage of electrons (in the order of $10^{-5}$-$10^{-6}$ Torr). The combination of vacuum environment plus the high temperature of the source due to the kinetic energy of the incoming electron beam results in a vapor, which covers the whole area inside the vacuum chamber including the wafer mounted in the direct line of sight of the metal source. The thickness of the deposited layer was controlled by a crystal-based thickness monitoring system.

The fabrication of the electrodes ended with lift-off in acetone to remove the photoresist remaining on the substrate with the deposited metal layer on top. Fig. 2-6 shows one of the devices after photolithography and after lift-off.

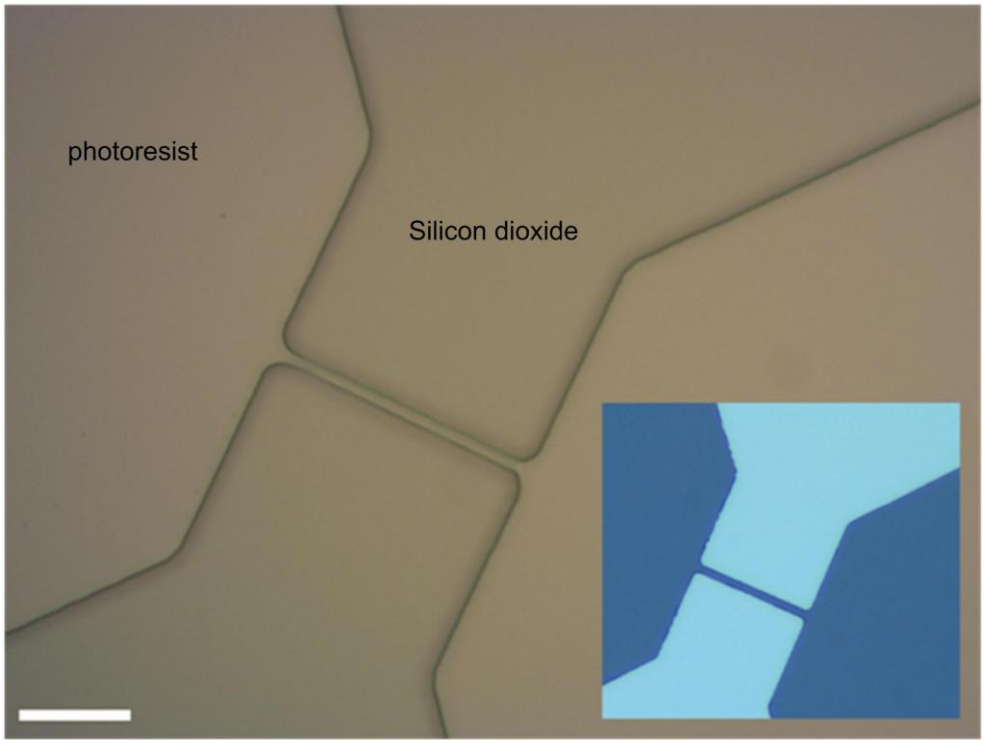


Fig. 2-6. Optical microscope images of a device after photolithography. The inset shows a similar device after the lift-off. Scale bar is 20 μm.

**Electron-beam (e-beam) lithography**

The fabrication of devices using e-beam lithography was made possible through CMC Microsystems'[60] NanoSOI competition. The process involved a combination of e-beam and optical lithography on diced silicon-on-insulator (SOI) substrates. The feature size achieved was of the order of 100 nm on the sections patterned with e-beam lithography.

The process started by the deposition of the metals. Then, the surface was covered by the resist. PMMA is usually the resist of choice in e-beam lithography. A 20-kV acceleration voltage was used for patterning the resist, followed by 20 s of development in an MIBK:IPA solution. Patterning of the metal layer was performed by chlorine-based reactive ion etching. An

inductively coupled plasma was used for etching the thin silicon layer with the thickness of 145 nm. Stripping the photoresist was the last step of the fabrication process.

The high resolution of the method was employed in making extremely sharp electrodes to capture a few and even single CNTs using DEP. Fig. 2-7 and Fig. 2-8 show the design and Fig. 2-9 shows images of the device after fabrication taken using an optical microscope.

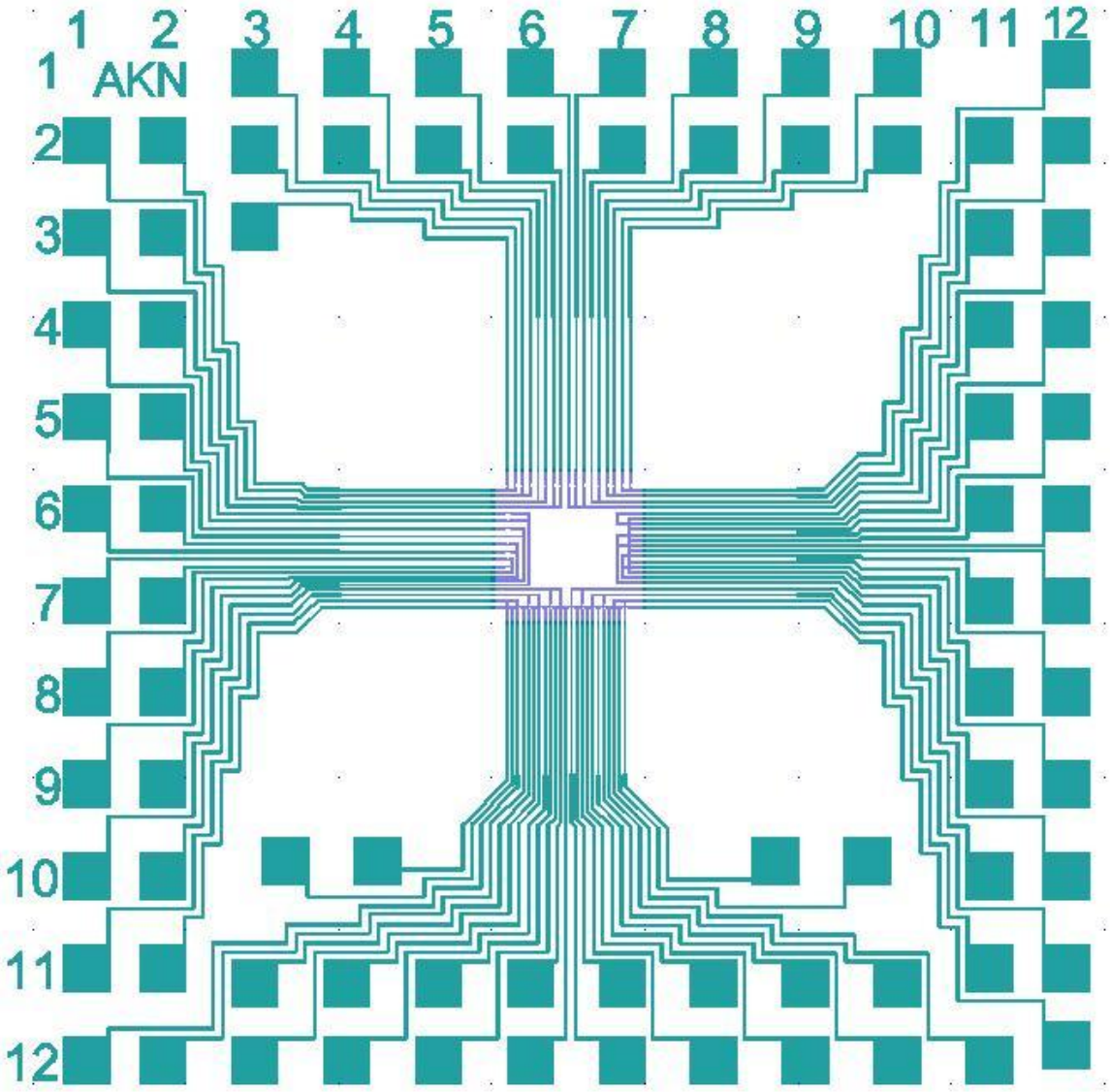


Fig. 2-7. Mask design for e-beam lithography.

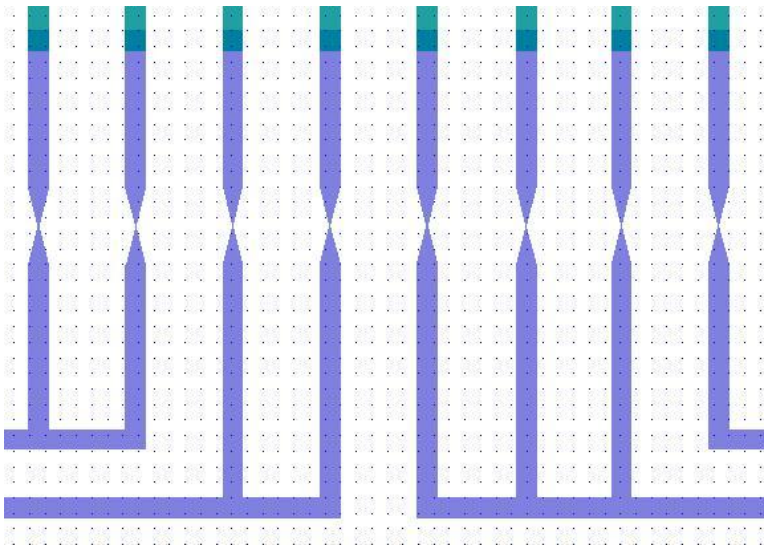

Fig. 2-8. Magnified view of a few of the devices. The gaps between the electrodes range from 100 nm to 2 μm.

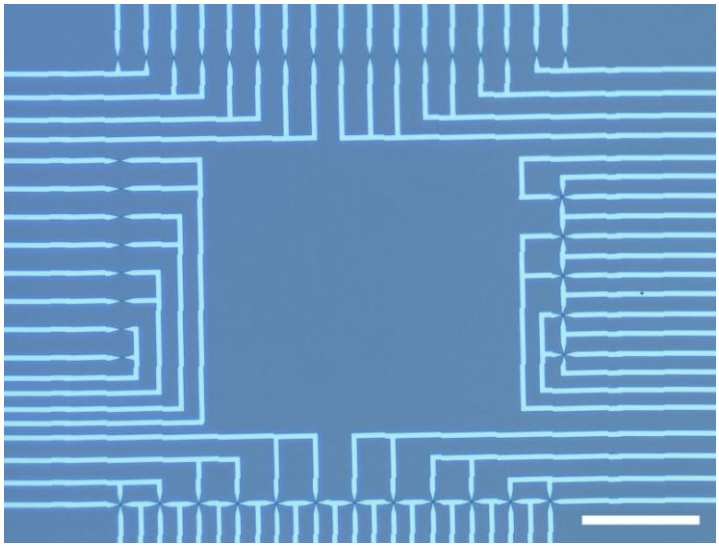

(a)

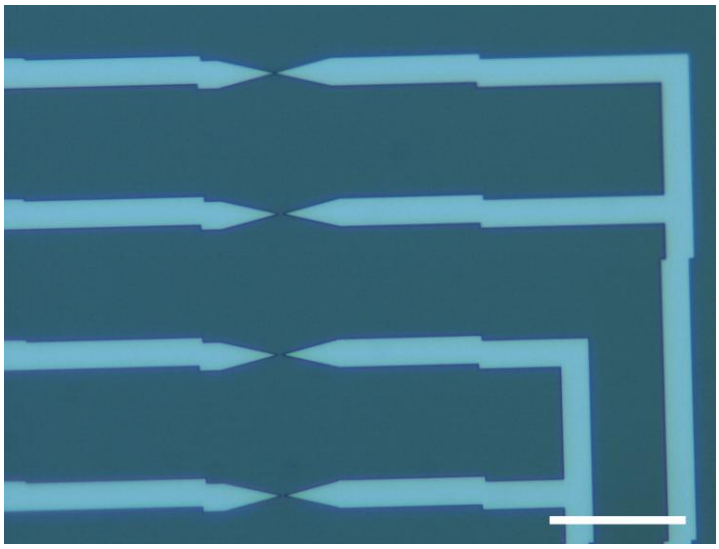

(b)

Fig. 2-9. Images of the fabricated device using e-beam lithography. The scale bars are 200 and 50 μm respectively.

### 2.1.3 Performing DEP

A typical DEP experiment started by cleaning the fabricated chip with a sequence of acetone, methanol/ isopropanol, and DI water, followed by blow-drying with nitrogen. The sample was then placed underneath an optical microscope. A drop of CNT-containing solution (with a volume of approximately 10 µl) was then poured on the sample to surround the tip of the electrodes. Alternatively, a small piece of glassware with a rectangular prism shape was used to immerse the sample in the CNT solution to improve the consistency between experiments. The height of the solution above the sample was 3 mm in the experiments. A set of microprobes with movement resolution of 25 µm was used to connect to the large pads of the electrodes. The probes were guided under the optical microscope to the electrodes and then lowered to connect to them. The tip of the probes were connected to a signal generator. Fig. 2-10 shows schematics of the two setups and Fig. 2-11 contains pictures of the actual setup used for the experiments.

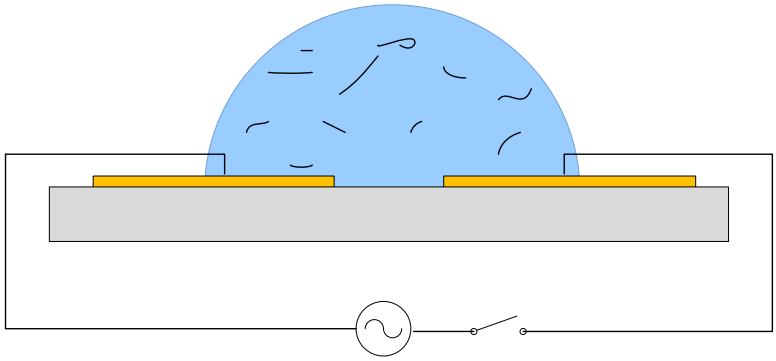

(a)

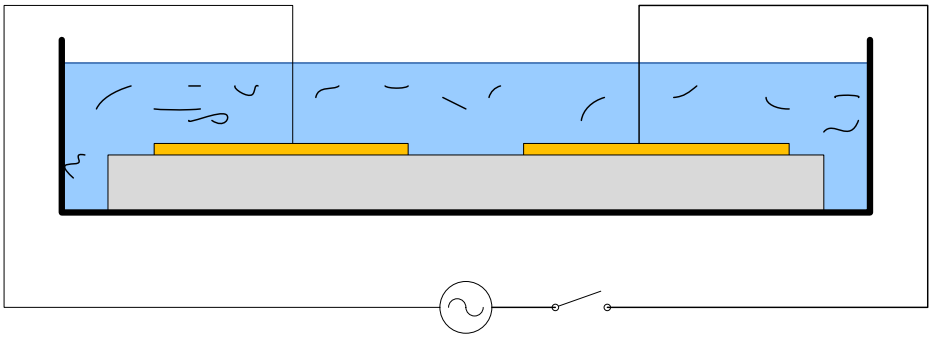

(b)

Fig. 2-10. Schematics of the DEP setups, (a) a drop of solution on the sample, and (b) the sample immersed in the solution.

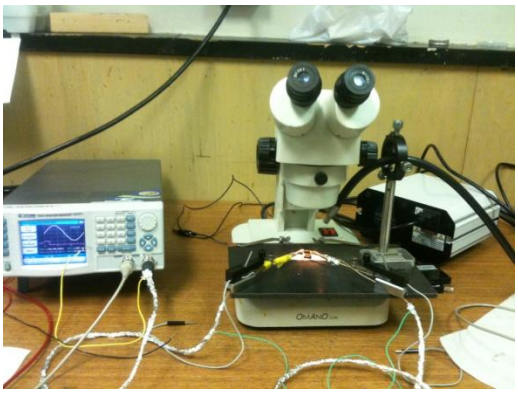

(a)

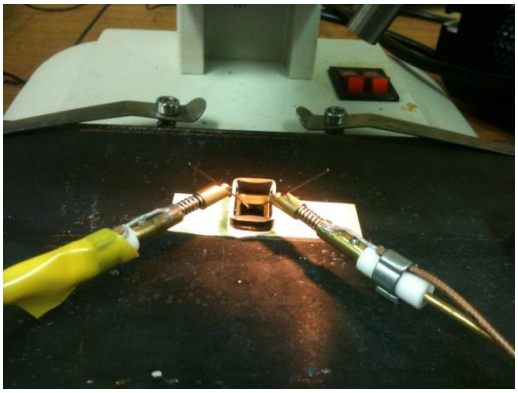

(b)

Fig. 2-11. Images showing (a) the DEP setup, and (b) the microprobes connecting to the sample.

The equivalent circuit of the DEP set up is shown in Fig. 2-12. $R_{solv}$ is the resistance between the two electrodes through the solution. It is inversely proportional to the conductivity of the solution and will be discussed in further detail in the following chapters. $C_{solv}$ denotes the capacitance between the two electrodes (and the pads connected to them) in the solution. $C_{BG\ is}$ the capacitance between the electrodes combined with the pads and the conductive back gate with the silicon dioxide layer as the dielectric (the calculated value for the large connector pads and the back gate of the devices presented in this work is 2.7 pF for each electrode). The double

layer between the electrolyte and the electrodes is represented by a pseudo-capacitor ($C_{DL}$) in the equivalent circuit [39], [44].

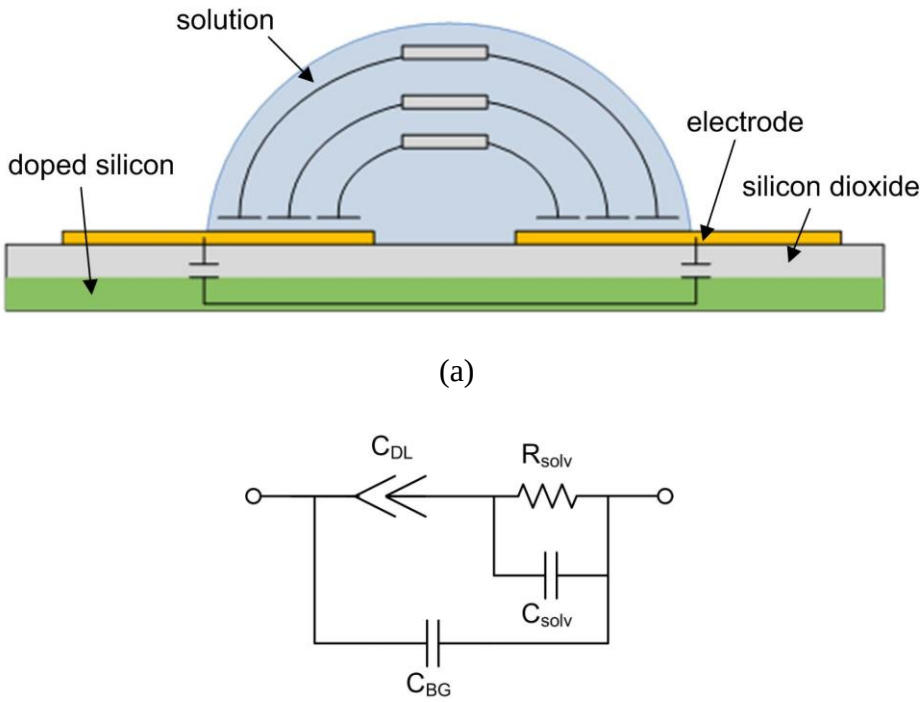


Fig. 2-12. (a) DEP setup modeled by circuit elements. (b) The equivalent circuit between the two electrodes.

Various frequencies and voltage amplitudes were applied in different experiments using a waveform generator (WW5061 Tabor Electronics). The range of applied frequencies was from 100 kHz to 10 MHz, and the potential differences were between 0.5 V/μm to 2 V/μm multiplied by the gap distance between the electrodes.

Once the experiment was finished the sample was rinsed with DI water and blow-dried with nitrogen.

Atomic force microscopy (Nanosurf Easy Scan 2, in the tapping mode with an ACLA tip from APPNANO) and scanning electron microscopy (Hitachi S-4700 field emission scanning electron microscope and Zeiss Sigma field emission scanning electron microscope) were used for characterizing the results of the experiments.

## 2.2 Simulation framework

In order to gain an understanding of the role of various forces during DEP, the development of a multiphysics simulation framework, which could enable coupling of forces with completely different origins, was necessary. Several partial differential equations describe the electric, thermal and fluidic components of the system. The electric field can be found by solving Maxwell's equations. The forces resulting from the electric field present in a medium with non-zero temperature gradients generate the electrothermal force on the fluid. The fluid movement is governed by the Navier-Stokes equation.

A finite-element approach provides the means of finding the solution to differential equations in two and three dimensions [61]. A series of two- and three-dimensional (2-D and 3-D) finite-element simulations were thus performed using COMSOL Multiphysics software package [62] to find the direction and magnitude of the fluid flow in the solution. In the 2-D case, a larger section of the system (containing the electrodes, substrate and solution) could be simulated. On the other hand, in 3-D models, the shapes of the electrodes could be directly implemented in the model, making the simulations more realistic, and the solution movement could be investigated in all three directions. The computational limitations dictated the inclusion of a smaller section of the system in the 3-D simulations.

The electric potential and field in the system were calculated using phasor-based quasi-static Maxwell's equations. The electrodes were set to appropriate potential values and the back gate was grounded. Electric insulation was applied to the boundaries of the system and, therefore, the perpendicular component of the current density was set to zero on all the outer boundaries.

When a potential is applied between the electrodes, the current passing through the solution as a result of the electric field can raise the temperature around the gap region between the electrodes because of Joule heating,

$$Q = < \sigma E^2 > = \frac{1}{2}\sigma|\vec{E}|^2, \qquad \text{Eq. 2-1}$$

where Q is the generated power, σ is the solution conductivity and $\vec{E}$ is the AC electric field. This effect rapidly establishes a stationary temperature field with a negligible oscillating component [40]. The thermal convective motion of the solution is negligible in micro-systems. The energy balance equation can be written as

$$k\nabla^2 T + Q = 0\,, \qquad \text{Eq. 2-2}$$

in which k is the thermal conductivity of the medium and T is the temperature [40], [44]. The boundary conditions applied for the thermal calculations were different in 2-D and 3-D simulations. For the 2-D case, the system boundaries were far away from the heat source and their temperature was supposed to be very close to that of the surroundings; therefore, in this case the temperature of the boundaries was set equal to the ambient temperature. On the other hand, due to computational limitations, the boundaries of the 3-D models were closer to the heat source, and could affect the results unrealistically if they were set to a constant temperature. To avoid this problem, instead we set the normal temperature gradient component at the boundaries

to zero. In both cases, the electrodes were assumed to be thick enough to conduct the heat easily and stay at room temperature.

The temperature gradient leads to gradients in conductivity and permittivity. These spatial changes in the presence of an electric field give rise to the electrothermal force. The time-averaged electrothermal force per unit volume can be approximated using

$$< \overrightarrow{f_E} >= -\frac{1}{2}[\left(\frac{\nabla\sigma}{\sigma} - \frac{\nabla\varepsilon}{\varepsilon}\right).\vec{E}\frac{\varepsilon\vec{E}}{1+(\omega\tau)^2} + \frac{1}{2}\left|\vec{E}\right|^2\nabla\varepsilon], \qquad \text{Eq. 2-3}$$

in which $\varepsilon$ is the permittivity of the solution and $\tau = \varepsilon/\sigma$ is the charge relaxation time in the solution. This expression can be rewritten as a function of temperature gradient as

$$< \overrightarrow{f_E} > = \frac{1}{2}[(\alpha - \beta)\left(\nabla T.\vec{E}\right)\frac{\varepsilon\vec{E}}{1+(\omega\tau)^2} - \frac{1}{2}\left|\vec{E}\right|^2\varepsilon\alpha\nabla T], \qquad \text{Eq. 2-4}$$

where $\alpha = \partial\varepsilon/(\varepsilon\,\partial T) = -0.4\%$ and $\beta = \partial\sigma/(\sigma\,\partial T) = 2\%$ per Kelvin for an aqueous solution [63]. This formula was manually entered into COMSOL. Using the temperature profile calculated by COMSOL based on Eq. 2-2 as explained before, the electrothermal body force was computed for all the meshes covering the model. In order to calculate the velocity of the fluid at each point, the electrothermal force was used in the following equation, which is derived from the Navier-Stokes equation, combined with the mass conservation equation,

$$\eta\nabla^2\vec{u} - \nabla p + \vec{f} = 0 \qquad \text{Eq. 2-5}$$

and

$$\nabla.\vec{u} = 0, \qquad \text{Eq. 2-6}$$

in which $\eta$ is the dynamic viscosity of the solution, p is the pressure, $\vec{u}$ is the velocity vector and $\vec{f}$ is the general volumetric force (here, the electrothermal force, $\overrightarrow{f_E}$, calculated as described above).

The electrothermal force formula has two terms. The first term on the right hand side of Eq. 2-3, which represents the Coulomb force, is dominant at low frequencies. The dielectric force (the second term) is the major component at high frequencies. The transition frequency, at which the dominant term changes, is of the order of the inverse of the relaxation time. The two components are in different directions and, therefore, the direction of the electrothermal flow is different at low and high frequencies [39], [41], [44].

The DEP force depends on the gradient of the square of the field and, for a rod-shaped particle with ellipsoidal shape, can be calculated using

$$< \vec{F}_{DEP} >= \frac{\pi abc}{3}\varepsilon_m \mathrm{Re}\{\frac{\varepsilon_p^* - \varepsilon_m^*}{\varepsilon_m^*}\}\nabla\left|\vec{E}\right|^2, \qquad \text{Eq. 2-7}$$

in which a, b, and c are half of the lengths of the major ellipsoid axes and $\varepsilon_p^*$ and $\varepsilon_m^*$ are the particle (in our case CNT) and medium's permittivities, respectively.

The movement of a particle suspended in a fluid influenced by a deterministic force such as DEP is described by the Langevin equation,

$$m\frac{d\vec{u}_{CNT}}{dt} = \vec{F}_{DEP} - f(\vec{u}_{CNT} - \vec{u}), \qquad \text{Eq. 2-8}$$

in which $\vec{u}_{CNT}$ denotes the velocity of the particle (CNT in this work), m its mass, $\vec{F}_{DEP}$ the deterministic force (here DEP), f the friction factor between the particle and the fluid, and finally $\vec{u}$ the velocity of the fluid at the point where the particle is located at time t [42]. The forces affecting the nanotube movement are DEP, Brownian and the drag imposed on the particle by the solution as it moves at a different speed compared to the surrounding fluid. For now, we neglect the Brownian force but it will be accounted for later on.

The solution of Eq. 2-8 can be written as

$$\vec{u}_{CNT} = \left(\vec{u}_{CNT0} - \vec{u} - \frac{\vec{F}_{DEP}}{f}\right)e^{-\left(\frac{f}{m}\right)t} + \vec{u} + \frac{\vec{F}_{DEP}}{f}. \qquad \text{Eq. 2-9}$$

Here, $\vec{u}_{CNT0}$ is the initial velocity of the nanotube. The characteristic time of acceleration, $\tau = m/f$, is very small and in the range of nano seconds for CNTs, which means that the nanotubes almost instantly accelerate to the velocity determined by the solution velocity, DEP force, and the friction factor. f can be estimated for a randomly moving prolate ellipsoid with a length of l and a radius of r in a solution with a dynamic viscosity of η by [39]

$$f = \frac{3\pi\eta l}{\ln\left(\frac{l}{r}\right)}. \qquad \text{Eq. 2-10}$$

As mentioned in the first chapter, the CNTs become aligned with the field during DEP. However, parasitic phenomena such as Brownian motion interfere with the aligned movement of nanotubes, leading to their having random orientations as they move.

CNT bundles are also usually present in the solutions. Since there are usually at least some metallic nanotubes present in the bundles, they feel a considerable DEP force. One other difference between single CNTs and bundles is the higher stiffness of bundles. While the simulations in this work concentrate on individual CNTs, bundles act in a similar manner during DEP.

The 2-D model consisted of a 200 μm x 150 μm segment representing the solution above the 70-nm-thick electrodes and 2-μm-thick oxide. The electrodes were set at ±V/2 (V is the applied potential difference between the electrodes). The electrostatic potential on the back side of the substrate was set equal to zero to represent the potential of the conductive body of a doped silicon chip. In practice, the substrate is capacitively coupled to the electrodes and, therefore, acquires a potential equal to the average of those of the two electrodes (here, +V/2 and –V/2).

The 2-D simulations cannot take the shape of the electrodes into account. To gain a better understanding of the fluid movement in the third direction, three types of electrodes – narrow,

wide and sharp - were simulated using 3-D models. The computationally expensive nature of 3-D simulation limits the size of the simulation domains. The simulation structure consisted of a pair of electrodes over 2 μm of silicon dioxide, plus a 16 x 20 x 10 μm medium representing the solution. Fig. 2-13 shows the 3-D models.

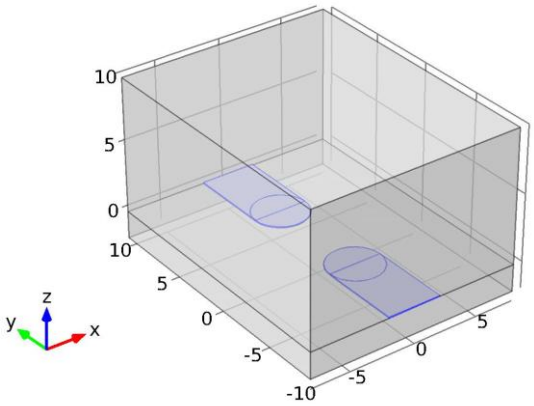


(a)

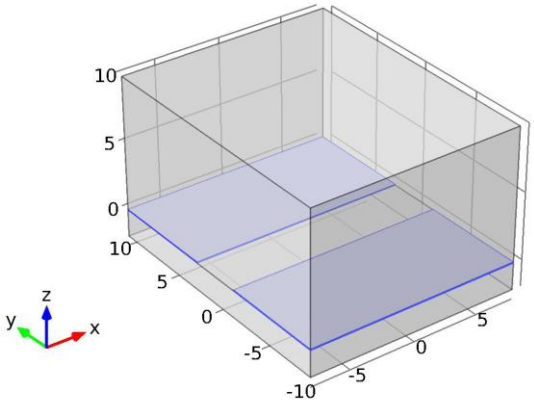


(b)

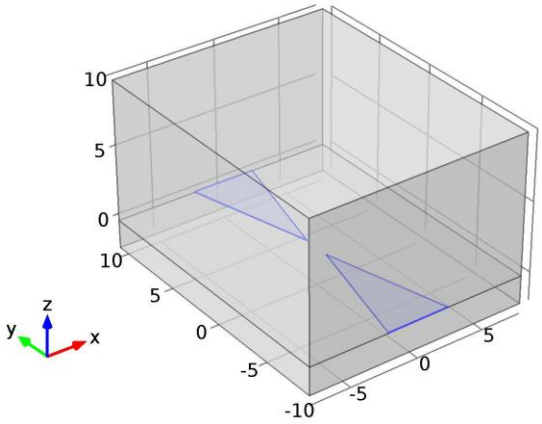


(c)

Fig. 2-13. 3-D models used for simulations. The lengths are in micrometers. The electrodes are highlighted in blue, (a) narrow, (b) wide, and (c) sharp electrodes.

Fig. 2-14 shows the steps taken to find the velocity of nanotubes because of the DEP and electrothermal forces.

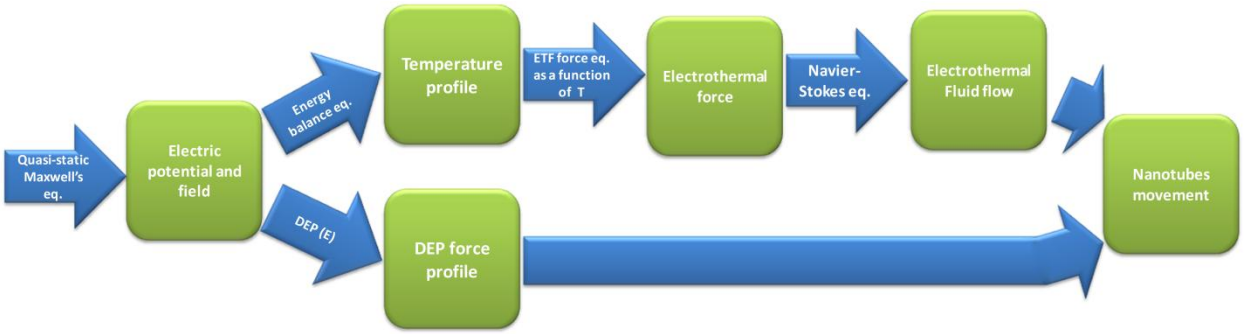


Fig. 2-14. Schematic showing the steps of finite-element method simulations.

## 2.3 Summary

The DEP experiments were performed using solutions made with chemical and physical methods. Electrodes were fabricated with normal photolithography and also e-beam lithography. The large extensions of the electrodes were used to connect the devices to external circuitry during DEP experiments.

The simulations were carried out using a commercial finite-element method software package. A combination of fluid flow as well as electrical simulations for various scenarios was used for estimating the forces acting on nanotubes in different regions of the medium. The experimental and simulation methodology described in this chapter was used in the various aspects of the work reported in the subsequent chapters.

# Chapter 3: **Effect of solution motion on the deposition of carbon nanotubes using DEP**[2]

Although DEP is very promising for fabricating CNT devices, repeatability is still a challenge. There are various parameters that can affect the results, such as the frequency, duration and amplitude of the applied voltage, the shape of the electrodes and the solution properties. Several studies have investigated the effect of each of these parameters to varying degrees as discussed in the first chapter; however, the effect of solution properties in the resulting deposition patterns has not been fully explored.

Among the media typically used for making CNT solutions, water is a popular one. CNT solutions prepared with various methods can have different conductivities and the motion of the solution because of the electrothermal phenomenon can affect the DEP deposition differently in each case. The aqueous solutions commonly used either contain surfactants for suspending CNTs or use some form of pre-treatment to functionalize the originally hydrophobic CNTs so they can dissolve in water [48], [64]. Although both methods result in stable CNT solutions, these solutions have different physical and electrical properties. Even for the solutions made using surfactants, the percentage of surfactant dissolved in the solution can have a significant impact on the conductivity of the final solution.

The current passing through the solution during DEP creates a spatial temperature gradient, which leads to significant movement in parts of the solution.

---

[2] A version of this chapter has been published in a peer-reviewed journal (Reused with permission from "A. Kashefian Naieni, and A. Nojeh, 'Effect of solution conductivity and electrode shape on the deposition of carbon nanotubes from solution using dielectrophoresis,' Nanotechnology, vol. 23, p. 495606, 2012", Copyright 2012, Institute of Physics).

Although the effect of the electrothermal force on creating movement in the solution has been shown previously, no systematic experimental report on the effect of solution conductivity on the deposition of CNTs with DEP is available. We used CNT solutions with different conductivities, but similar in every other respect, to perform such a systematic study, with particular emphasis on how the deposition patterns are affected. We analyze the differences and explain them using finite element simulations. The effect of electrothermal movement in the solution caused by Joule heating was simulated for the various solutions. The simulation results show good agreement with the experiments and can shed light on the drastic changes that the solution conductivity can cause in the deposition patterns.

### 3.1 Methodology

In order to allow for a meaningful comparison between the results of DEP experiments using solutions with different conductivities, one needs solutions with the same number of suspended nanotubes per unit volume but with different concentrations of a surfactant material such as SDBS. Normally, surfactant concentration affects the nanotube concentration [45]. To overcome this issue, we used a surfactant-free CNT solution, commercially available from NanoLab Inc. [49], where the suspended single-walled nanotubes are carboxylated prior to suspension in water, and have a length in the range of 1-5 μm and an average diameter of 1.5 nm. The initial concentration of the solution was 1 g/l and it contained both metallic and semiconducting nanotubes. By adding de-ionized water and the appropriate amounts of SDBS, we prepared three solutions with 0, 0.5, and 1 weight percent (wt%) surfactant with a CNT concentration of 50 mg/l. The role of the surfactant here was merely to change the conductivity of the solution. Although the surfactant might interact with the CNTs in the 0.5 and 1 wt% solutions, this would

not affect the CNT concentration in the solution as the CNTs are already separated and suspended. The conductivities of these solutions were 20, 1010, and 2100 µS/cm, respectively, as measured by a YSI 3200 conductivity meter. The following diagram shows the magnitude of the impedance between the two electrodes (narrow electrodes, 4 µm apart) of the devices, measured using an Agilent 4294A impedance analyzer. The results are shown for the cases where there is no solution on the surface, as well as where the sample is immersed in different solutions.

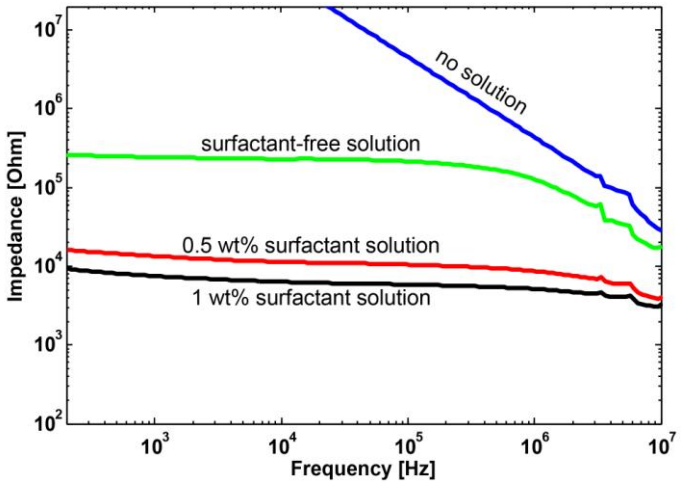


Fig. 3-1. Magnitude of the impedance between the two electrodes (narrow electrodes, 4 µm apart) in different solutions.

The model presented in Fig. 2-12 can be used to explain this diagram. For a bare sample, the capacitances between the electrodes and the conductive back-gate are the main elements playing a role. When a solution covers the electrodes, the electrolyte resistance and capacitance and the double layer capacitance come into play. The effect of the double layer is observed in the non-zero slope of the impedance at low frequencies (up to a few kHz). At intermediate frequencies (between a few kHz and a few MHz) the resistance of the solution is the most influential

element. At higher frequencies (higher than a few MHz) the back gate capacitance is the dominant factor and considerably reduces the magnitude of the impedance between the two electrodes.

It should be noted that, although a surfactant was used for changing the conductivity of the solutions (because of the popularity of the surfactants and their widespread use, which could make the results of the current work more useful) this could effectively be achieved with other ionic salts such as sodium sulfate. This was done in order to perform a control experiment (to evaluate the effect of surfactants on the deposition pattern) with the same concentration of CNTs and the same conductivity as those of the 1 wt% surfactant solution. The solution was prepared by making a concentrated sodium sulfate (BDH Inc.) aqueous solution and diluting it to the desired conductivity level. The final solution had a concentration of 0.011 M of sodium sulfate. As mentioned before, the electrothermal phenomenon can lead to solution movement, which can adversely interfere with the movement of CNTs caused by the DEP force. As the conductivity of the solution increases, this interference is expected to be more significant. A series of experiments at various voltages were performed to investigate how these two forces shape the deposition of CNTs in DEP experiments using solutions with different conductivities and electrodes with different shapes. The three types of electrodes –narrow, wide, and sharp- were used in the DEP experiments.

The DEP experiments were performed starting by pouring and spreading a 10-µl drop of solution on a chip containing 24 pairs of electrodes for narrow and wide electrode designs. For sharp electrodes, the design has electrodes with various gap distances on the same chip. In the case of the solution with no surfactant, the solution could not be spread at the same level as the other two solutions because of the hydrophobicity of the surface. In this case, a 5-µl solution drop was

poured around the target electrodes. Electrodes with different shapes were used. A signal generator was connected to one of the electrodes and the other electrode was grounded through a 200 KΩ resistor in parallel with an oscilloscope. The duration of each experiment was 1 minute. This gives enough time to the CNTs to be deposited on the electrodes and, at the same time, is not excessively long to the point of having nanotubes cover everywhere and mask the difference that using various voltages make. In all of the experiments, the frequency of the applied voltage was set to 5 MHz, which is a typical DEP frequency used in several previous reports [21], [22], [33]. After each experiment, the chip was rinsed with DI water and blow-dried using nitrogen gas. The samples were imaged using a Hitachi S4700 field-emission scanning electron microscope at 1 kV of primary beam acceleration voltage.

## 3.2 Results and discussion

### Experimental results

Fig. 3-2 shows the results of the DEP experiments using narrow electrodes at voltages ranging from 3.5 to 5.5 V. For the solution with no surfactant (Fig. 3-2a), the CNTs deposit in the entire area between the electrodes even at the lowest applied potential. At low voltages, the CNTs deposit in the central regions between the electrodes where the electric field has its maximum value. As the voltage is increased, they start covering the entire gap. The number of deposited CNTs increases as the applied voltage is increased. Therefore, there is a direct relation between the applied voltage and the average driving force on the CNTs. This suggests that DEP, which increases in strength with applied voltage, plays a prominent role in this case.

The morphology of the deposited CNTs is drastically different for the cases where the solution contains surfactants. Instead of covering the whole gap, the CNTs are concentrated more on the

edges of the electrodes. For the solution with 0.5 wt% surfactant (Fig. 3-2b), and specially at lower voltages, few nanotubes bridge the gap. However, at higher voltages and also for the 1 wt% surfactant case (Fig. 3-2c), the CNTs mostly cover the electrodes' surroundings. There is no direct relationship between the applied voltage – and, therefore, the magnitude of the DEP force – and the number of deposited nanotubes. The electrothermal force is thus more dominant in these cases, and is expected to be more pronounced for the more conductive solutions and at higher voltages.

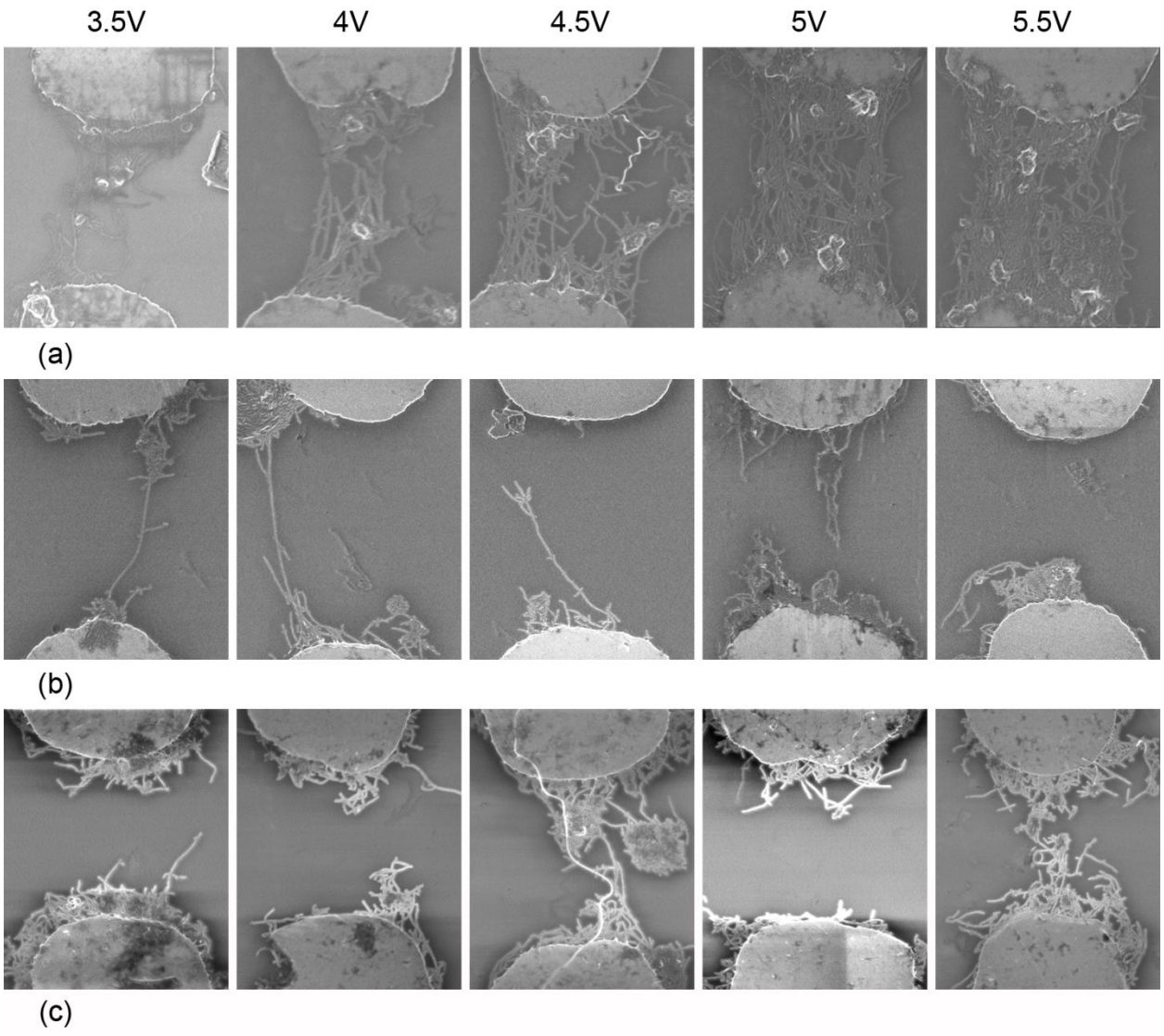


Fig. 3-2. Scanning electron micrographs of the devices made from solutions with (a) 0, (b) 0.5, and (c) 1 wt% surfactant, at voltages ranging from 3.5 V to 5.5 V. The gap between the electrodes is 4 μm long.

Fig. 3-3 shows the results of DEP experiments using a 5.5 V potential difference applied to wide electrodes. While the CNTs from the surfactant-free solution fill the gap between the electrodes completely, for the other two solutions the CNTs mostly cover the electrodes' edges.

Occasionally, at places where the edges of the electrodes are already covered, some CNTs may deposit in the gap and bridge the CNTs on the two sides.

The experiments on the wide and narrow electrodes were performed at least for three separate devices for each voltage setting and solution conductivity shown on Fig. 3-2, for a total of over 45 devices. The results of all the experiments showed deposition patterns similar to what is shown here. The only exceptions were 3 devices with narrow electrodes using the solution with no surfactant, where no CNT or few CNTs were deposited, most likely due to the lack of proper electrical contact between the delicate micro-probes and the electrodes. More experimental results are presented in appendix B.

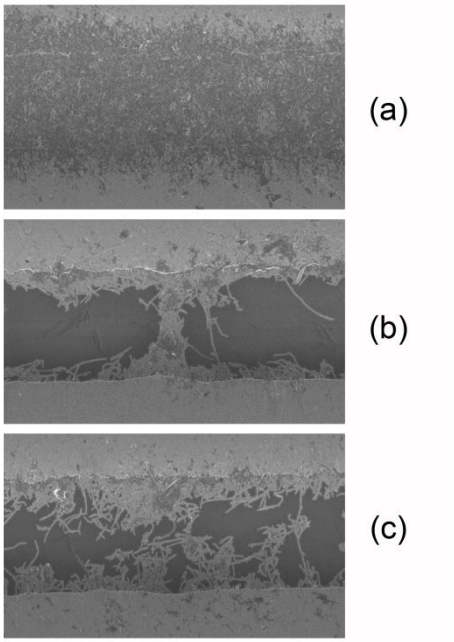


Fig. 3-3. Scanning electron micrographs of the devices made with wide electrodes, using solutions with (a) 0, (b) 0.5, and (c) 1 wt% surfactant. The gap between the electrodes is 4 μm long.

In the case of DEP experiments with wide electrodes, in the gap and away from the corners there is no change in the DEP and electrothermal forces in the direction parallel to the electrode edges.

Therefore, the deposition is expected to be more uniform compared to that in the narrow electrodes, in which case the CNTs are more concentrated in the central region of the gap. The latter point is even more evident if sharp electrodes – for which the central region is practically a point – are used (Fig. 3-4): the gap is bridged by two CNTs when the solution has no surfactant and the DEP force plays the primary role, but there is no CNT deposited in the case of the solution with 1 wt% surfactant.

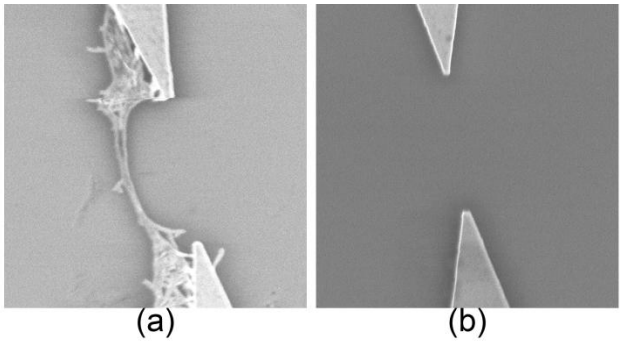


Fig. 3-4. Scanning electron micrographs of the devices made using sharp electrodes with (a) surfactant-free, and (b) 1wt% surfactant solutions. A 3 V potential difference was applied to the electrodes. The gap between the electrodes is 2 μm long.

We now turn to a more detailed analysis of the effect of the electrothermal force, as well as a look at the potential effects of surfactants.

**The effect of the electrothermal force**

To understand the effectiveness of electrothermal flow in each case, a series of two- and three-dimensional (2-D and 3-D) finite element simulations were performed using COMSOL Multiphysics [62] to find the direction and magnitude of the fluid flow in the solution.

Fig. 3-5 demonstrates the diagrams of temperature profiles for different cases when a 5 V potential difference was applied to the electrodes. While the profile pattern is almost the same for all of the surfactant levels, the maximum temperature increases proportional to the conductivity of the solution.

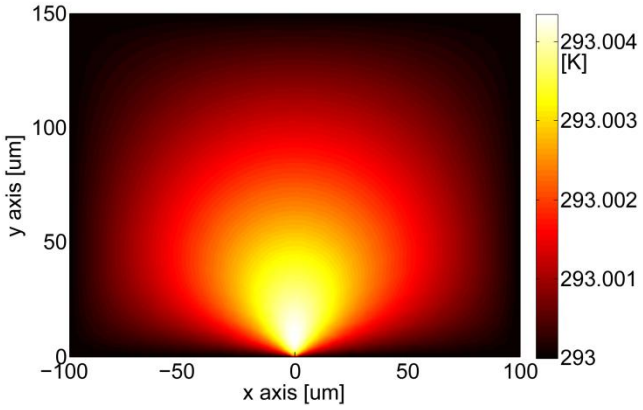


(a)

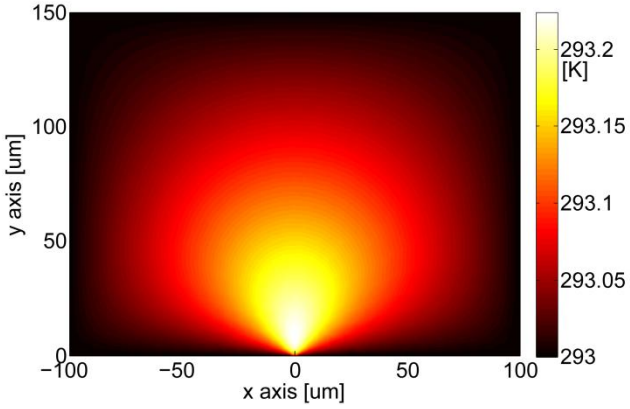


(b)

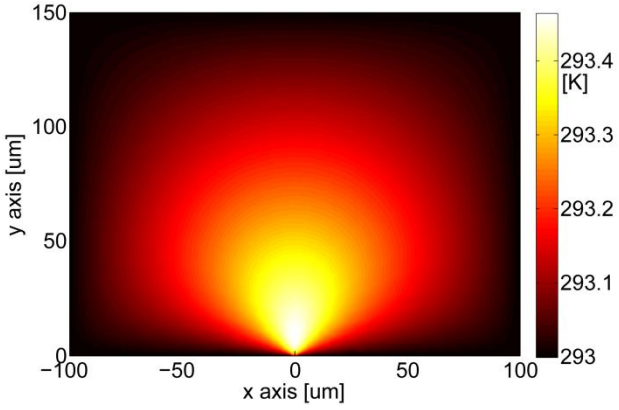


(c)

Fig. 3-5. Temperature distributions in the solution during DEP calculated using 2-D FEM simulations for (a) 0, (b) 0.5, and (c) 1 wt% surfactant solutions. The gap between the electrodes is between -2 to 2 μm on the x axis.

Fig. 3-6 shows the results of the 2-D simulations of the fluid movement. The direction and magnitude of the flow are shown in this figure. Not only the velocities in the surfactant-free solution are orders of magnitude smaller than those in the solutions with surfactant, but also, and importantly, they are in the opposite direction in the two cases. The reason is the much higher relaxation time of the surfactant-free solution, which makes the transition frequency considerably lower than in the other two cases. The maximum velocity for the surfactant-free solution is on the order of a tenth of a micrometer per second, which means that considering the size of the system, the solution is almost stationary.

For the solutions containing surfactant, electrothermal flow is at maximum velocity in the close vicinity of the gap, and it creates a circular motion in a large portion of the bulk of the solution. The direction of the flow is from above the gap toward the edges of the electrodes, and then it continues outward over the electrodes and eventually back over the gap. The long-range movement of the CNTs is governed by the fluid flow and the CNTs are pushed toward the edges of the electrodes. This can explain the difference between the experimental results of the various cases. While the solution is almost stationary in the case of the surfactant-free solution, in the presence of surfactants (leading to considerable conductivity), electrothermal flow carries the CNTs with very high velocities toward the edges of the electrodes and, after that, away from the gap, which gives a short time to the DEP force to make the CNTs deposit only close to the edge of the electrodes.

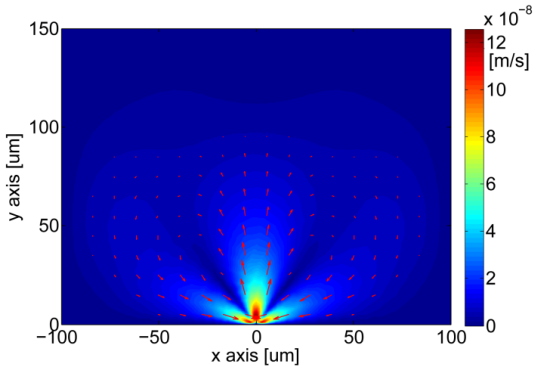


(a)

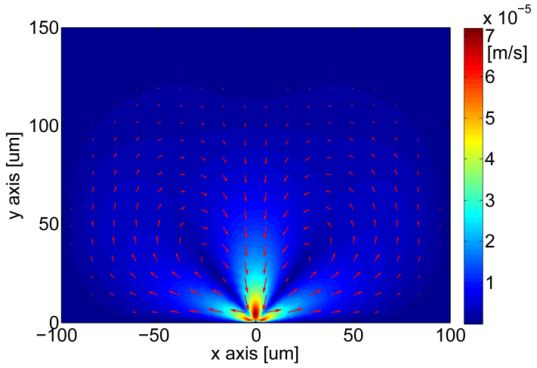


(b)

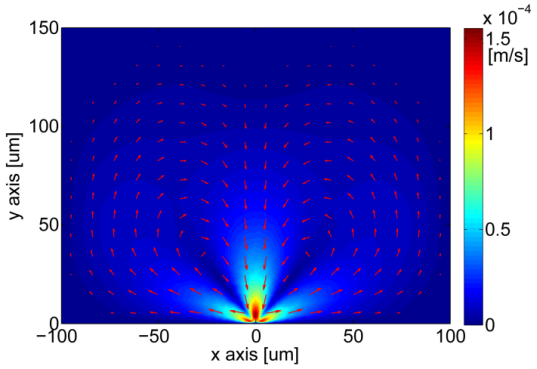


(c)

Fig. 3-6. The fluid flow induced by the electrothermal force for (a) 0, (b) 0.5, and (c) 1 wt% surfactant solutions. The electrode edges are at -2 and 2 μm on the horizontal axis. The colors show the magnitude of the velocity in the entire bulk of the solution. The gap between the electrodes is between -2 to 2 μm on the x axis. The vectors are logarithmically related with the solution velocity at each point.

In order to understand the changes in the fluid velocity as a function of the applied potential, a series of simulations were performed for both 0.5 wt% and 1 wt% solutions with the same range of applied voltages as in the experiments. Fig. 3-7 shows the magnitude of the velocity of the electrothermal flow at a point 10 µm above the center of the gap. The results show a non-linear increase in the velocity as the applied voltage increases. This can explain the presence of some CNTs in the middle of the gap at low applied voltages with the medium conductivity solution. At higher voltages or for the higher-conductivity solution, the velocity is considerably higher and the nanotubes are pushed toward the edges and away from the middle of the gap.

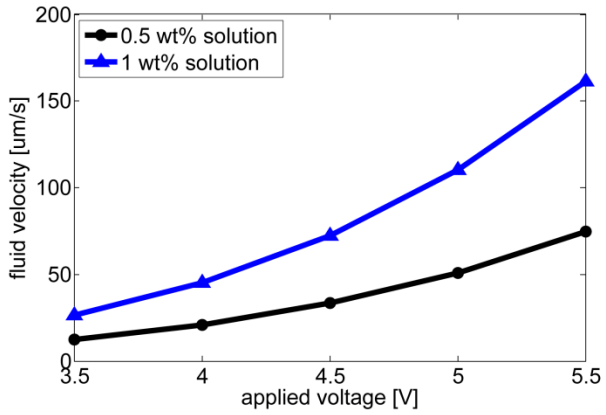


Fig. 3-7. The magnitude of the fluid velocity as a function of the applied voltage. The black line with circles shows the velocity values for the solution with 1 wt% surfactant. The blue line with triangles shows the values for the solution containing 0.5 wt% surfactant.

Fig. 3-8 shows the overall movement of the nanotubes in the medium for the case of 1 wt% surfactant solution under a 5-V applied potential. It can be seen that the long range movement of the CNTs is dictated by the electrothermal flow, but the DEP force is dominant near the gap and captures the CNTs as they pass in the close vicinity of the gap. The maximum of the color-bar in

Fig. 3-8 is set to 200 µm/s to allow for more detail to be visible over the entire figure. It should be noted that the velocity of nanotubes as a result of the DEP force is much higher close to the edges of the gap, whereas the fluid velocity is zero on the boundaries because of the no-slip boundary condition. Without the DEP force, the nanotubes would move with the fluid because of the electrothermal force and, although they would approach the gap, they would not deposit there. Fig. 3-8b and c show the magnified version of the nanotubes' velocities near the gap as a result of the electrothermal flow (Fig. 3-8b) and electrothermal and DEP combined (Fig. 3-8c) to ease the comparison.

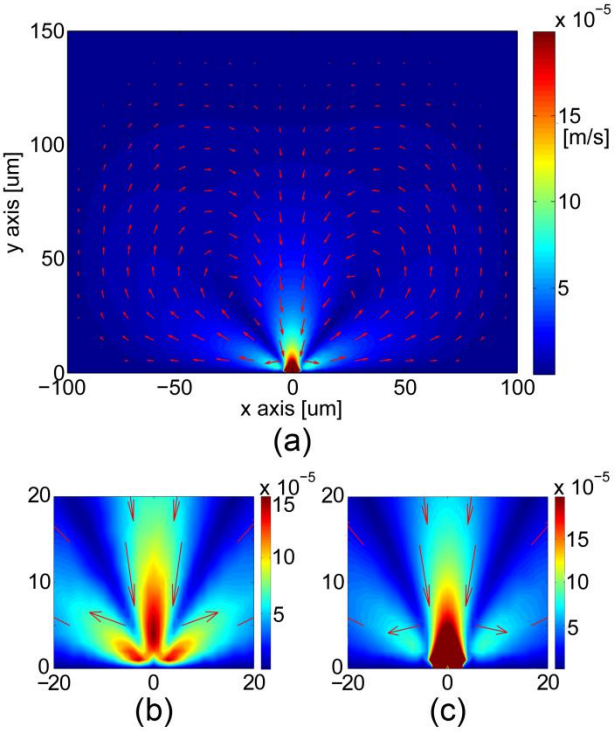


Fig. 3-8. (a) The overall velocity of movement of the CNTs as a result of electrothermal flow and DEP force for the 1 wt% surfactant solution at 5 V, (b) the movement of nanotubes in the 1 wt% solution in the presence of electrothermal flow only, near the gap region (magnified view of Fig. 3-5c near the gap), (c) the magnified view of Fig. 3-8a near the gap region. The vectors are logarithmically related with the solution velocity at each point.

The 2-D simulations cannot take the shape of the electrodes into account. To gain a better understanding of the fluid movement in the third direction, two types of electrodes – narrow and wide- were simulated using 3-D models. The temperature gradient created by the wide electrodes is higher than in the case of the narrow electrodes and also sharp electrodes due to the larger total current passing through the solution. This higher temperature gradient causes faster movements in the solution. Fig. 3-9 shows the temperature profiles for different cases.

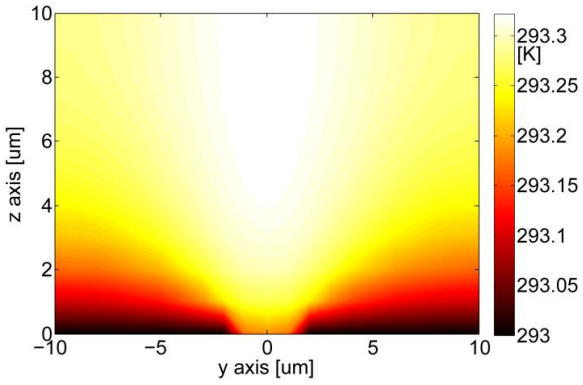


(a)

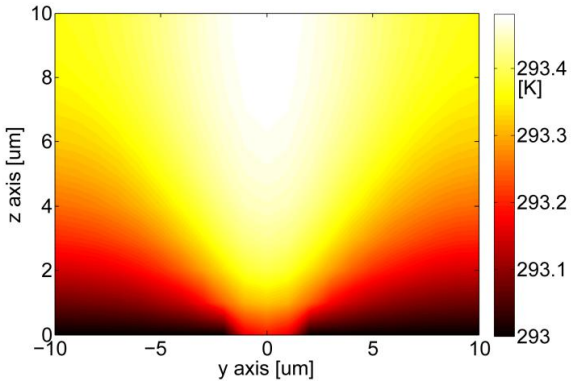


(b)

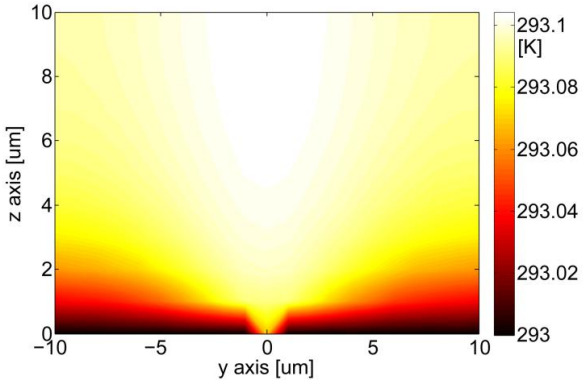


(c)

Fig. 3-9. Temperature distributions in the solution during DEP calculated using 3-D FEM simulations for (a) narrow electrodes, (b) wide electrodes, and (c) sharp electrodes. The gap between the electrodes is between -2 to 2 μm on the y axis.

Fig. 3-10 shows the simulated fluid motion pattern in the plane of symmetry between the two electrodes (x-z plane in Fig. 2-13). The fluid has a very homogeneous movement straight from the top toward the gap when the width of the electrodes is considerably larger than the gap. In this case, the fluid has an in-plane movement in the planes parallel to the y-z plane (Fig. 3-10a). This results in a rather uniform deposition of the nanotubes in the x direction. For the narrow electrodes, the fluid not only moves in the z direction, but also moves in the x direction toward the gap (Fig. 3-10b). For the sharp electrodes, the movement is even more concentrated toward the line connecting the tips of the electrodes (Fig. 3-10c). This movement and the electric field distribution lead to the nanotubes depositing primarily in the narrow region between the electrodes.

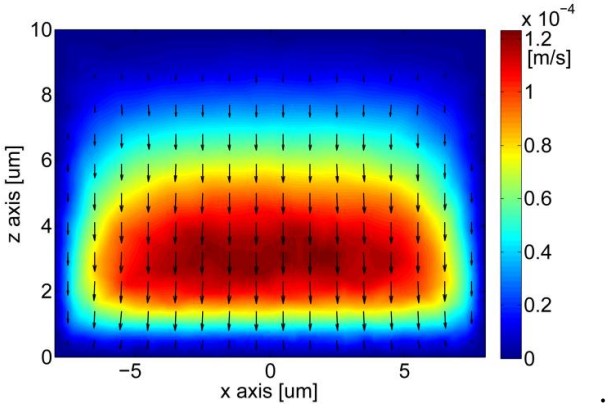


(a)

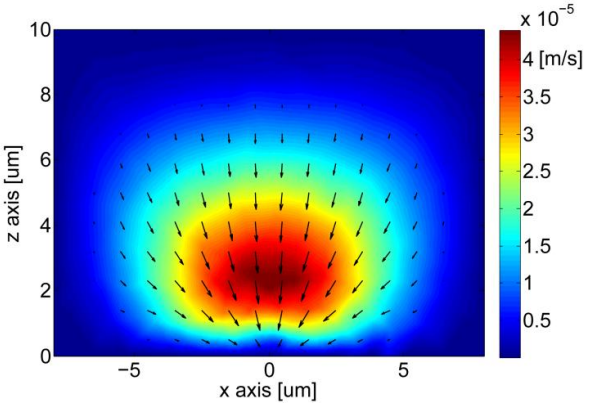


(b)

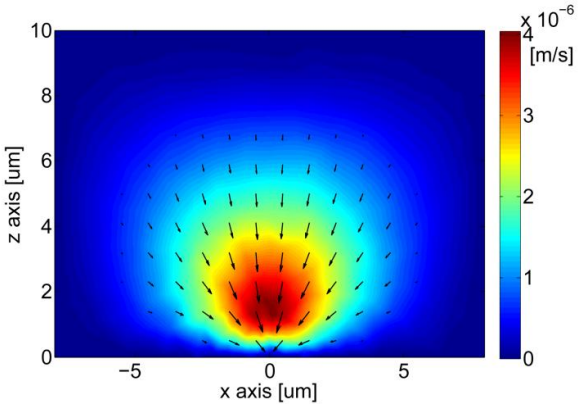


(c)

Fig. 3-10. The fluid flow pattern in the x-z plan in the middle of the gap of (a) wide, (b) narrow, and (c) sharp electrodes. The vectors are logarithmically related with the solution velocity at each point.

As it was discussed, the simulation results are consistent with the experimental observations, and demonstrate that the electrothermal force plays a key role in the deposition of nanotubes especially for solutions in which surfactant materials are used for the separation of the CNTs.

**The effect of surfactants**

The modeling results presented in the previous section strongly suggest that the electrothermal force has a significant effect on the results of DEP deposition, and can explain the morphology of the devices made using low- and high-conductivity solutions (without or with surfactant, respectively). However, other factors might also influence the morphology of the nanotube layer on the surface. For example, surfactants affect not only the nanotubes, but also the other surfaces in contact with the solution, notably the palladium electrodes. They can thus potentially cause important interactions between the suspended nanotubes and the electrodes. Here, we will attempt to shed light on the extent of such influence on the results.

The first question is whether the surfactant molecules can enable the attachment of nanotubes to the electrodes even in the absence of the DEP force. Fig. 3-11 shows four devices after having been submerged in a 1 wt% surfactant solution for more than 5 minutes. The lack of CNTs on the electrodes indicates that, acting alone, it is highly unlikely for surfactants to lead to nanotube deposition.

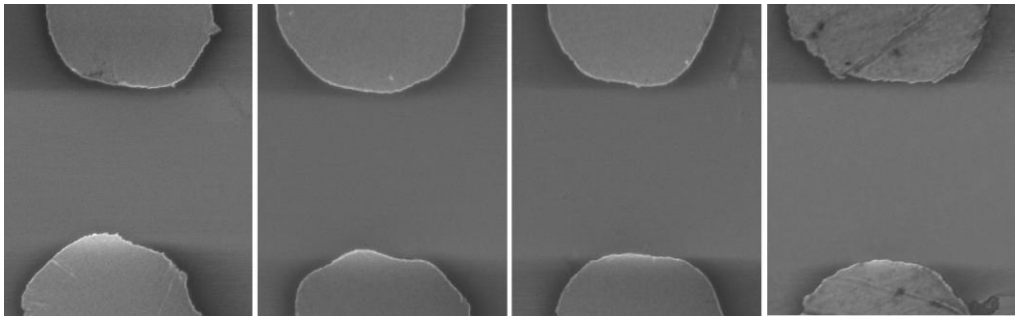

Fig. 3-11. Scanning electron micrographs of the electrodes after being submerged in surfactant-containing CNT solutions for more than 5 minutes. The gap between the electrodes is 4 μm.

Next, we consider the role of surfactants in the presence of the electric field, which creates the DEP force on the nanotubes. Ideally, control experiments completely separating the effect of surfactant molecules in the solution and the electrothermal motion are needed. However, this is not possible since the presence of ionic surfactants always leads to increased conductivity and thus electrothermal flow. An alternative control experiment consists of using solutions made with ionic salts (such as sodium sulfate as explained in the methodology section of this chapter) with conductivities similar to those of the surfactant-containing solutions. This would reveal the effect of electrothermal movement in the absence of surfactants. Fig. 3-12 shows two repetitions of such a control experiment, using the same DEP parameters as those of Fig. 3-2.

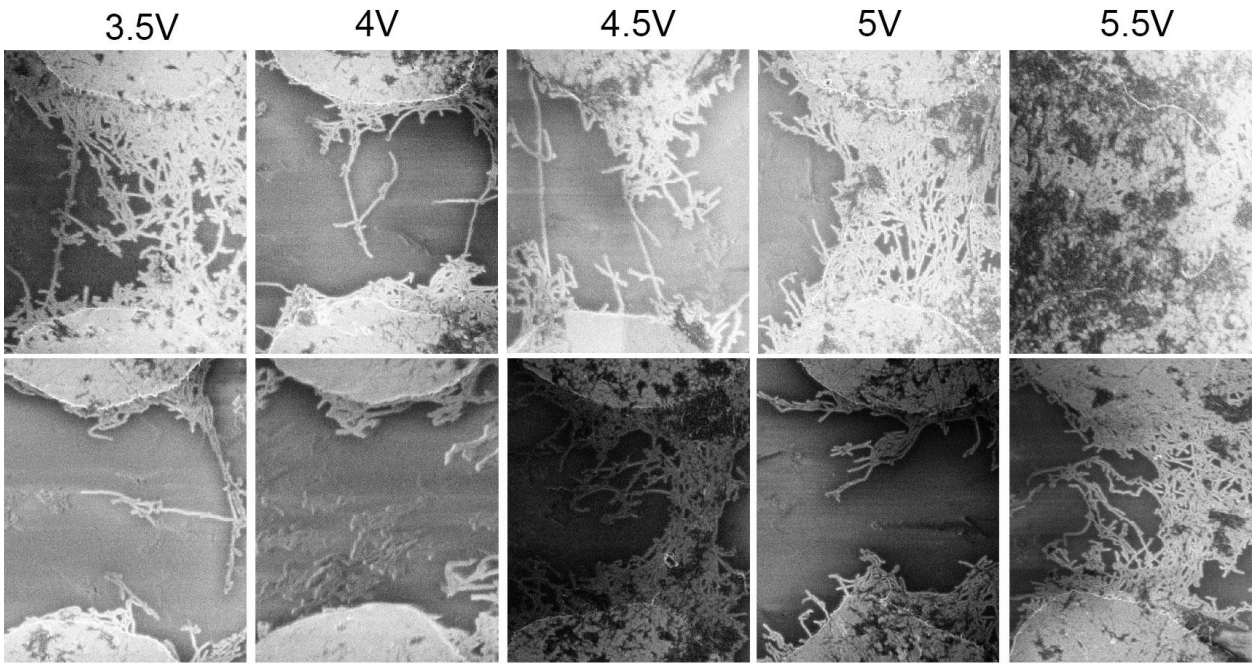


Fig. 3-12. Scanning electron micrographs of the devices made in control experiment. The conductivity of the CNT solution was altered using sodium sulfate rather than surfactants. Each column shows two repetitions of the experiment with the same applied voltage. The gap between the electrodes is 4 µm.

In order to be able to compare the results of the original and control experiments, an image processing procedure was implemented to quantify the outcome. To compensate for the areas that the electrodes occupy (which could be different from image to image), images were individually cropped so they include 1 µm of the length of each electrode. Considering the 4 µm distance between the pair of electrodes, the images included a total length of 6 µm of the device. The ratio of the area covered by nanotubes and the total area of the image was then calculated in each case. Details of the image processing method are presented in Appendices B and C.

Fig. 3-13a shows the ratio of the area covered by nanotubes to the total area of the image. The variation in the total number of nanotubes deposited from the solutions with higher conductivity was an obstacle on the way of meaningfully quantifying the coverage on different parts of the

image (e.g. close to the electrodes, or the middle of the gap). We thus adopted the following normalization procedure: for each image, nanotube coverage in regions within a distance of approximately 1 μm from the electrodes on each side was calculated. This was divided by the total coverage of the nanotubes (as calculated in the previous step) as a measure of the percentage of nanotubes deposited in the close vicinity of the electrodes. The results are shown in Fig. 3-13b.

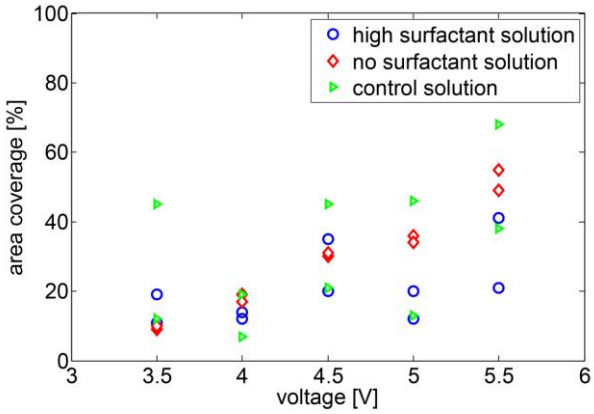


(a)

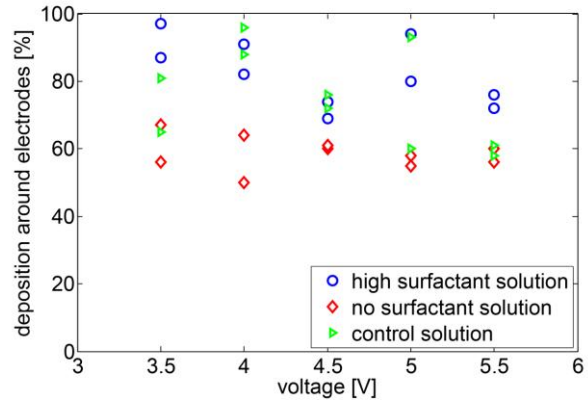


(b)

Fig. 3-13. (a) Ratio of the area covered by the nanotubes and the total area between the two electrodes, and (b) ratio of the area covered by the nanotubes near the electrodes and the total area covered by them. Both graphs are plotted for DEP experiments using different solutions at various voltages. The green triangles, blue circles, and red diamonds denote the results for the control solution, the 1 wt% surfactant solution and the no surfactant solution, respectively.

The total coverage area of the nanotubes deposited in the control experiment show strong variations, not only for different voltages but also at each voltage point. This lack of trend with voltage can also be observed for the devices made using the surfactant-containing solution. On

the other hand, for the solution with no surfactant, there is significantly less variation in the results and a clear monotonic increase with voltage. A similar trend was observed in numerous other experiments using surfactant-free solutions, some of which are presented in Appendix B.

The percentage of the nanotubes deposited around the electrodes using the surfactant-free solution did not vary much as a function of voltage (Fig. 3-13b). This shows that the number of deposited nanotubes increases homogeneously in the area around the electrodes as well as in the middle of the gap for the surfactant-free solution. The average value of all the data points was 58%. For the case of the control solution and the 1 wt% solution, the overall deposition percentage around the electrodes was significantly higher than for the surfactant-free solution. This is an indication that, for both of these cases, the nanotubes tend to deposit around the electrodes rather than in the middle of the gap. The average values of all the data points for the devices made using the control solution and 1 wt% solution were 75% and 82%, respectively. These values are both substantially higher than the 58% observed in the deposition from the surfactant-free solution, supporting the argument that the electrothermal motion of the solution has a detrimental effect. Therefore, at the very least, the surfactants have the detrimental effect of changing the conductivity, and thus play an important role in the deposition process. Nonetheless, this study falls short of quantifying the extent of effectiveness of the interaction between the surfactant-affected electrodes and suspended nanotubes in the solution. The higher variations in the number of deposited nanotubes from the control solution compared to the surfactant containing solution, as shown in Fig. 3-13a, suggest a positive role for the surfactants. While one might be tempted to draw conclusions, many more repetitions of such experiments in the form of a systematic study would be needed to confirm this, which is beyond the scope of this work.

## 3.3 Summary

Dielectrophoresis experiments were performed and accompanied by simulations in order to study the effect of the electrothermal force on the deposition pattern of CNTs from solutions with various conductivities, using electrodes with different shapes. The results show that in the case of the surfactant-free solution, there is negligible movement in the solution under applied voltage. Experimentally, this results in the deposition of CNTs all around the gap between the electrodes. The presence of surfactants in the solution increases the conductivity and, therefore, the Joule heating effect. The resulting electrothermal force can be of primary significance in the morphology of the deposited nanotube collection on the surface; the CNTs deposit mostly on the electrode edges. Simulations show that the reason behind this is the movement of the fluid from the upper regions of the solution toward the gap, and then its deflection toward the edges of the electrodes and onto the electrodes' surfaces on each side.

The direction of the electrothermal movement of the solution depends on the shape of the electrodes. For electrodes with a width considerably larger than their gap, the flow takes place in planes perpendicular to the gap edge. For electrodes with narrow widths, the movement has a 3-D profile.

Taking the electrothermal force into account appears to be of primary importance in designing DEP deposition processes for CNTs.

## Chapter 4: **The evolution of forces with frequency during DEP**[3]

The physical properties of the solution play a major role in determining the nanotube patterns deposited using DEP; the non-uniform temperature profile generated by the passage of current can create forces in the solution, which result in agitations and can interfere with the DEP force.

In the previous chapter we investigated the simultaneous effects of the electrothermal and DEP forces on CNTs and the resulting deposition pattern at a single frequency for solutions with different levels of conductivity. It was observed that the electrothermal force cannot be neglected in solutions containing surfactants. In addition, the effect of this force does not depend strongly on the percentage of surfactant in stable nanotube solutions; however, it is drastically less pronounced for solutions without surfactant. For solutions with 1wt% SDBS, which is typical for CNT deposition, the electrothermal force is the dominant player in the long-range drift of the CNTs, and affects the deposition pattern dramatically compared to the situation in the solution with no surfactant.

The forces that induce movement in the solution, as well as the DEP force, all vary with frequency in different manners. An important question here is how the effects of the two main forces – the DEP force and the electrothermal force – evolve with respect to each other as the frequency of the applied voltage is varied. This is a critical issue that requires detailed investigation. In this chapter, results of experiments and finite element simulations investigating the interplay between these two forces at different frequencies are discussed. We show that there exists a threshold frequency beyond which the number of deposited CNTs bridging the

[3] A version of this chapter has been published in a peer-reviewed journal (Reused with permission from "A. Kashefian Naieni, and A. Nojeh, 'Dielectrophoretic deposition of carbon nanotubes: the role of field frequency and its dependence on solution conductivity,' Microelectronic Engineering, vol. 114, p. 26, 2014", Copyright 2014, Elsevier).

electrodes reduces drastically. For low-conductivity solutions (those made using pre-treated nanotubes), this threshold falls within the frequency range used in practice, whereas in high-conductivity solutions (those including surfactants), it is orders of magnitude higher.

### 4.1 Methodology

Two nanotube solutions were prepared from the commercially available NanoLab solution. The nanotube solutions were diluted to the desired concentrations. For each sample with a certain concentration of CNTs, two solutions with 0 and 1 wt% SDBS were prepared. Each of the solutions was ultrasonicated for 5 minutes.

The DEP experiments were conducted by applying a 5-V AC signal with a range of frequencies to the electrodes using microprobes. The sample was immersed 3 mm deep into the solution during each experiment. It was then rinsed with DI water followed by blow drying using nitrogen. The samples were imaged using a Hitachi S4700 field-emission scanning electron microscope under 1 kV of primary beam acceleration voltage.

In order to be able to explain the experimental results 2-D finite element simulations were performed at the same frequencies as in the experiments as was explained in the second chapter.

The electric field distribution was used to calculate the DEP force using

$$< \vec{F}_{DEP} >= \frac{\pi abc}{3} \varepsilon_m \mathrm{Re}\{f_{CM}\} \nabla \left|\vec{E}\right|^2 \qquad \text{Eq. 4-1}$$

$$f_{CM} = \frac{\varepsilon_p^* - \varepsilon_m^*}{\varepsilon_p^*}, \qquad \text{Eq. 4-2}$$

where $f_{CM}$ is the Clausius-Mossoti (CM) factor, and $\varepsilon_p^*$ and $\varepsilon_m^*$ are the particle (in this case the CNT) and medium's complex permittivities, respectively. Also, we have

$$\varepsilon^* = \varepsilon - j\frac{\sigma}{\omega}, \qquad \text{Eq. 4-3}$$

in which ε is the permittivity, σ is the conductivity and ω is the angular frequency. The CM factor is the frequency dependent part of the DEP force formula. At lower frequencies, the real part of the CM factor depends mostly on the conductivities of the particle and the solution, but in the higher limit the permittivities play the main roles. The border between these higher and lower limits is determined by the relative values of the conductivity and permittivity of the solution and the particle. The DEP force was calculated for metallic CNTs with a length of 1 μm and a radius of 1 nm.

## 4.2 Results and discussion

DEP experiments were performed at 200 kHz, 500 kHz, 1 MHz, 5 MHz, and 10 MHz. We observed that not only does the frequency of the applied voltage affect the results, but also the trends are different for the two solutions. Fig. 4-1 shows the outcome of DEP experiments using solutions with a concentration of 2.5 μg/ml of CNTs and a deposition time of 30 s. For the no-surfactant case, at lower frequencies most of the nanotubes bridge the electrodes. Increasing the frequency from 200 kHz to 1 MHz directly increases the number of deposited nanotubes. For higher frequencies, the pattern of nanotube deposition changes considerably. The number of deposited nanotubes decreases and, instead of long nanotubes bridging the gap, mostly shorter CNTs deposit along the edges of the electrodes.

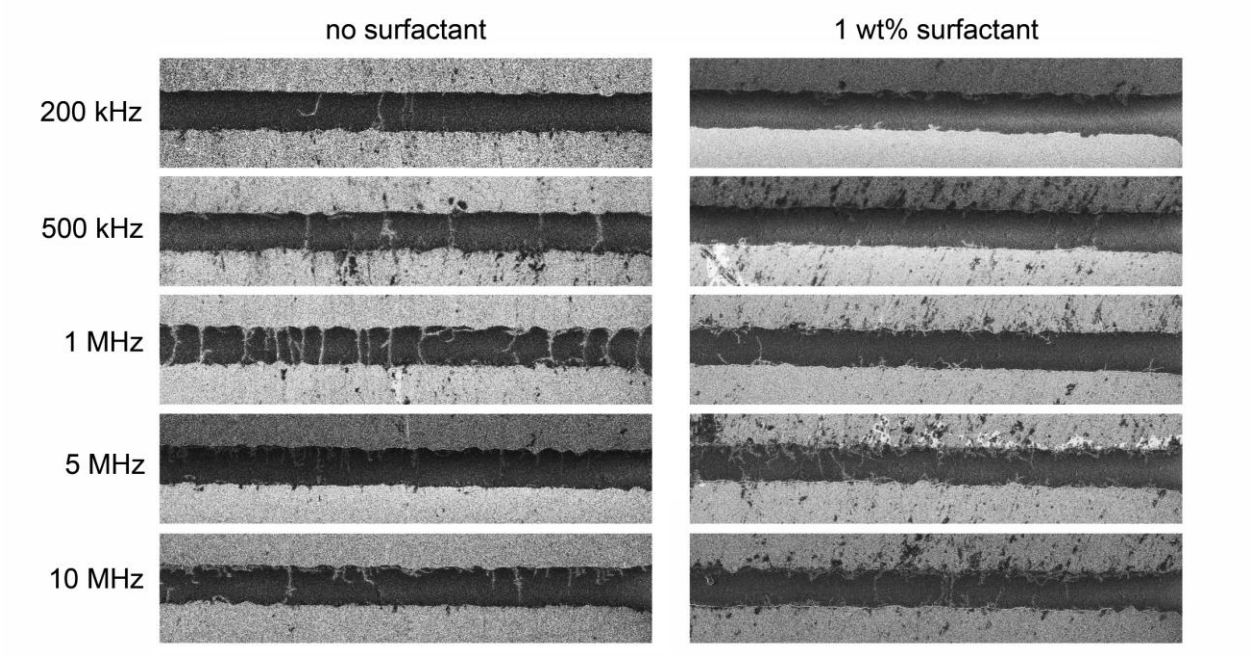


Fig. 4-1. Scanning electron micrographs of structures fabricated at various frequencies using solutions with no surfactant and 1 wt% surfactant with 2.5 µg/ml of CNTs in water. The gap between the electrodes is 4 µm.

For the solution with 1 wt% surfactant, the CNTs deposit near the electrode edges for all frequencies. Although there seems to be a slight increase in the number of deposited nanotubes as the frequency increases, this trend is weaker than in the no-surfactant case. As will be seen later, the thermal effects are the root cause of this lack of clear trends with frequency in this range.

Fig. 4-2 shows the results of DEP experiments using the 50-µg/ml solution and narrow electrodes. The voltage was applied for 30 s in each experiment. Although the number of deposited nanotubes is much higher compared to the previous case because of the higher CNT concentration, the behavior at different frequencies follows the same pattern. For the no-surfactant solution, at low frequencies the gap between the electrodes is completely filled with CNTs. The area covered by nanotubes increases as the frequency increases from 200 kHz to 1

MHz. At 5 MHz, the number of deposited nanotubes experiences a drastic drop, and increasing the frequency to 10 MHz further decreases this number to just a few. In the 1 wt% surfactant case, CNTs deposit mostly around the edges of the electrodes. There is no direct relationship between the number of nanotubes and the frequency, and the results appear to be somewhat random.

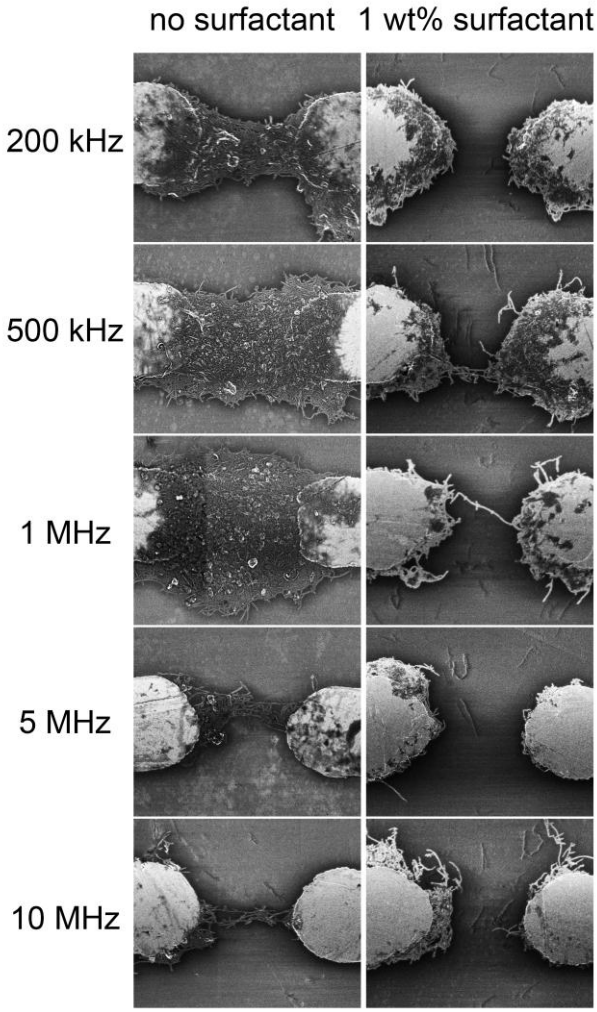


Fig. 4-2. Scanning electron micrographs of structures fabricated at various frequencies using solutions with no surfactant and 1 wt% surfactant with 50 µg/ml of CNTs in water. The gap between the electrodes is 4 µm.

We now turn to the simulation results in order to gain a better understanding of the effective parameters and the forces at work. In the simulations, as expected, the amount of heat generated by the passage of current through the solution was not affected by the frequency in any substantial way and, therefore, the resulting temperature profile was similar at different frequencies. Fig. 4-3 shows these profiles for the no-surfactant and 1 wt% surfactant cases.

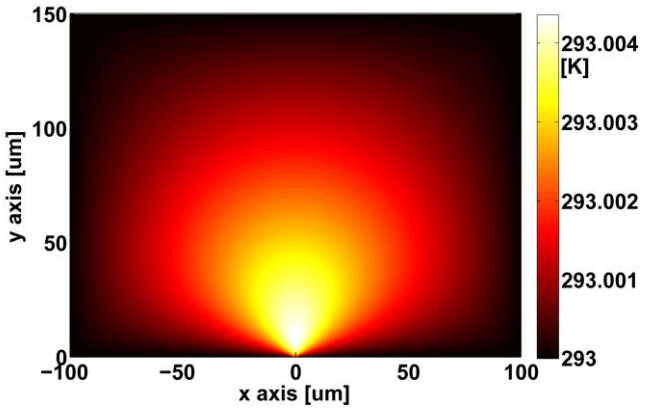


(a)

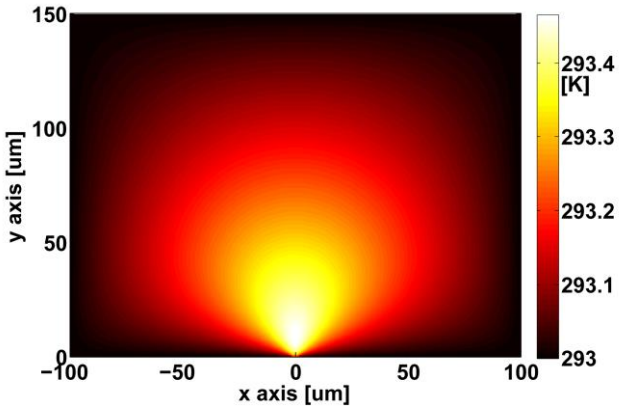


(b)

Fig. 4-3. Side view of the calculated temperature profile in the (a) no-surfactant, and (b) 1 wt% surfactant solutions. The two electrodes are located at -100 µm to -2 µm and 2 µm to 100 µm on the x axis. Note that the maximum temperature difference between the hot and cold areas is approximately 100 times higher in case (b).

The gradient of the temperature profile is very high in the case of the 1 wt% solution, especially near the edges of the electrodes. The electrothermal force directly depends on the temperature gradient; therefore, this leads to much higher electrothermal forces in this case compared to when no surfactant is present. Fig. 4-4 depicts the electrothermal flow pattern in the solution with no surfactants, as well as the movement of the nanotubes as a result of both electrothermal flow and DEP forces acting on them, for three of the simulated frequencies. The maximum velocity on the color coded figures of nanotube movement is set to 200 μm/s in order to bring out the details.

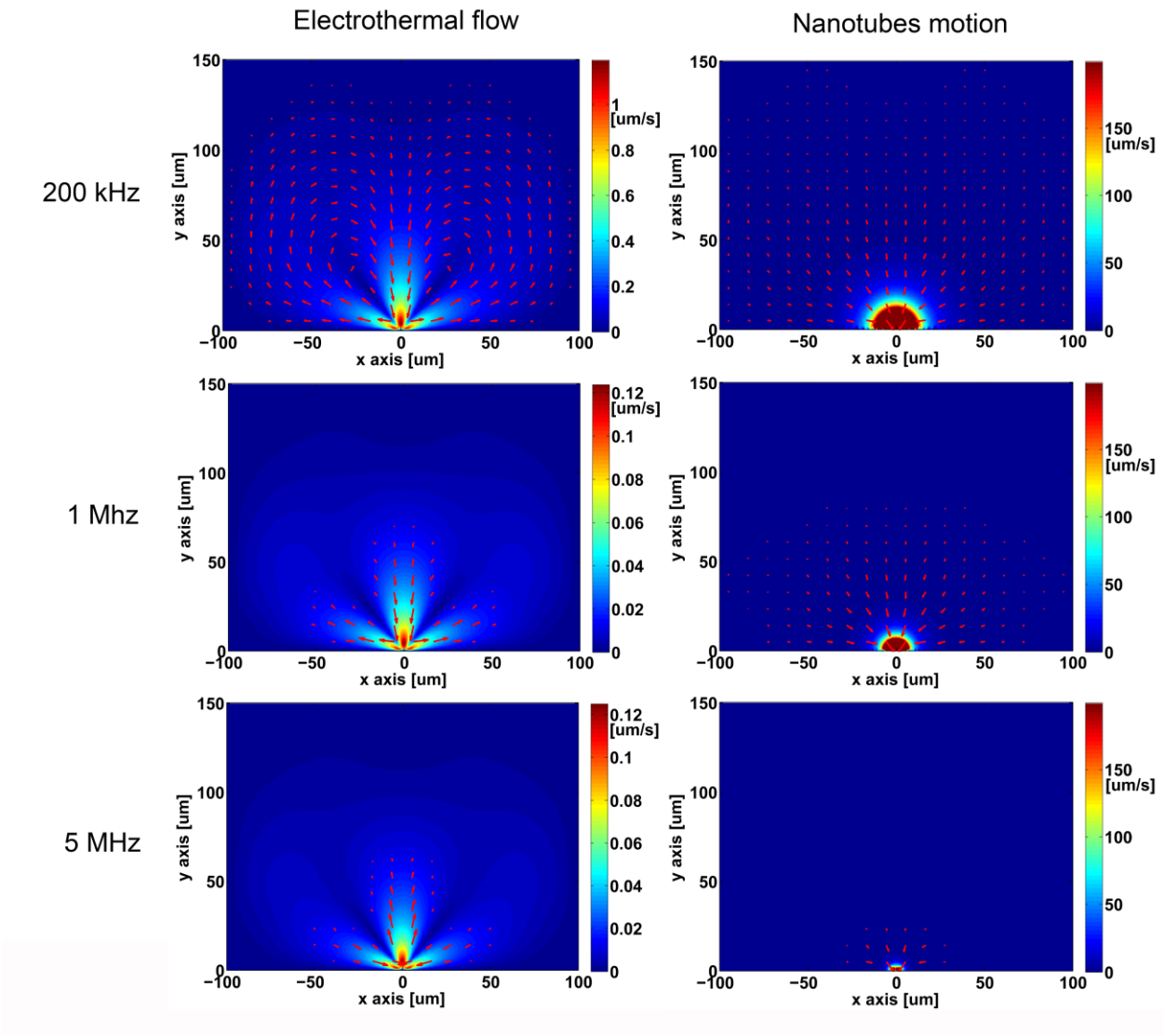


Fig. 4-4. Electrothermal flow and movement of the nanotubes in the solution caused by electrothermal flow and DEP forces at different frequencies for the no-surfactant solution. The vectors are logarithmically related with the velocity at each point. The gap between the electrodes is between -2 to 2 µm on the x axis.

For the no-surfactant solution, the electrothermal force not only weakens at higher frequencies, but also changes direction, pushing the solution upward above the gap between the two electrodes rather than downward. For frequencies up to 1 MHz, the electrothermal force assists the overall deposition process by driving the CNTs toward the gap between the two electrodes.

The DEP force is dominant in the close vicinity of the gap. For frequencies higher than 5 MHz, electrothermal flow actually repels the nanotubes from the gap. On the other hand, the DEP force gradually loses its domain of effectiveness and is increasingly restricted to near the edges of the electrodes. This is due to the decrease in the magnitude of the real part of the CM factor for the case of the no-surfactant solution as the frequency increases. The initial increase in the number of deposited nanotubes with increase in frequency (from 200 kHz to 1 MHz) is probably due to the better alignment of the CNTs with the field and, therefore, the higher effect of the DEP force as the frequency increases [27], [65]. A perfectly aligned nanotube has a stronger dipole, compared to one which is not in alignment with the field, and therefore feels a larger DEP force.

When a solution containing surfactants is used, the electrothermal force plays a much more pronounced role. In this case, the CM factor does not change in the range of frequencies used here, which means that the DEP force should not change with frequency as much as in the previous case; the simulations also do not show any significant changes in the DEP and electrothermal forces for different frequencies. Fig. 4-5 shows the electrothermal flow as well as the overall movement of the nanotubes because of both solution movement and the DEP force in this case.

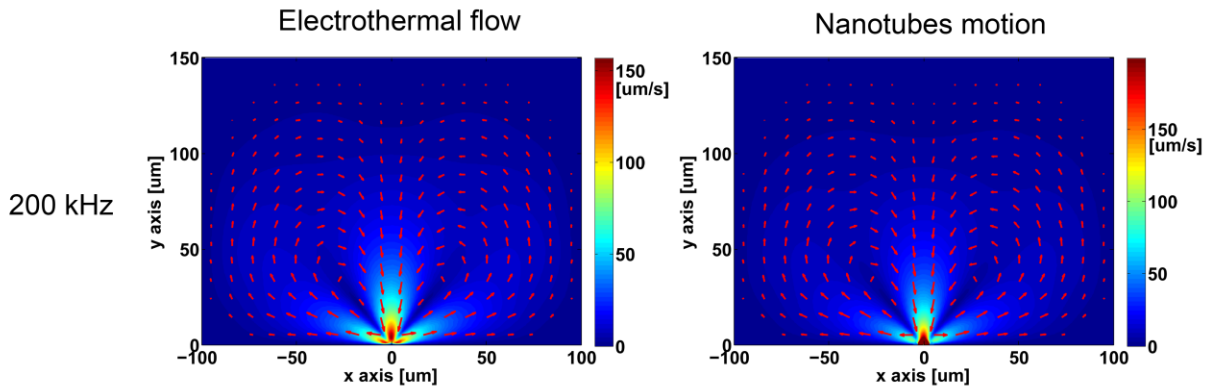


Fig. 4-5. Electrothermal flow and movement of the nanotubes in the solution with 1 wt% surfactant. The results at other frequencies are similar. The vectors are logarithmically related with the velocity at each point.

As a final note, the randomness in the deposition patterns caused by thermal agitations seems to be aggravated when a solution with a higher concentration of CNTs is used (see the right-hand side panel of Fig. 4-2). We believe this is due to the fact that, when a nanotube is deposited, it affects the electric field gradient in its surroundings significantly. This could result in a substantial change in the magnitude and direction of the DEP force acting on other, nearby nanotubes. Added to the thermal movements, this leads to inconsistent and pseudo-random results.

## 4.3 Summary

The change in the frequency of the applied voltage during DEP experiments affects the outcome differently for different nanotube solutions. For solutions with low conductivity, the change in the frequency affects the electrothermal flow direction and magnitude significantly and, more importantly, as the frequency increases, the DEP force becomes more concentrated in the immediate vicinity of the edges of the electrodes. This results in a sudden decrease in the number

of nanotubes which bridge the gap between the electrodes at higher frequencies. On the other hand, in the range of frequencies used in practice, changing the frequency does not affect the movement of the solution or the DEP force for solutions with high conductivities. The electrothermal force induces high-velocity movements in the body of the solution and creates a passage for the solution above the gap toward it. In the close proximity of the gap, the DEP force attracts the nanotubes and the combination of the DEP and electrothermal forces drive them toward the edges, which makes the nanotubes deposit on the edges rather than bridge the electrodes.

# Chapter 5: **The mutual interactions of CNTs during DEP**[4]

We showed that the solution properties and electrode shapes, among other parameters, significantly affect the DEP results. While the DEP force plays the major role in the close proximity of the gap between the electrodes, other forces such as the electrothermal force agitate the liquid environment and particularly alter the long range movement of the nanotubes and affect the deposition patterns for solutions with high conductivity. For aqueous solutions with no surfactant, the heat generated because of the current passing through the medium is considerably less than the previous case and, therefore, the electrothermal force is suppressed, leaving the DEP force as the dominant factor in the nanotubes' motion and deposition.

When low-conductivity solutions are used for making CNT devices on electrodes with a few tens of micrometers in width, the deposited nanotubes show a distinct periodic pattern (see figure 4 in [37] or figure 1 in [66]). This is especially more pronounced in cases where there is a considerable gap between the electrodes (see figure 2 in [26]).

Vijayaraghavan et al. stated that the deposition of a CNT on sharp electrodes results in a change in the DEP force around the electrodes from attraction to repulsion during the rest of the process [46]. While this may be the case for sharp electrodes, it cannot explain why the stripes in wide electrodes are made of multiple nanotubes; an opposite mechanism appears to be at play in this case.

---

[4] A version of this chapter has been published in a peer-reviewed journal (Reused with permission from "A. Kashefian Naieni, and A. Nojeh, 'The mutual interactions of carbon nanotubes during dielectrophoresis,' IEEE Transactions on Nanotechnology, vol. 15, p. 1068, 2013", Copyright 2013, IEEE).
Part of this chapter has been published as a conference paper (Reused with permission from "A. Kashefian Naieni, and A. Nojeh, 'Investigation of the dynamics of carbon nanotube deposition in dielectrophoresis,' IEEE 5th International Nanoelectronics Conference (INEC), pp. 52-55, 2013' Copyright 2013, IEEE).

There are two scenarios that can potentially explain the formation of nanotube stripes: the alteration of the electric field around the deposited nanotubes, and/or the alteration in the movement of the solution around the electrodes and the deposited CNT due to the change in the temperature profile because of the high current passing through the deposited nanotubes.

In this chapter, we reveal the mechanism of pattern formation due to the mutual interactions of nanotubes through a quasi-static study of the evolution of the device during the DEP deposition process from low-conductivity solutions. The results of this combined experimental-simulation study take us one step closer toward engineering the morphology of CNT based devices.

We first demonstrate the results of experiments using devices with different gap distances between the electrodes and different deposition times to investigate the described effect in more details. 3-D finite element simulations are used to elucidate the mechanism behind the deposition of nanotubes in striped patterns.

The experiments show a clear trend in the formation of the stripes from the very beginning of the process. Throughout the DEP experiments, the stripes attract more nanotubes and expand their width. These stripes have a periodicity, which depends on the geometry of the sample. The results of different scenarios for nanotube deposition are presented here. In each case, the DEP force, as well as the electrothermal motion of the CNTs, are calculated. The results show that, while the electrothermal force is greatly enhanced when there is a CNT bridging the two electrodes, the interaction between the suspended nanotubes and the electric field altered by the deposited nanotubes - even if the latter do not bridge the electrodes - plays the key role in the formation of the patterns.

## 5.1 Methodology

The CNT solution was prepared by diluting the solution from NanoLab Inc. with the final CNT concentration of 2.5 µg/ml.

Three different types of devices with 4, 8 and 20 µm gap between the opposing electrodes were used for the DEP experiments. The DEP experiments were performed by applying a potential difference with a frequency of 500 kHz to the electrodes while the sample was immersed about 3 mm deep in the solution. The applied voltages were chosen so as to maintain an applied electric field of 1 V/µm between the electrodes. After the deposition, the samples were rinsed with deionized water and blow-dried with nitrogen.

To capture the 3-D nature of the problem, and to be able to investigate the changes of the forces in different directions, 3-D finite element simulations were performed using COMSOL Multiphysics software package as explained in the second chapter. To briefly recap, because of the limitation on the total number of points that could be used for meshing due to the computationally expensive character of the 3-D simulations, the size of the structure needed to be small. A 16 x 20 x 10 $\mu m^3$ structure (x, y, and z directions, respectively) represented the solution and was placed over a pair of 70-nm-thick electrodes, which were 4 or 8 µm apart in the y direction. The substrate was represented by a 2-µm-thick silicon dioxide piece. The potential of the backside of this layer was set to emulate the potential of the highly doped part of the silicon wafer.

## 5.2 Results and discussion

To reach a clear understanding of the dynamics of deposition of nanotubes, a series of DEP experiments with time durations ranging between 15 seconds and 4 minutes were performed

using electrodes with 8 μm of gap between them. Fig. 5-1 shows the scanning electron microscopy (SEM) viewgraphs of the deposited nanotubes between the two electrodes. The results show a clear trend in the formation of CNT stripes from the very beginning. The stripes start to take shape even for the shortest experiment with a time of t = 15 sec. Since the gap between the two electrodes is almost twice as large as the length of the longest nanotubes suspended in the solution, the stripes can bridge only if two or more (often several) nanotubes connect in alignment with each other. For longer deposition times, the half bridging CNTs turn into fully bridging stripes, and from then on the stripes thicken until the whole gap is covered.

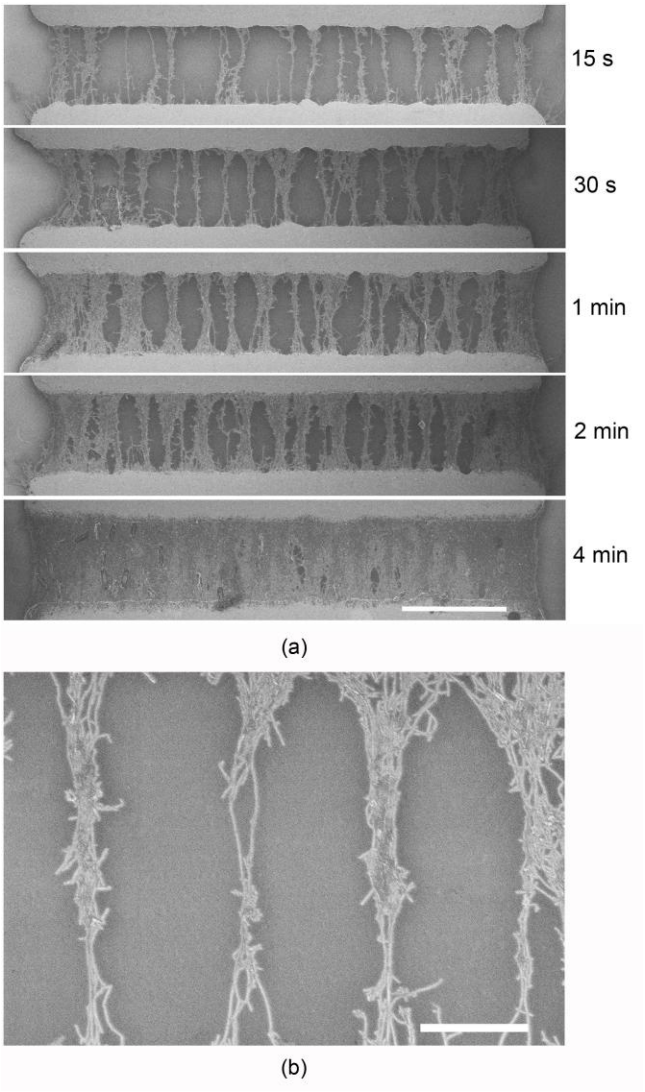


Fig. 5-1. (a) SEM images of the deposition patterns for different times. The gap between the electrodes is 8 μm. The scale bar is 10 μm. (b) Magnified view of the DEP result for t = 30 sec device. The scale bar is 2 μm.

The overall process of CNT deposition on the electrodes seems to start by the deposition of nanotubes on the edge of the electrodes. Other CNTs are then deposited in alignment with the previously deposited nanotubes to form bridges between the two electrodes. The stripes form parallel to each other. The number of stripes forming between the two electrodes and, therefore, the distance between them, seem to be almost equal for different experiments. Considering that

the results shown in Fig. 5-1 are from different devices, each used for DEP separately, the consistent trend observed means that the number of stripes shaped between the electrodes during DEP is not random and the results of the process are repeatable. Once the stripes are formed, other nanotubes are attracted toward them (especially toward the nanotubes-electrode contact region), and deposit on the edges of the stripes until they fill the gap.

The ratio of the area covered by the nanotubes to the surface between the two electrodes was investigated for the two repetitions of the experiments for different times using image processing and is presented in Fig. 5-2. The rate of coverage increases rapidly at the beginning but slows down as the time increases. The coverage varies by less than 10% between the two experiments for all time durations, except for the case of t = 15 sec, in which the stripes have not fully formed yet.

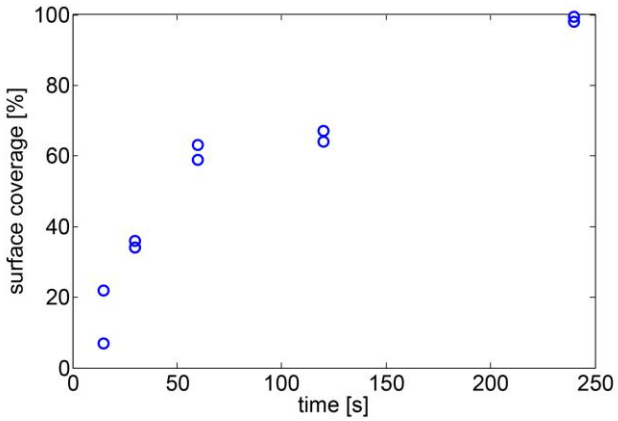


Fig. 5-2. Surface coverage ratio for different experiment times.

The results of the atomic force microscopy performed on the devices show a clear two dimensional expansion for the stripes: the nanotubes mostly deposit beside the stripes rather than creating stripes consisting of multi layers. In all cases, the maximum heights of the stripes are in the range of 15-20 nm, with variations of a few nm from device to device.

Similar experiments were performed with devices with 4 and 20 µm gaps. Fig. 5-3 shows the results when t = 4 min. The experiments were performed on two devices for each time setting. The results show good repeatability especially for devices with longer duration. For shorter times (15 and 30s) the stripes are not fully formed yet and the number of bridges between the electrodes can be different for different devices with the same experimental settings.

The randomness present in the devices made from solutions containing surfactants in the previous two chapters was considerably suppressed in the experimental results of this chapter. This led to a high yield for the fabrication process as mentioned above. This can be attributed to less agitation of the solution because of lower conductivity.

Although the overall look of the samples is the same and the CNTs create stripes during deposition, the gap between the stripes is different for devices with different gap distances. While the distance between adjacent stripes is in the range of 2.8 to 3.2 µm when the gap between the electrodes is 8 µm, it is in the range of 3.6 to 4 µm when the gap is 20 µm and less than 1.8 µm for 4 µm of gap. Also, the phenomenon is not as pronounced in 4-µm-gap devices as it is in devices with larger gaps. It seems that the periodicity of the stripes depends on the geometry of the sample.

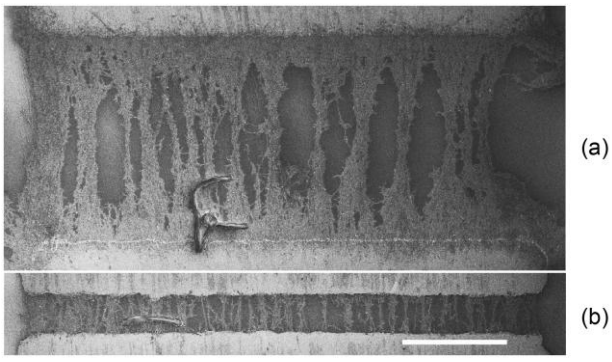


Fig. 5-3. SEM images of the deposition patterns using 4 minutes of deposition time and devices with (a) 20 µm and (b) 4 µm of gap. The scale bar is 10 µm.

To understand the various steps of the nanotube deposition process, finite element simulations were carried out for devices with 4 µm and 8 µm of gap for three cases: no nanotube, one nanotube half bridging, and one nanotube fully bridging the gap. In the second and third case, a rectangular prism with a 2 nm x 2 nm cross section was used to emulate the CNT bridging/half bridging the gap between the electrodes. For the case of a CNT half bridging the gap, the potential of the CNT was set equal to the potential of the electrode that it was connected to. When the CNT was connected to both of the electrodes, the potential of the rectangular prism surface was set to ground. This value was chosen based on a work by Chen et al. in which it is shown that the potential drop on a metallic nanotube bridging two electrodes happens primarily within 5 nm of the nanotube-metal junction at each side [67] and, therefore, almost the entire nanotube body is at the average potential of the two electrodes, which is zero in our case.

Fig. 5-4 shows the velocity of the nanotubes in the solution on an xy plane (parallel to the substrate surface), 400 nm above the substrate when no CNT has deposited yet. The gradient of the electric field is highest around the edges of the electrodes and therefore the CNTs are mainly attracted toward there at this stage.

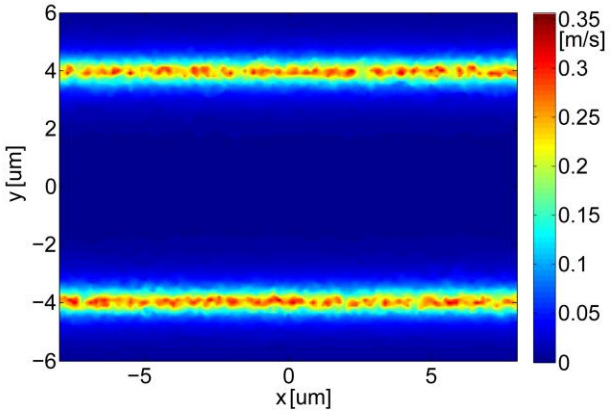


Fig. 5-4. Magnitude of the velocity of the nanotubes on a plane 400 nm above the substrate surface and parallel to it.

The velocity of the CNTs in the half-bridging nanotube situation in the same plane as in the previous figure is shown in Fig. 5-5. The nanotubes' motion is clearly affected by the presence of the deposited nanotube and the DEP force pushes the suspended nanotubes toward the tip of the deposited nanotube. This is due to the very high aspect ratio of the CNT, which considerably enhances the electric field on the tip, and results in a larger DEP force around it. This argument can explain why the half bridging nanotubes attract other nanotubes to deposit aligned and connected with them toward the opposite electrode.

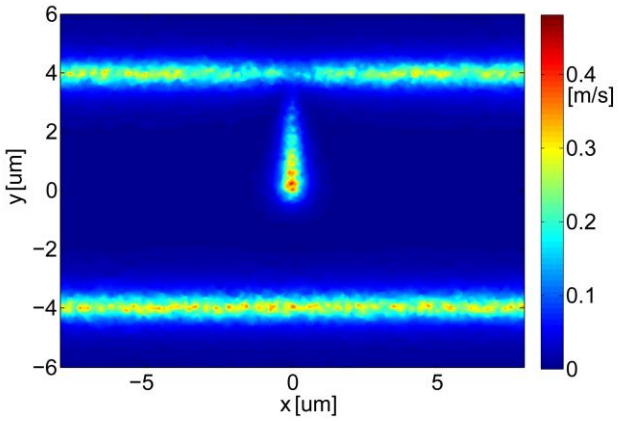


Fig. 5-5. Same as in Fig. 3, but in the presence of a deposited nanotube half-bridging the gap.

A detailed view of the velocity components for the case of a bridging nanotube is shown in Fig. 5-6. The x (parallel to the electrode edges) and z (vertical direction) components of the velocity of the nanotubes at two different heights from the surface of the substrate are presented. At 500 nm above the surface, the x component of the velocity pushes the suspended CNTs away from the deposited nanotube in the central regions of the gap. The z component is very low (compared to part d of the same image) at this height.

Fig. 5-6c and Fig. 5-6d show the velocity components 50 nm away from the substrate surface. The x component attracts the suspended CNTs toward the deposited nanotube especially near the edges; only in a very small region around the center of the gap is this force repulsive. The z component is strongly negative (toward the surface) in the close vicinity of the deposited CNT and pins the suspended CNTs in that region to the surface. As a result, the suspended nanotubes are attracted toward (especially the base of) the fully bridging deposited nanotubes and, once they are close to the edge of the latter, a very large DEP force makes them deposit. Thus, the combined effects of these two components explain the peculiar shape of the nanotube stripes and their thickening near the electrodes (see the experimental results of Fig. 5-1 and Fig. 5-3 for the shape of the stripes).

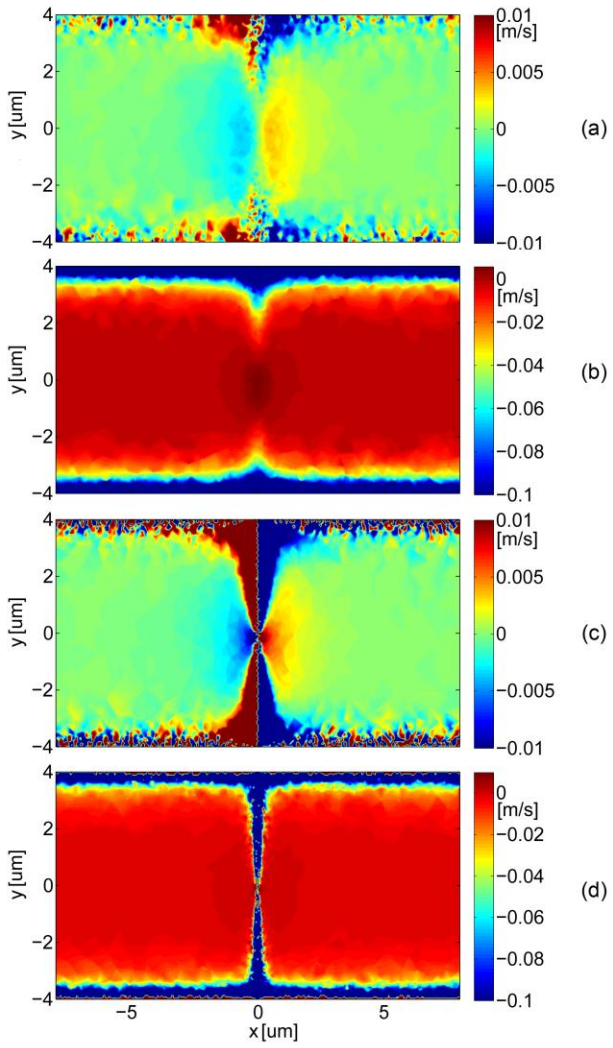


Fig. 5-6. Components of the velocity of the nanotubes in planes parallel to the substrate surface: (a) x, and (b) z components in the plane at a height of 500 nm above the surface; (c) x, and (d) z components in a plane 50 nm high.

Similar simulations were performed for devices with 4 µm of gap between the two electrodes. A particular case with three nanotubes deposited at a distance of 2 µm from each other was simulated for the 4-µm-gap device as well. Simulating an equivalent structure with a larger gap was not possible due to the computational limitations. The velocity components of the CNTs on a plane 50 nm above the substrate and parallel to it are shown in Fig. 5-7. Again the nanotubes

are attracted toward the base of the deposited CNTs. It should be noted that the x-component of the force around the middle of the gap is more repulsive compared to the area around the nanotube- electrode connection. The shorter nanotubes feel the force as shown in the figure, but the longer nanotubes align themselves with the field prior to deposition and experience an average force, which is determined by the electric field and solution motion along their entire lengths. The diamond-shaped regions seen in Fig. 5-7 bear a striking resemblance to the empty regions in-between the nanotube stripes seen in the experimental results shown in Fig. 5-1 and Fig. 5-3, a confirmation that the simulations are, indeed, capturing the mechanism behind the pattern formation process.

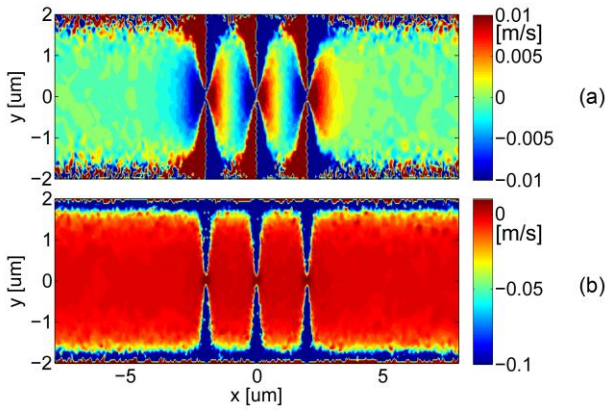


Fig. 5-7. Components of the velocity of the nanotubes in a plane parallel to the substrate surface and 50 nm above it in the case with three CNTs already deposited: (a) x, and (b) z components.

Fig. 5-8 shows the x velocity component of the nanotubes due to the DEP force on a line parallel to the edges of the electrodes in the middle of the device at a height of 500 nm from the surface for both the 4-µm- and 8-µm-gap devices. It can be seen that the extent for which the CNTs are pushed away for the latter device is almost double that for the former. This can explain the difference in the distance between the stripes in these two devices.

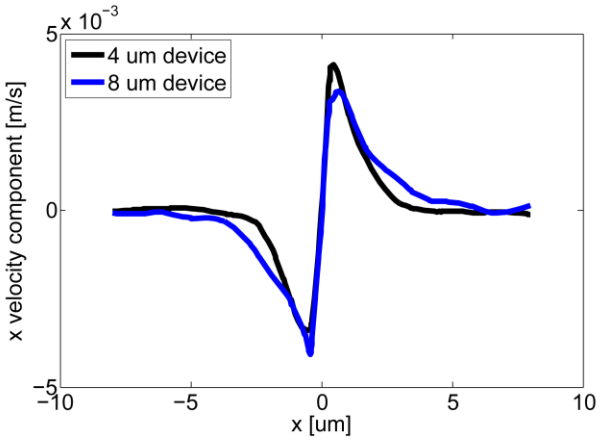


Fig. 5-8. The x component of the velocity for 4-µm- and 8-µm-gap devices on a line parallel to the edges of the electrodes in the middle of the gap at a height of 500 nm above the substrate surface.

We have previously demonstrated that the solution motion caused by inhomogeneities induced by the non-uniform temperature profile –especially the movement of the solution because of electrothermal force– can be a substantial factor in the deposition pattern of nanotube devices made using DEP. This effect is more pronounced when the solution is made using surfactants and has a high conductivity, whereas in low-conductivity solutions it is minimal due to the small change in the temperature profile because of the small amount of heat generated by Joule heating in the solution. Although the solution used in the experiments reported here had low conductivity, the electrothermal force could be significant in the case of a nanotube bridging the two electrodes. The high current passing through the CNT, plus the defect prone structure of solution processed nanotubes, can potentially lead to the generation of non-negligible amounts of heat and a high temperature gradient during the DEP experiment. To examine this possibility, an estimate of the temperature of the bridging CNT was needed.

The temperature of a CNT on a substrate conducting current was estimated by Pop et al. [68]. They showed that, for the largest part of the CNT structure on the surface, the temperature difference could be obtained from p/g, where p is the Joule heating rate per unit length and g is the net heat loss rate to the substrate per unit length. It was stated that g depends primarily on the interface and not on the thermal conductivity of the substrate. In order to obtain a rough estimate of the temperature of a nanotube conducting current in a solution, we assumed the heat loss rate to be double the case when the CNT is in air. The total resistance of a device containing a single CNT between the two electrodes without any post-deposition treatment was measured to be around 5 MΩ. The average resistivity of a solution processed metallic CNT per μm of length is estimated to be 200±10 kΩ [69]. p is equal to the square of current times the resistance per unit length. The current itself can be calculated by the division of the rms value of the voltage over the total resistance. The resulting temperature change was found to be around 0.18 K.

Fig. 5-9 shows the temperature profile and the electrothermal motion in the solution with and without a nanotube bridging the two electrodes. Although the change in the temperature because of the presence of the conducting CNT considerably increases the electrothermal motion of the solution (the maximum increases from less than one to more than forty micrometers per second on the plane of Fig. 5-9), this force is still negligible compared to the DEP force that the nanotubes experience (the maximum of DEP velocity is around 1.5 mm/s on the same plane), as seen by comparison with the velocity values shown in Fig. 5-4 to Fig. 5-7, which are primarily due to DEP. (It should be noted that all of the simulation results include both the DEP and the electrothermal induced movement of the nanotubes in the solution but, as discussed, the main driving force is DEP).

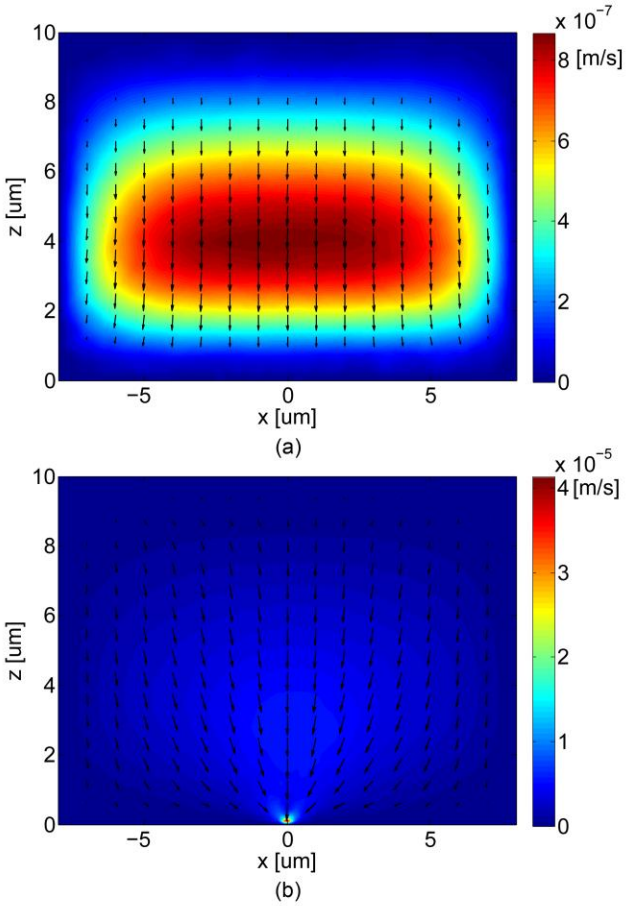


Fig. 5-9. Solution velocity due to the electrothermal force in a vertical plane in the middle of the two electrodes: (a) no CNT deposited, and (b) one CNT bridging.

## 5.3 Summary

In summary, CNTs form stripes during DEP deposition on wide electrodes due to changes in the electric field pattern because of the already deposited nanotubes. The process starts by the deposition of a few nanotubes on the edges of the electrodes. The DEP force is considerably enhanced around the tip of half bridging nanotubes and, therefore, other nanotubes are attracted and deposited in alignment and connection with them. The CNT bridges between the two electrodes push most of the suspended ones away laterally. On the other hand, a downward force

pushes the suspended CNTs toward a bridging nanotube if they are close enough to it. The result of these interactions is the formation of stripes of nanotubes between the two electrodes. This effect is more pronounced for devices with larger gap distances.

The DEP force plays the dominant role in CNT pattern formation and the thermal-induced solution movement does not affect the final results for low conductivity solutions, even when a CNT conducts current and warms up as a result of Joule heating. In such a case, the electrothermal agitation increases considerably compared to the situation where there is no connection between the opposite electrodes, but still cannot take away from the dominance of the DEP.

# Chapter 6: **A step by step evaluation of the forces affecting the movement of carbon nanotubes in the solution during dielectrophoresis**

In this chapter, a particle tracing approach is used to follow the path of carbon nanotubes (CNTs) from suspension in the solution to deposition on the substrate surface, taking into account several influential factors: the DEP force, the movement of the solution itself, and the Brownian movement of the CNTs.

We previously investigated the interaction of metallic nanotubes suspended in a low-conductivity solution with those already deposited on the substrate, through the changes the latter create in the DEP force field. The corresponding pattern formation process was studied using experiments and finite-element simulations. However, in order to evaluate the degree of involvement of the various forces in different stages of the deposition–from having the CNTs suspended in the solution to their transfer toward the electrodes and finally their deposition–is only possible if we can track the CNTs throughout these steps. Moreover, the Brownian motion of the particles can be taken into account using this approach. Such a particle-tracing study forms the basis of the work presented in this chapter.

Particle tracing was used by Dimaki and Boggild in order to find the probability of CNTs being captured by a set of microelectrodes in a microliquid channel for different fluid velocities [70]. They considered the DEP force as well as the Brownian motion of the nanotubes in isopropanol and in a 1-weight-percent aqueous solution of SDS. While DEP is the dominant force in low-conductivity solutions, in the high-conductivity SDS aqueous solution other hydrodynamic forces such as the electrothermal force, which were neglected in this study, can stir up the solution and hinder the effect of the DEP force.

Lu et al. investigated the influence of electrode type (parallel and comb-shaped electrodes) on the movement of nanotube bundles suspended in isopropanol using a similar approach [71]. The properties of the bundles were considered to be close to metallic CNTs due to their much higher conductivity and permittivity compared to semiconducting nanotubes. They also showed that the final distribution of the nanotubes on the surface is less affected by thermal fluctuations under higher applied voltages.

We use a dynamic step-by-step tracing approach to follow the nanotubes in their journey from the solution to the substrate in low- and high-conductivity solutions considering DEP, electrothermal and Brownian forces. The relative strength of each depends on the type of nanotube, conductivity of the solution, and the changes in the electric field by the previously deposited nanotubes. In order to find out exactly how the nanotubes move toward the substrate and the main forces at play at each step, the movement path of randomly distributed semiconducting and metallic nanotubes and their final deposition pattern was investigated for three different cases: no nanotube deposited, one nanotube connected to one of the electrodes, and finally one nanotube bridging the two electrodes. The simulated results show that for the low-conductivity solution, while DEP is the dominant force for the metallic nanotubes, for semiconducting nanotubes the Brownian motion has a pronounced role and makes the deposition outcome much more unpredictable compared to when metallic nanotubes are used. When surfactants are used to suspend CNTs, the long-range movement of the nanotubes is affected mainly by the electrothermal force and the resulting circular agitation of the solution; the DEP force captures the metallic nanotubes only once they are sufficiently close to the electrodes. For semiconducting nanotubes the DEP force is not as strong and, therefore, these CNTs do not deposit as effectively as the metallic ones.

## 6.1 Methdology

As discussed earlier, Langevin equation describes the movement of a particle suspended in a fluid influenced by a deterministic force such as DEP. The non-deterministic forces such as the Brownian can also be added to the equation.

$$m\frac{d\vec{u}_{CNT}}{dt} = \vec{F}_{DEP} + \vec{F}_{Brownian} - f(\vec{u}_{CNT} - \vec{u}) \qquad \text{Eq. 6-1}$$

The stochastic nature of the Brownian force makes solving this differential equation analytically impossible. A numerical step-by-step approach was thus taken to track the path of the particles in the solution. The random Brownian force was added at each step.

In order to investigate the nanotube paths and their final deposition location, the DEP force and the velocity of the solution are needed. An approach similar to the previous chapter was taken to calculate the DEP and also electrothermal velocity fields. A structure with 4 μm gap between the electrodes was used. The frequency of the applied electric field was 500 kHz and the potentials of the electrodes were chosen so as to lead to an electric field of 1 V/μm.

The values used as the length and radius of the nanotubes were 1 μm and 1 nm, respectively. The metallic nanotubes have very high conductivities and permittivities; the values used in simulations for this type of nanotube have been $10^3$ S/m for the conductivity and $10^4$ for the relative permittivity [44], [72]. Semiconducting nanotubes, on the other hand, have much smaller conductivities. Semiconductors are insulating at zero temperature but show limited conductivity at higher temperatures due to the thermally excited carriers as well as dopings. Both the permittivity and conductivity decrease at higher frequencies. Benedict et al. reported a static relative permittivity of 2 to 5 for semiconducting nanotubes [73]. The estimated conductivity of semiconducting CNTs in surfactant solutions is 0.35 S/m [30]. While both of these values are

probably an overestimation for semiconducting nanotubes moving under the influence of an alternating electric field in a surfactant-free solution, as will be seen, the resulting DEP force is still weak compared to other forces that affect the semiconducting nanotubes in various cases.

A CNT velocity grid with a resolution of 0.1 μm was made using the extracted results from COMSOL. The solution velocity and also the velocity of the nanotubes as a result of the DEP force in x, y and z directions were estimated at each grid point and added up to find the total velocity vector of CNTs. 750 random initial positions were chosen and the nanotubes' movement was followed using the velocity grid by multiplying the velocity components in each direction with the time step. The default value of the time step was set to 10 ms. At each step the total displacement of each nanotube was compared to 0.2 μm. If larger, the time step for that step was reduced accordingly and the displacement in that step was calculated again to avoid unrealistic jumps on the nanotube path.

The movement of the particles as a result of the Brownian force has a random behavior with an average displacement of zero. The probability distribution of the particle position after time t can be described by a normal function with a standard deviation of $\sqrt{2Dt}$ in each direction. D is called the diffusion constant and is given by $D = kT/f$, k denotes the Boltzmann constant and T is temperature [18]. Accordingly, at each step of the simulation of the particle movement, a random number with a normal distribution was added to the nanotube displacement in each direction to account for the Brownian effect.

For each initial location, the program traced the nanotube until it was deposited on the substrate or a maximum tracing time of 60 seconds was reached. The code is attached in the Appendix.

## 6.2 Results and discussion

Fig. 6-1 shows the general movement pattern due to each of the DEP and electrothermal forces in the y-z plane (perpendicular to the electrodes). It should be noted that while the DEP force affects the nanotubes directly, the electrothermal force creates movement in the solution and as a result affects the nanotubes indirectly. In different scenarios the strength of each of these two forces is different but the overall pattern stays the same: the DEP force is strongest on the edges of the electrodes and quickly drops in strength with distance from the edges of the electrodes, whereas the electrothermal force induces a circular pattern of motion in a large portion of the solution.

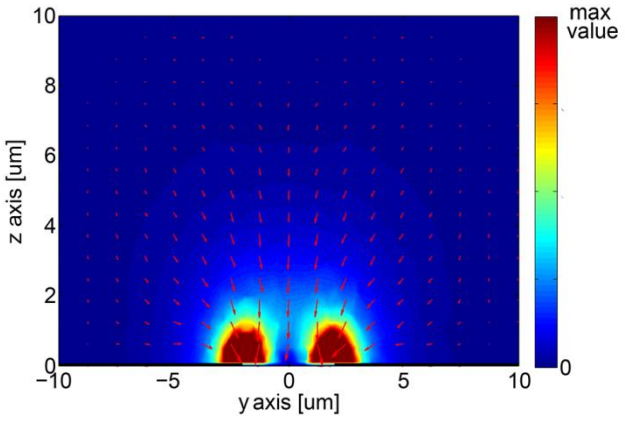


(a)

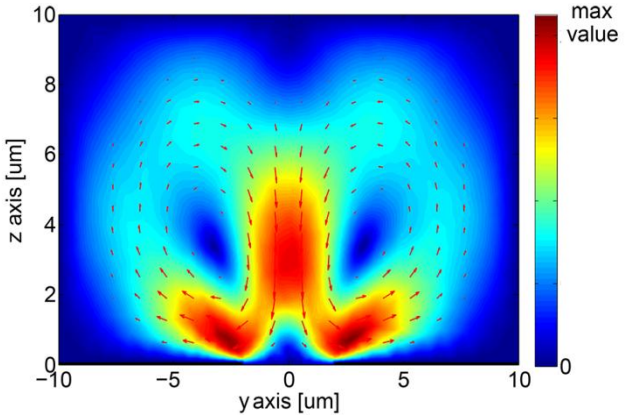


(b)

Fig. 6-1. The overall pattern of movement as a result of (a) DEP, and (b) electrothermal forces. The vectors are logarithmically related with the magnitude of the velocity at each point. The gap between the electrodes is between -2 to 2 μm on the y axis.

The results of the particle-tracing simulations for the low-conductivity solution will be discussed first. Fig. 6-2a shows the path of the metallic nanotubes moving toward the electrodes when there is no nanotube deposited previously. The movement of the nanotubes toward the edges in a pattern similar to Fig. 6-1a shows that DEP is strong enough to hinder the effect of the electrothermal force. The Brownian force creates small perturbations in the path of the nanotubes toward the electrodes but is of no serious consequence in the movement of the metallic CNTs;

they follow the field gradient until they deposit on or near the edges of the two electrodes. The percentage of deposited nanotubes (CNTs which ended up in the gap or on the electrodes within 0.5 μm of the electrode edge, on the z=0 plane) in this case is more than 91%. The dots in Fig. 6-2b represent the location of the deposition of the center of the CNTs. The majority of the metallic CNTs deposit on or around the edges where the DEP force has its maximum.

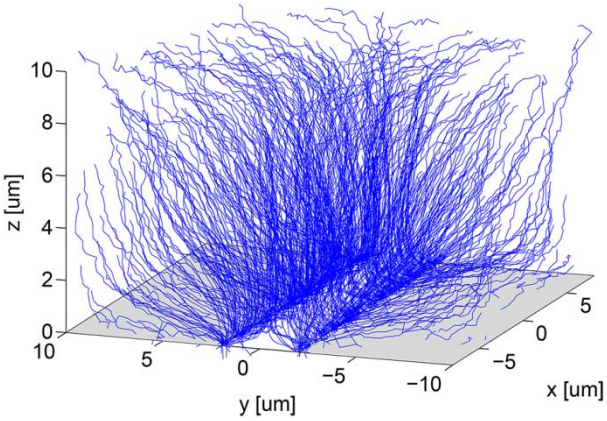


(a)

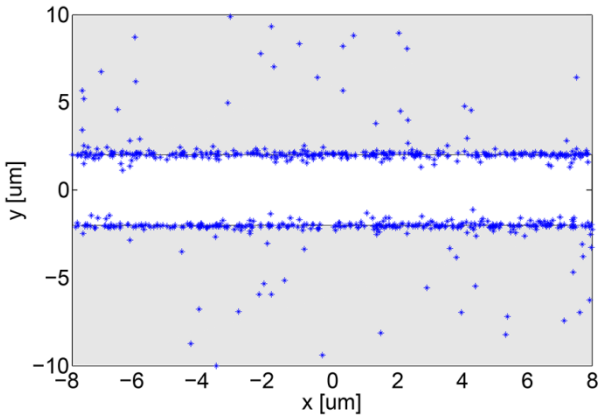


(b)

Fig. 6-2. (a) Metallic nanotubes' paths during DEP in a low-conductivity solution; (b) deposition locations on the z=0 plane. The dots show the centers of the deposited CNTs.

Because of their extremely high-aspect-ratio structure, CNTs enhance the electric field considerably. A common situation during the deposition of the nanotubes is when a nanotube is deposited on one of the electrodes, but is not long enough to reach the second one. In such a case the electric field and the DEP force become considerably enhanced around the CNT tip. As it was shown earlier, the DEP force is the main contributor in the movement of metallic nanotubes in low-conductivity solutions. The particle tracing simulation results show that CNTs are attracted toward the tip of the half-bridging nanotube and it is likely to have a bridge between the electrodes made of more than one nanotube due to this effect (Fig. 6-3a).

When a CNT is connecting the two electrodes, the electric field profile changes around that nanotube. We have shown that this change can alter the DEP force profile in the previous chapter. The DEP force attracts those CNTs that are very close to the deposited nanotube especially toward the junction between the CNT and the electrodes, but repels the rest from the vicinity of the deposited nanotube. Another effect of having a fully bridging nanotube is the change in the temperature profile around it. Joule heating resulting from the current passing through the CNT warms up the nanotube and, therefore, increases the electrothermal force, which is proportional to the temperature gradient. Fig. 6-3b shows the result of the particle tracing simulation when a CNT is fully bridging. The deposition locations show that a few CNTs are attracted toward the CNT-electrode junction, which is where the DEP force guides them. Therefore, although the electrothermal force is enhanced because of Joule heating, the DEP force still has the main influence over the metallic nanotubes in low-conductivity solutions in all situations.

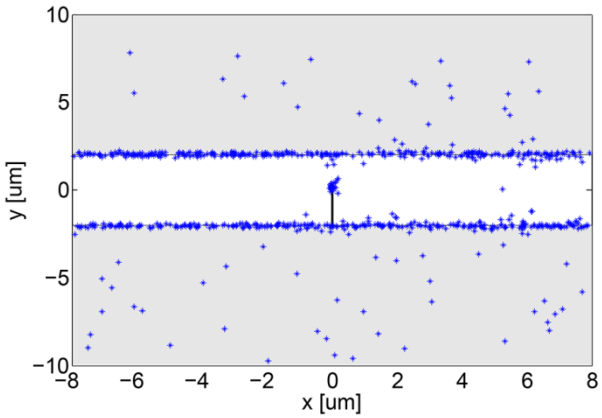


(a)

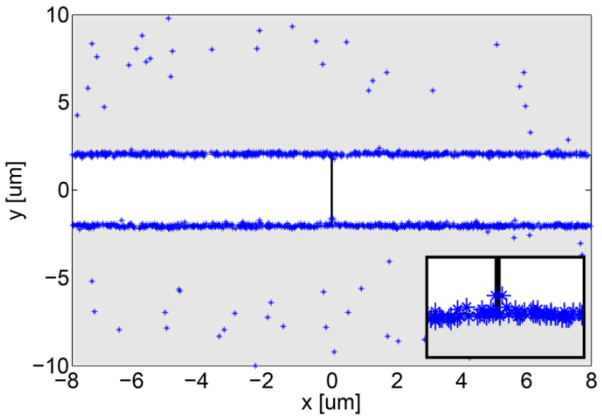


(b)

Fig. 6-3. The deposition pattern of metallic nanotubes in a low-conductivity solution when there is a CNT (a) half bridging, (b) fully bridging the two electrodes, the inset shows a magnified view of the electrode-nanotube junction.

The electrothermal and Brownian forces, which affect the semiconducting nanotubes in low-conductivity solutions, are similar in strength to those acting on metallic nanotubes, but the DEP force is not the same and is directly affected by their much lower conductivity and permittivity, which result in the lower CM factor. Fig. 6-4a demonstrates the path of the semiconducting nanotubes during the experiment. A high level of randomness is seen. The path of the CNTs that

ended up depositing on the gap between the electrodes is shown in red. Only the nanotubes very close to the gap have a chance of depositing and connecting to the electrodes. The deposition locations shown in Fig. 6-4b depict an almost uniform distribution with the exception of the edges, which have a slightly higher concentration. The total number of deposited nanotubes on or near the gap is 31% of the initial number of CNTs.

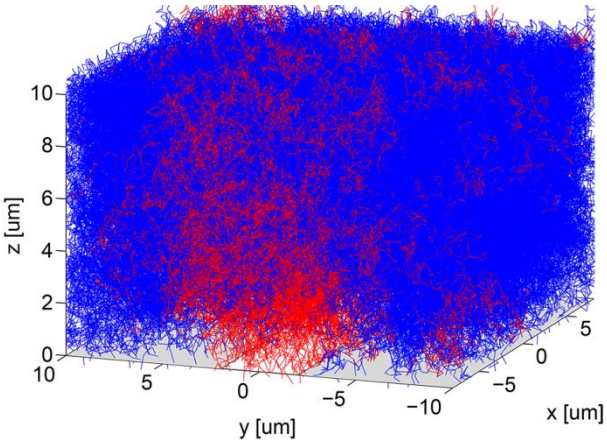


(a)

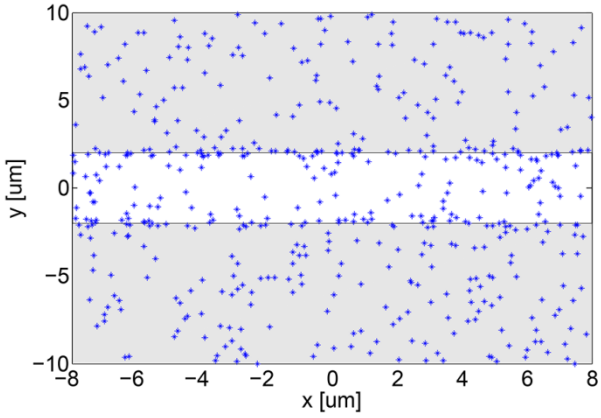


(b)

Fig. 6-4. (a) Semiconducting nanotubes' paths during DEP in a low-conductivity solution, the paths of the CNTs deposited on the gap are shown in red; (b) deposition locations on the z=0 plane. The dots show the centers of the deposited CNTs.

Fig. 6-5a shows the location of semiconducting nanotubes after DEP when there is a half-bridging nanotube on the surface. The overall random distribution is very similar to the previous case. A few nanotubes deposit around the tip of the previously deposited CNT. Fig. 6-5b shows the results when a CNT is fully bridging. The change in the deposition morphology is not as pronounced as in the case of metallic nanotubes. In general, for semiconducting nanotubes in low-conductivity solutions, the Brownian force is of more significance compared to the other two forces. The DEP plays a role when the CNTs are very close to the edges of the electrodes, and the electrothermal force is almost of no consequence.

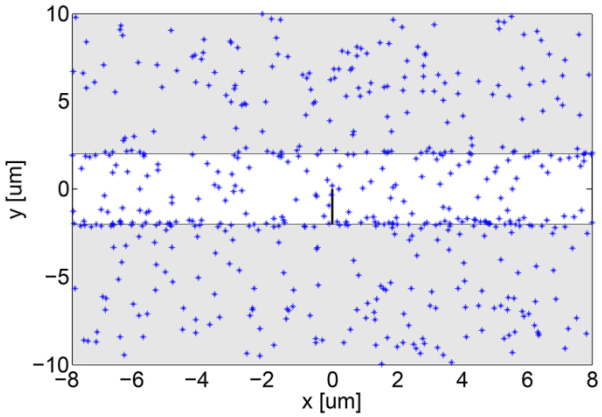


(a)

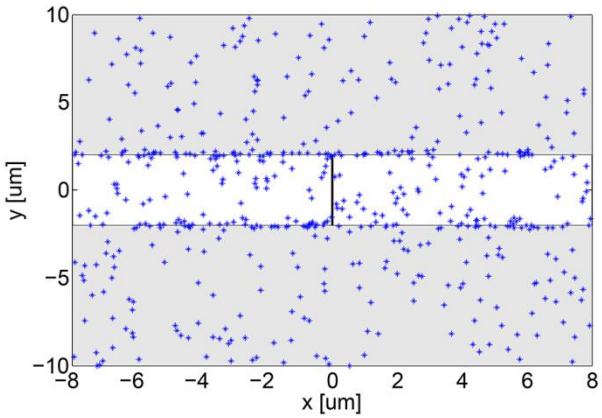


(b)

Fig. 6-5. The deposition pattern of semiconducting nanotubes in a low-conductivity solution when there is a CNT (a) half bridging, (b) fully bridging the two electrodes.

Solutions in which ionic surfactants have been used to help in separation and suspension of intrinsically hydrophobic nanotubes, have much higher conductivities. The higher electrical current during DEP causes the solution to heat up locally, which results in increased electrothermal motion. When no nanotube has yet deposited on the surface, the maximum of the velocity due to the electrothermal force in the solution increases from 0.2 μm/s for the low-conductivity solution to 60 μm/s for the high-conductivity one. Moreover, the higher conductivity of the surrounding medium lowers the CM factor and thus the DEP force compared to the previous case.

As shown in Fig. 6-6, in high-conductivity solutions the long-range movement of the nanotubes is mainly governed by the movement of the solution because of the electrothermal force, which follows a circular pattern. The electrothermal force moves the solution toward the region above the gap and then directly toward the gap, in a direction perpendicular to the plane of the substrate. The down-coming stream then splits into two diverging branches near the surface over the gap, each branch flowing over one of the electrodes. The CNTs initially move with the solution in this pattern toward the gap. Once the metallic nanotubes are close to the surface, the locally strong DEP force makes them deposit. The percentage of the deposited nanotubes on and around the gap is 90%.

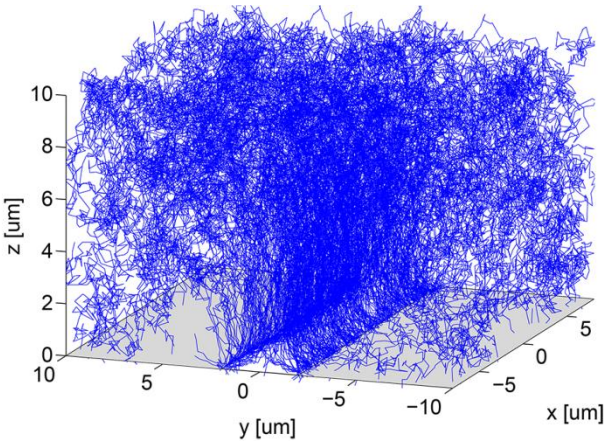


(a)

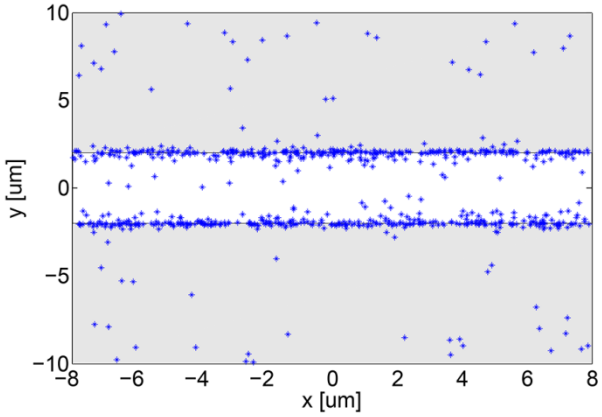


(b)

Fig. 6-6. (a) Metallic nanotubes' paths during DEP in a high-conductivity solution, (b) deposition locations on the z=0 plane. The dots show the centers of the deposited CNTs.

When a CNT is half-bridging the electrodes during a DEP experiment using a high-conductivity solution, other nanotubes deposit close to its tip. Due to the agitation of the solution, the CNTs drawn toward the tip become deposited not only on the very tip but also the area around it as shown in Fig. 6-7a. Fig. 6-7b shows the final locations of the CNTs for a fully bridging situation. Nanotubes are attracted toward the base of the deposited nanotube but are otherwise repelled from it. Even though the CNTs are brought toward the edges by the electrothermal force everywhere, the DEP force dictates the final morphology – which is attraction toward the edges,

especially the nanotube-electrode junction, and repulsion from the area around the deposited nanotube (see figure 4 in [37]) – on the surface because of its local strength in the close proximity of the electrodes. This can explain why often CNTs are separated with some distance from each other when deposited using DEP even in high-conductivity solutions.

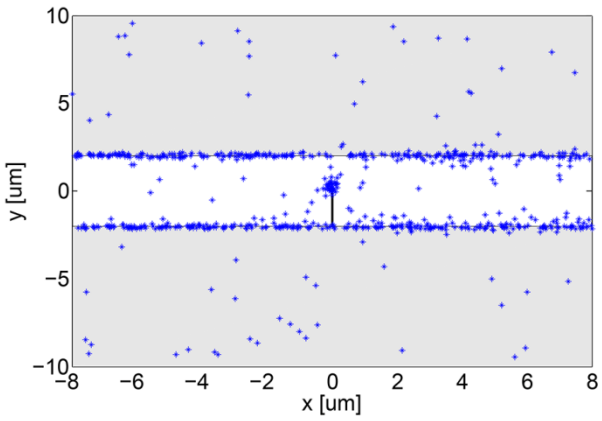


(a)

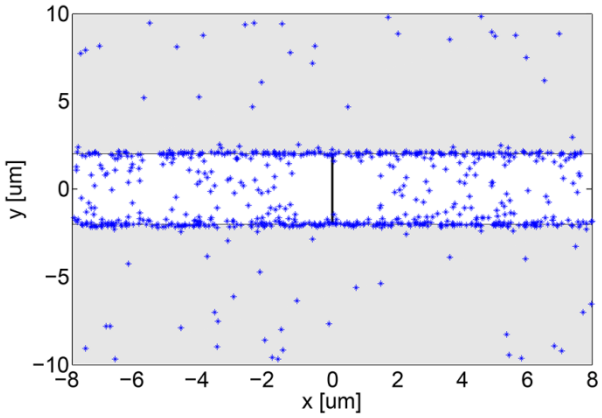


(b)

Fig. 6-7. The deposition pattern of metallic nanotubes in a high-conductivity solution when there is a CNT (a) half bridging, (b) fully bridging the two electrodes.

The electrothermal motion plays an important role in how the semiconducting nanotubes are manipulated during DEP using a high-conductivity solution. Contrary to the situation with metallic nanotubes, in this case the DEP force is not strong enough to be able to prevent them

from spinning with the solution, at least until they reach the region very close to the surface. Fig. 6-8a shows the path of the nanotubes in the solution. A closer look at the movement of 8 nanotubes chosen randomly out of the initial 750 nanotubes shows that the nanotubes undergo a circular movement in the solution because of the electrothermal flow. The small DEP force is not able to capture the CNTs the first time they approach the electrodes. Semiconducting nanotubes thus keep rotating until they are deposited on one of the electrodes (rather than on the gap between the electrodes) or are finally captured by the weak DEP force. 49% of the starting nanotubes deposit on or around the gap, which is higher than the percentage of the similar type of nanotubes in the low-conductivity solution. This is due to the rotating motion of the solution, which provides more opportunities for the semiconducting nanotubes to reach the substrate, gap or electrodes and eventually be captured.

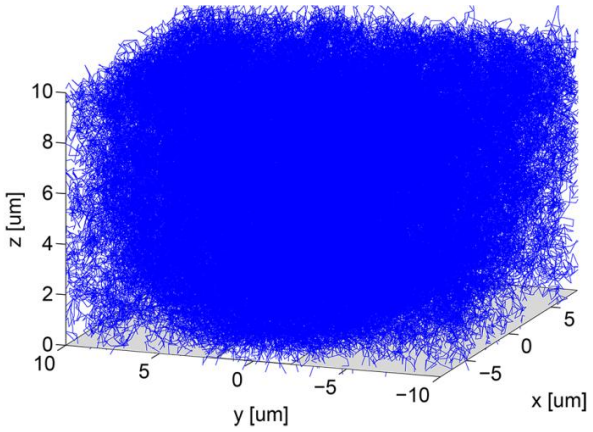


(a)

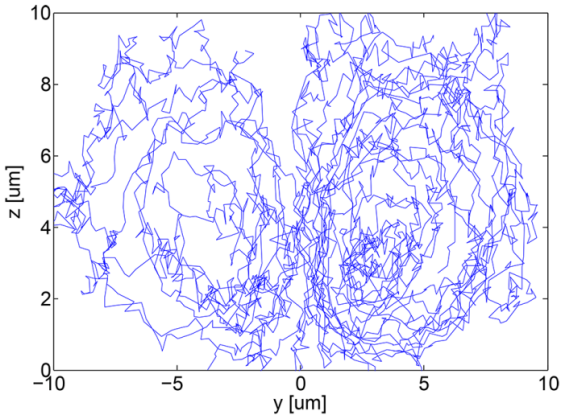


(b)

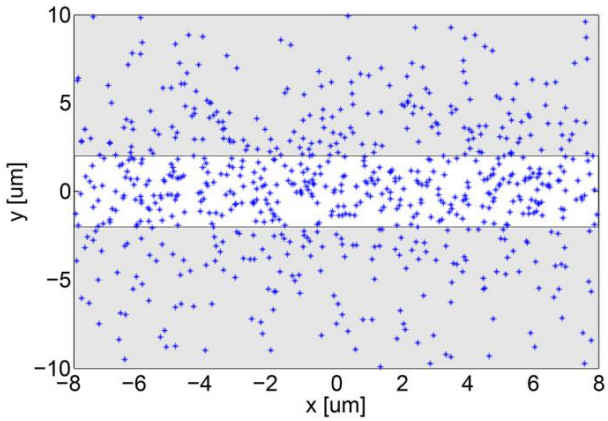


(c)

Fig. 6-8. (a) Semiconducting nanotubes' paths during DEP in a high-conductivity solution, (b) path of 8 randomly chosen nanotubes, (c) deposition locations on the z=0 plane. The dots show the centers of the deposited CNTs.

The DEP force on the semiconducting nanotubes is so small that even the higher field gradient due to the presence of a half-bridging nanotube does not change the deposition pattern appreciably. This is also true for the case of a fully bridging nanotube.

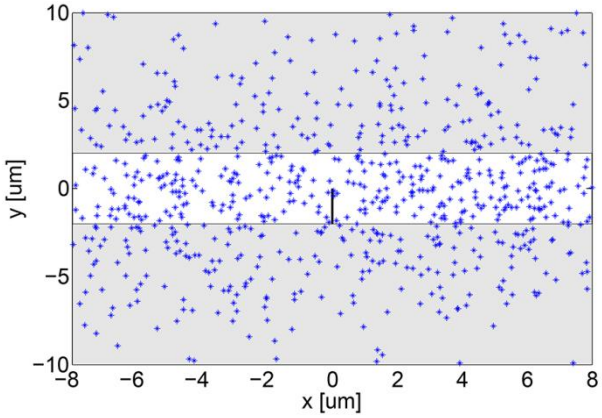


(a)

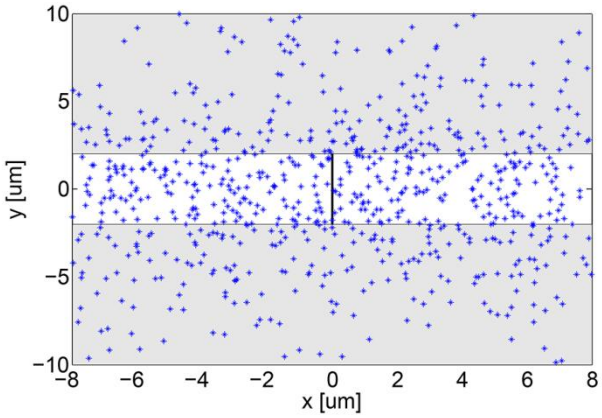


(b)

Fig. 6-9. The deposition pattern of semiconducting nanotubes in a high-conductivity solution when there is a CNT (a) half bridging, (b) fully bridging the two electrodes.

The following figure shows a summary of the effective forces during DEP experiments in various scenarios. As it is seen from this chart, the electrothermal force and Brownian motion of solution are not only not negligible in certain cases, but are of primary importance in moving the nanotubes in the solution.

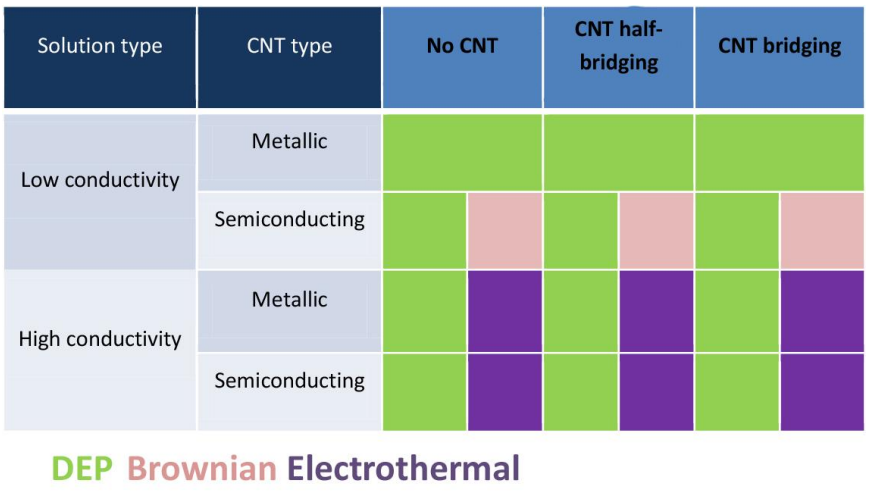


Fig. 6-10. The effective forces during DEP in different scenarios.

It is noteworthy that, while the DEP and electrothermal forces both depend on frequency, for the typical range of frequencies used in the DEP deposition of CNTs (up to a few MHz), the overall behavior in the different scenarios discussed here remains the same.

## 6.3 Summary

The effect of the forces dictating the movement of CNTs in the solution during DEP experiments was investigated using a step-by-step particle-tracing approach. It was shown that the electrothermal force acting on the solution and the Brownian force acting on the nanotubes can play an important, even critical role in the movement and deposition of nanotubes. Depending on the type of the CNT, DEP parameters and solution properties, the extent of effectiveness of these forces is different.

While for the metallic CNTs in a low-conductivity solution, the DEP force has the upper hand over electrothermal force, which agitates the solution, and the Brownian motion, which moves the nanotubes at random, in a high-conductivity solution, the electrothermal force dictates the

long-range circular movement of the nanotubes until they are captured by the DEP force. An already-deposited half-bridging nanotube increases the field gradient and results in the deposition of nanotubes in alignment with it no matter the conductivity of the solution. A fully-bridging nanotube also changes the electric field pattern and affects the final CNT deposition pattern.

Semiconducting nanotubes have a lower chance of deposition compared to metallic ones due to the lower DEP field. The small magnitude of the DEP force allows the Brownian force in low-conductivity solutions, and the electrothermal force in high-conductivity solutions, to be of primary importance during the DEP of semiconducting nanotubes.

In summary, forces other than DEP cannot be neglected in the deposition of particles using the DEP method. Understanding the interplay between them in different cases can help us engineer the DEP process more effectively in order to obtain a higher deposition yield with the desired morphology of particles on the substrate.

# Chapter 7: **Summary, conclusion and future work**

In this thesis, a combined experimental and numerical simulation study on evaluating the effect of various parameters in the DEP deposition of CNTs was presented. The DEP force, the hydrodynamic movement of the solution and the Brownian motion of the suspended CNTs, as well as the interplay among them in different stages of the transport of nanotubes from the solution to the substrate, were investigated. A summary of the contributions as well as some suggestions for future works are given in this chapter.

## 7.1 Contributions

1. In chapter 3, we showed that the effect of electrokinetic movement of the solution during DEP of nanotubes can be of significance depending on the physical properties of the solution. We investigated the effect of this movement in solutions with various levels of conductivity through experiments as well as numerical modeling. Our results showed that electrothermal motion in the solution can alter the deposition pattern of the nanotubes drastically for high-conductivity solutions, while DEP remains the dominant force when a low-conductivity (surfactant-free) solution is used. The extent of effectiveness of each force was discussed in the various cases and the fluid movement model was investigated using two- and three-dimensional finite-element simulations.
2. In chapter 4, we took our efforts on unveiling the effect of solution properties on the CNT deposition pattern through DEP one step further, and characterized the effective forces at different frequencies. The forces that induce movement in the solution, as well as the dielectrophoresis force, all vary with frequency in different manners. Experiments and simulations were used to investigate the interplay between the solution conductivity and

the frequency of the applied voltage, and their effects on the deposition patterns. We demonstrated that changes in the frequency affect solutions with different physical properties differently: while the frequency directly influences the number of deposited carbon nanotubes when using solutions with low conductivity, it is almost of no consequence in the case of solutions that include surfactants and thus have a higher conductivity.

3. In chapter 5, we discussed the results of experiments that showed that the interactions among deposited and suspended nanotubes during the deposition process can considerably affect the dynamics and the final results of the deposition. Semi-periodic stripes of nanotubes bridging the two electrodes were formed from solutions containing no surfactant. The periodicity of the patterns depended on the geometry of the electrodes. The devices made using the low conductivity solution showed much better repeatability compared to the devices produced in the previous chapters. Finite-element method simulations were used to explain the mechanisms underlying the observed experimental outcomes. The pattern formation mechanism was shown to be related to the mutual effects of CNTs on each other during the experiment. The reason lies behind the changes in the electric field as a result of the deposition of CNTs. These changes directly alter the DEP force field and, therefore, the way the CNTs are guided. The extent of effectiveness of the electrothermal force was also investigated, and it was shown that, although in some situations the heat generated by the current passing through the nanotubes considerably increases this force, the DEP force remains dominant when a surfactant-free solution is used.

4. In chapter 6, a framework for evaluating all the considerable forces during various steps of DEP was developed. The mechanisms involved in the deposition of metallic and semiconducting nanotubes, as well as the extent of effectiveness of each force in various scenarios during deposition, were explored using particle tracing simulations. We showed that the Brownian and electrothermal forces are by no means negligible in many cases and, in fact, can be of primary importance in the final results. While the DEP force constitutes the main cause of movement for metallic nanotubes in low-conductivity solutions, the Brownian movement has the upper hand for semiconducting nanotubes. For high-conductivity solutions, the electrothermal movement of the solution determines the long-range movement of the nanotubes toward the electrodes.

Although DEP has many advantages for the deposition of micro/nano objects such as CNTs, there are many parameters that must be considered in order to fabricate devices in a controlled and repeatable fashion. This thesis is a step toward engineering the DEP process. Our results suggest that not only the parameters directly affecting the DEP force, *e.g.* voltage amplitude and deposition time, are important, but also other effects such as hydrodynamic motion of the solution and mutual interaction of CNTs must be taken into account. These effects are clearly not negligible in many cases, and in fact are of primary influence for certain situations.

## 7.2 Future work

Because of the findings of this thesis, more repeatable fabrication of the CNT devices, especially made of multiple nanotubes, is possible. These devices have the potential to be used in many different applications such as electronics, sensing and field-emission.

Single nanotube devices are the candidates for many quantum-dot-based applications, such as single-electron transistors and electron turnstiles. Because of the special structure of nanotubes, they are considered 1-D conductors. The only step needed to make quantum-dot-based devices is transforming them from 1-D to 0-D by inducing some sort of confinement for the carriers. Repeatable fabrication of single nanotube devices is the first step on this path.

Although in our simulations we covered the most important forces affecting the nanotubes during DEP, there is still potential for expanding the model and capturing other possibly effective phenomena into account, one of which can be the mutual effects of suspended nanotubes on each other before even their deposition. The electric field polarizes the particles in the solution and the field resulting from the polarization of these particles can affect the other particles. To be able to simulate this effect, the movement of all of the nanotubes in the solution should be simulated at once in each step. A term originating from the overall influence of the rest of the CNTs should be added to the Langevin equation solved for each of the nanotubes. Another neglected, potentially effective phenomenon is the interaction of surfactants and the surfaces of the sample. Solutions containing surfactant, especially at high concentrations, can electrochemically modify the surfaces of the electrodes and make them more attractive for the nanotubes. Running more experiments with solutions with the same conductivity but with and without surfactants can shed some light on the extent of importance of this phenomenon in the final results.

As shown in the last chapter, fluid motion can bring the nanotubes toward the electrodes. This is of more importance when the DEP force is too weak to capture a certain type of nanotube (mostly semiconducting ones). This can be used to engineer the solutions for fabricating devices with a stronger semiconducting characteristics. For this purpose, nanotube solutions can be

prepared with conductivities in the range of a few hundreds of μS/cm in order to create some moderate movement in the solution to carry the nanotubes toward the gap between the electrodes.

One other approach for improving the simulations is trying to take the effect of the nanotubes' lengths into account. While the model we used is appropriate for short nanotubes, for longer nanotubes it cannot be directly applied due to the variations in the electric field through their length. Moreover, the flexible structure of nanotubes makes them hard to track if the change in the movement of the fluid is considerable for adjacent points. A thorough study in which the longer nanotubes are modeled as small segments connected to each other can shed some light on how the longer nanotubes actually move in the solution during DEP.

Finally, we are now at a point where we have established some of the important parameters affecting DEP results, as well as achieved a higher level of repeatability through the use of solutions without surfactants. This work could thus form the basis of subsequent studies, where the effect of these parameters on the outcome could be quantified empirically through a number of systematic experiments covering a broad range for these parameters.

## Bibliography


[1] M. Meyyappan, *Carbon Nanotubes: Science and Applications*. CRC Press, 2004.

[2] S. Reich, C. Thomsen, and J. Maultzsch, *Carbon Nanotubes*. John Wiley & Sons, 2008.

[3] C. T. White and J. W. Mintmire, "Fundamental Properties of Single-Wall Carbon Nanotubes," *J. Phys. Chem. B*, vol. 109, no. 1, pp. 52–65, Jan. 2005.

[4] M. Kumar and Y. Ando, "Chemical Vapor Deposition of Carbon Nanotubes: A Review on Growth Mechanism and Mass Production," *J. Nanosci. Nanotechnol.*, vol. 10, no. 6, pp. 3739–3758, 2010.

[5] M. Meyyappan, "A review of plasma enhanced chemical vapour deposition of carbon nanotubes," *J. Phys. Appl. Phys.*, vol. 42, no. 21, p. 213001, Nov. 2009.

[6] E. Joselevich, H. Dai, L. Jie, and K. Hata, "Carbon Nanotube Synthesis and Organization," in *Carbon Nanotubes: Advance Topics in the Synthesis, Structure, Properties, and Applications*, A. Jorio, G. Dresselhaus, and M. S. Dresselhaus, Eds. .

[7] A. M. Cassell, N. R. Franklin, T. W. Tombler, E. M. Chan, J. Han, and H. Dai, "Directed Growth of Free-StandingSingle-Walled Carbon Nanotubes," *J. Am. Chem. Soc.*, vol. 121, no. 34, pp. 7975–7976, Sep. 1999.

[8] A. Nojeh, A. Ural, R. F. Pease, and H. Dai, "Electric-field-directed growth of carbon nanotubes in two dimensions," in *The 48th International Conference on Electron, Ion, and Photon Beam Technology and Nanofabrication*, San Diego, California (USA), 2004, vol. 22, pp. 3421–3425.

[9] L. Ding, D. Yuan, and J. Liu, "Growth of High-Density Parallel Arrays of Long Single-Walled Carbon Nanotubes on Quartz Substrates," *J. Am. Chem. Soc.*, vol. 130, no. 16, pp. 5428–5429, Apr. 2008.

[10] C. Kocabas, S.-H. Hur, A. Gaur, M. A. Meitl, M. Shim, and J. A. Rogers, "Guided growth of large-scale, horizontally aligned arrays of single-walled carbon nanotubes and their use in thin-film transistors," *Small Weinh. Bergstr. Ger.*, vol. 1, no. 11, pp. 1110–1116, Nov. 2005.

[11] P. Avouris, J. Appenzeller, R. Martel, and S. J. Wind, "Carbon nanotube electronics," *Proc. IEEE*, vol. 91, no. 11, pp. 1772–1784, 2003.

[12] R. Pethig, "Review Article—Dielectrophoresis: Status of the theory, technology, and applications," *Biomicrofluidics*, vol. 4, no. 2, pp. 022811–022811–35, Jun. 2010.

[13] C. Zhang, K. Khoshmanesh, A. Mitchell, and K. Kalantar-zadeh, "Dielectrophoresis for manipulation of micro/nano particles in microfluidic systems," *Anal. Bioanal. Chem.*, vol. 396, no. 1, pp. 401–420, Jan. 2010.

[14] R. Martinez-Duarte, "Microfabrication technologies in dielectrophoresis applications—A review," *ELECTROPHORESIS*, vol. 33, no. 21, pp. 3110–3132, 2012.

[15] K. Khoshmanesh, S. Nahavandi, S. Baratchi, A. Mitchell, and K. Kalantar-zadeh, "Dielectrophoretic platforms for bio-microfluidic systems," *Biosens. Bioelectron.*, vol. 26, no. 5, pp. 1800–1814, Jan. 2011.

[16] C. H. Kua, Y. C. Lam, C. Yang, and K. Youcef-Toumi, "Review of bio-particle manipulation using dielectrophoresis," Jan. 2005.

[17] R. Krupke, F. Hennrich, H. v Löhneysen, and M. M. Kappes, "Separation of Metallic from Semiconducting Single-Walled Carbon Nanotubes," *Science*, vol. 301, no. 5631, pp. 344–347, Jul. 2003.

[18] S.-H. Yoon, S. Kumar, G.-H. Kim, Y.-S. Choi, T. W. Kim, and S. I. Khondaker, "Dielectrophoretic Assembly of Single Gold Nanoparticle into Nanogap Electrodes," *J. Nanosci. Nanotechnol.*, vol. 8, no. 7, pp. 3427–3433, 2008.
[19] S. Raychaudhuri, S. A. Dayeh, D. Wang, and E. T. Yu, "Precise Semiconductor Nanowire Placement Through Dielectrophoresis," *Nano Lett.*, vol. 9, no. 6, pp. 2260–2266, Jun. 2009.
[20] J. Tang, G. Yang, Q. Zhang, A. Parhat, B. Maynor, J. Liu, L.-C. Qin, and O. Zhou, "Rapid and Reproducible Fabrication of Carbon Nanotube AFM Probes by Dielectrophoresis," *Nano Lett.*, vol. 5, no. 1, pp. 11–14, Jan. 2005.
[21] H.-W. Seo, C.-S. Han, D.-G. Choi, K.-S. Kim, and Y.-H. Lee, "Controlled assembly of single SWNTs bundle using dielectrophoresis," *Microelectron. Eng.*, vol. 81, no. 1, pp. 83–89, Jul. 2005.
[22] A. Arun, P. Salet, and A. M. Ionescu, "A Study of Deterministic Positioning of Carbon Nanotubes by Dielectrophoresis," *J. Electron. Mater.*, vol. 38, no. 6, pp. 742–749, Jun. 2009.
[23] J. Moscatello, V. Kayastha, B. Ulmen, A. Pandey, S. Wu, A. Singh, and Y. K. Yap, "Surfactant-free dielectrophoretic deposition of multi-walled carbon nanotubes with tunable deposition density," *Carbon*, vol. 48, no. 12, pp. 3559–3569, Oct. 2010.
[24] J. Li, Q. Zhang, N. Peng, and Q. Zhu, "Manipulation of carbon nanotubes using AC dielectrophoresis," *Appl. Phys. Lett.*, vol. 86, no. 15, pp. 153116–153116–3, Apr. 2005.
[25] N. Peng, Q. Zhang, J. Li, and N. Liu, "Influences of ac electric field on the spatial distribution of carbon nanotubes formed between electrodes," *J. Appl. Phys.*, vol. 100, no. 2, pp. 024309–024309–5, Jul. 2006.
[26] A. H. Monica, S. J. Papadakis, R. Osiander, and M. Paranjape, "Wafer-level assembly of carbon nanotube networks using dielectrophoresis," *Nanotechnology*, vol. 19, no. 8, p. 085303, Feb. 2008.
[27] M. Dimaki and P. Bøggild, "Frequency dependence of the structure and electrical behaviour of carbon nanotube networks assembled by dielectrophoresis," *Nanotechnology*, vol. 16, no. 6, p. 759, Jun. 2005.
[28] B. K. Sarker, S. Shekhar, and S. I. Khondaker, "Semiconducting Enriched Carbon Nanotube Aligned Arrays of Tunable Density and Their Electrical Transport Properties," *ACS Nano*, vol. 5, no. 8, pp. 6297–6305, Aug. 2011.
[29] K. W. C. Lai, N. Xi, and U. C. Wejinya, "Automated process for selection of carbon nanotube by electronic property using dielectrophoretic manipulation," *J. Micro-Nano Mechatron.*, vol. 4, no. 1–2, pp. 37–48, Nov. 2008.
[30] R. Krupke, F. Hennrich, M. M. Kappes, and H. v. Löhneysen, "Surface Conductance Induced Dielectrophoresis of Semiconducting Single-Walled Carbon Nanotubes," *Nano Lett.*, vol. 4, no. 8, pp. 1395–1399, Aug. 2004.
[31] S. Blatt, F. Hennrich, H. v. Löhneysen, M. M. Kappes, A. Vijayaraghavan, and R. Krupke, "Influence of Structural and Dielectric Anisotropy on the Dielectrophoresis of Single-Walled Carbon Nanotubes," *Nano Lett.*, vol. 7, no. 7, pp. 1960–1966, Jul. 2007.
[32] D. Xu, A. Subramanian, L. Dong, and B. J. Nelson, "Shaping Nanoelectrodes for High-Precision Dielectrophoretic Assembly of Carbon Nanotubes," *IEEE Trans. Nanotechnol.*, vol. 8, no. 4, pp. 449–456, 2009.

[33] S. Banerjee, B. E. White, L. Huang, B. J. Rego, S. O'Brien, and I. P. Herman, "Precise positioning of single-walled carbon nanotubes by ac dielectrophoresis," 2006, vol. 24, pp. 3173–3178.
[34] C. W. Marquardt, S. Blatt, F. Hennrich, H. v Löhneysen, and R. Krupke, "Probing dielectrophoretic force fields with metallic carbon nanotubes," *Appl. Phys. Lett.*, vol. 89, no. 18, pp. 183117–183117–3, Nov. 2006.
[35] M. Duchamp, K. Lee, B. Dwir, J. W. Seo, E. Kapon, L. Forró, and A. Magrez, "Controlled Positioning of Carbon Nanotubes by Dielectrophoresis: Insights into the Solvent and Substrate Role," *ACS Nano*, vol. 4, no. 1, pp. 279–284, Jan. 2010.
[36] P. Stokes and S. I. Khondaker, "Directed assembly of solution processed single-walled carbon nanotubes via dielectrophoresis: From aligned array to individual nanotube devices," 2010, vol. 28, pp. C6B7–C6B12.
[37] S. Shekhar, P. Stokes, and S. I. Khondaker, "Ultrahigh Density Alignment of Carbon Nanotube Arrays by Dielectrophoresis," *ACS Nano*, vol. 5, no. 3, pp. 1739–1746, Mar. 2011.
[38] P. Li and W. Xue, "Selective Deposition and Alignment of Single-Walled Carbon Nanotubes Assisted by Dielectrophoresis: From Thin Films to Individual Nanotubes," *Nanoscale Res. Lett.*, vol. 5, no. 6, pp. 1072–1078, Jun. 2010.
[39] H. Morgan and N. G. Green, *AC Electrokinetics: Colloids and Nanoparticles*. Research Studies Press Limited, 2003.
[40] A. Ramos, H. Morgan, N. G. Green, and A. Castellanos, "Ac electrokinetics: a review of forces in microelectrode structures," *J. Phys. Appl. Phys.*, vol. 31, no. 18, p. 2338, Sep. 1998.
[41] N. G. Green, A. Ramos, A. González, A. Castellanos, and H. Morgan, "Electrothermally induced fluid flow on microelectrodes," *J. Electrost.*, vol. 53, no. 2, pp. 71–87, Aug. 2001.
[42] A. Castellanos, A. Ramos, A. González, N. G. Green, and H. Morgan, "Electrohydrodynamics and dielectrophoresis in microsystems: scaling laws," *J. Phys. Appl. Phys.*, vol. 36, no. 20, p. 2584, Oct. 2003.
[43] Y. Lin, J. Shiomi, S. Maruyama, and G. Amberg, "Electrothermal flow in dielectrophoresis of single-walled carbon nanotubes," *Phys. Rev. B*, vol. 76, no. 4, p. 045419, Jul. 2007.
[44] B. R. Burg, V. Bianco, J. Schneider, and D. Poulikakos, "Electrokinetic framework of dielectrophoretic deposition devices," *J. Appl. Phys.*, vol. 107, no. 12, pp. 124308–124308–11, Jun. 2010.
[45] A. J. Blanch, C. E. Lenehan, and J. S. Quinton, "Optimizing Surfactant Concentrations for Dispersion of Single-Walled Carbon Nanotubes in Aqueous Solution," *J. Phys. Chem. B*, vol. 114, no. 30, pp. 9805–9811, Aug. 2010.
[46] A. Vijayaraghavan, S. Blatt, D. Weissenberger, M. Oron-Carl, F. Hennrich, D. Gerthsen, H. Hahn, and R. Krupke, "Ultra-Large-Scale Directed Assembly of Single-Walled Carbon Nanotube Devices," *Nano Lett.*, vol. 7, no. 6, pp. 1556–1560, Jun. 2007.
[47] L. Vaisman, H. D. Wagner, and G. Marom, "The role of surfactants in dispersion of carbon nanotubes," *Adv. Colloid Interface Sci.*, vol. 128–130, pp. 37–46, Dec. 2006.
[48] B. I. Kharisov, O. V. Kharissova, H. Leija Gutierrez, and U. Ortiz Méndez, "Recent Advances on the Soluble Carbon Nanotubes," *Ind. Eng. Chem. Res.*, vol. 48, no. 2, pp. 572–590, Jan. 2009.
[49] "http://www.nano-lab.com." .

[50] J.-M. Bonard, T. Stora, J.-P. Salvetat, F. Maier, T. Stöckli, C. Duschl, L. Forró, W. A. de Heer, and A. Châtelain, "Purification and size-selection of carbon nanotubes," *Adv. Mater.*, vol. 9, no. 10, pp. 827–831, 1997.
[51] H. Wang, W. Zhou, D. L. Ho, K. I. Winey, J. E. Fischer, C. J. Glinka, and E. K. Hobbie, "Dispersing Single-Walled Carbon Nanotubes with Surfactants: A Small Angle Neutron Scattering Study," *Nano Lett.*, vol. 4, no. 9, pp. 1789–1793, Sep. 2004.
[52] J. Hilding, E. A. Grulke, Z. George Zhang, and F. Lockwood, "Dispersion of Carbon Nanotubes in Liquids," *J. Dispers. Sci. Technol.*, vol. 24, no. 1, pp. 1–41, 2003.
[53] S. J. Tans, A. R. M. Verschueren, and C. Dekker, "Room-temperature transistor based on a single carbon nanotube," *Nature*, vol. 393, no. 6680, pp. 49–52, May 1998.
[54] A. Javey, J. Guo, D. B. Farmer, Q. Wang, D. Wang, R. G. Gordon, M. Lundstrom, and H. Dai, "Carbon Nanotube Field-Effect Transistors with Integrated Ohmic Contacts and High-κ Gate Dielectrics," *Nano Lett.*, vol. 4, no. 3, pp. 447–450, Mar. 2004.
[55] P. Stokes and S. I. Khondaker, "Evaluating Defects in Solution-Processed Carbon Nanotube Devices via Low-Temperature Transport Spectroscopy," *ACS Nano*, vol. 4, no. 5, pp. 2659–2666, May 2010.
[56] "http://www.4dlabs.ca." .
[57] A. Javey, J. Guo, Q. Wang, M. Lundstrom, and H. Dai, "Ballistic carbon nanotube field-effect transistors," *Nature*, vol. 424, no. 6949, pp. 654–657, Aug. 2003.
[58] "http://nanofab.ubc.ca/." .
[59] C. Mack, *Fundamental Principles of Optical Lithography: The Science of Microfabrication*. John Wiley & Sons, 2008.
[60] "http://www.cmc.ca." .
[61] D. V. Hutton, *Fundamentals of finite element analysis*. Boston: McGraw-Hill, 2004.
[62] "http://www.comsol.com." .
[63] W. M. Haynes and D. R. Lide, *CRC handbook of chemistry and physics a ready-reference book of chemical and physical data: 2011-2012*. Boca Raton (Fla.); London; New York: CRC Press, 2011.
[64] H. Wang, "Dispersing carbon nanotubes using surfactants," *Curr. Opin. Colloid Interface Sci.*, vol. 14, no. 5, pp. 364–371, Oct. 2009.
[65] X. Q. Chen, T. Saito, H. Yamada, and K. Matsushige, "Aligning single-wall carbon nanotubes with an alternating-current electric field," *Appl. Phys. Lett.*, vol. 78, no. 23, pp. 3714–3716, Jun. 2001.
[66] P. Stokes, E. Silbar, Y. M. Zayas, and S. I. Khondaker, "Solution processed large area field effect transistors from dielectrophoreticly aligned arrays of carbon nanotubes," *Appl. Phys. Lett.*, vol. 94, no. 11, pp. 113104–113104–3, Mar. 2009.
[67] Z. Chen, J. Appenzeller, J. Knoch, Y. Lin, and P. Avouris, "The Role of Metal−Nanotube Contact in the Performance of Carbon Nanotube Field-Effect Transistors," *Nano Lett.*, vol. 5, no. 7, pp. 1497–1502, Jul. 2005.
[68] E. Pop, D. A. Mann, K. E. Goodson, and H. Dai, "Electrical and thermal transport in metallic single-wall carbon nanotubes on insulating substrates," *J. Appl. Phys.*, vol. 101, no. 9, pp. 093710–093710–10, May 2007.
[69] Q. Cao, S.-J. Han, G. S. Tulevski, A. D. Franklin, and W. Haensch, "Evaluation of Field-Effect Mobility and Contact Resistance of Transistors That Use Solution-Processed Single-Walled Carbon Nanotubes," *ACS Nano*, vol. 6, no. 7, pp. 6471–6477, Jul. 2012.

[70] M. Dimaki and P. Bøggild, “Dielectrophoresis of carbon nanotubes using microelectrodes: a numerical study,” *Nanotechnology*, vol. 15, no. 8, p. 1095, Aug. 2004.
[71] Y. Lu, C. Chen, L. Yang, and Y. Zhang, “Theoretical Simulation on the Assembly of Carbon Nanotubes Between Electrodes by AC Dielectrophoresis,” *Nanoscale Res. Lett.*, vol. 4, no. 2, p. 157, Nov. 2008.
[72] B. Kozinsky and N. Marzari, “Static Dielectric Properties of Carbon Nanotubes from First Principles,” *Phys. Rev. Lett.*, vol. 96, no. 16, p. 166801, Apr. 2006.
[73] L. X. Benedict, S. G. Louie, and M. L. Cohen, “Static polarizabilities of single-wall carbon nanotubes,” *Phys. Rev. B*, vol. 52, no. 11, pp. 8541–8549, Sep. 1995.

# Appendices

## Appendix A - Publications not included in the thesis

**Book Chapter:**

- A. Kashefian Naieni, A. Nojeh, "Quantum dot devices based on carbon nanotubes," in Nanoelectronics: Fabrication, Interconnects and Device Structures, Ed. K. Iniewski, McGraw-Hill, 2011.

**Journal Papers:**

- A. Kashefian Naieni, P. Yaghoobi, A. Nojeh, "Structural deformations and current oscillations in armchair-carbon nanotube cross devices: a theoretical study," Journal of Physics D: Applied Physics, 44, 085402, 2011.
- Y. Choi, M. Michan, J. L. Johnson, A. Kashefian Naieni, A. Ural, A. Nojeh, "Field-emission properties of individual GaN nanowires grown by chemical vapor deposition," Journal of Applied Physics, 111, 044308, 2012.
- A. Kashefian Naieni, P. Yaghoobi, A. Nojeh, "First-principles study of field-emission from carbon nanotubes in the presence of methane," Journal of Vacuum Science and Technology B, 30, 021803, 2012.

**Conference Presentations:**

- A. Kashefian Naieni, P. Yaghoobi, A. Nojeh, "Mechanical, electronic and transport properties of carbon nanotubes in a cross structure," Eleventh international conference on the science and application of nanotubes, Montreal Jun-Jul 2010, and the 6th international symposium on computational challenges and tools for nanotubes, Montreal, Canada, Jun 2010.

- A. Kashefian Naieni, A. Nojeh, “Fabrication of carbon nanotube thin films with predetermined morphology from solution,” 15th Canadian semiconductor science and technology conference, Vancouver, Canada, Aug 2011.

**Appendix B - Additional DEP results and image processing procedure related to chapter 3**

The following figure shows more results for the experiments described in the third chapter for the two cases of solutions with no surfactant and 1 wt% surfactant.

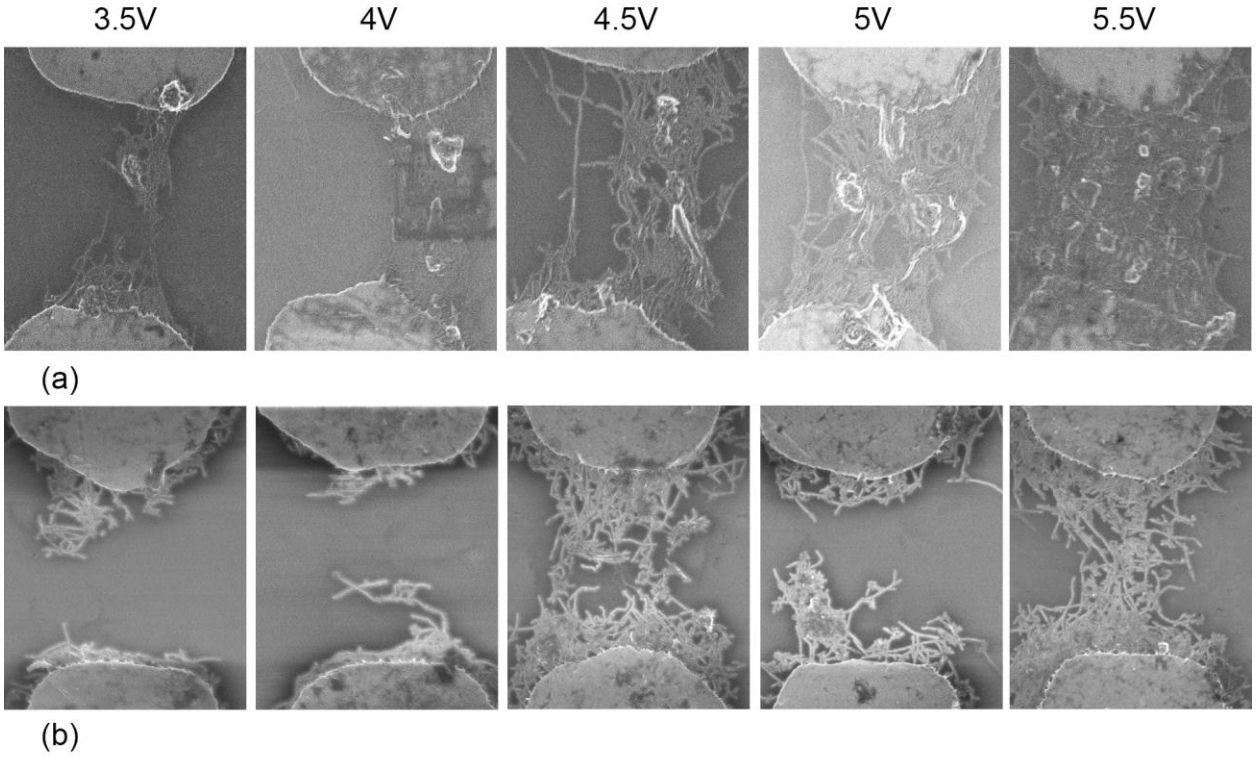


Fig. B-1. DEP results of experiments with (a) no surfactant, and (b) 1 wt% surfactant solutions.

The following figures (Fig. B-2 to B-7) show the results of DEP experiments using different parameters (compared to those shown above or in chapter 3) with solutions containing no surfactant and different CNT concentrations. In each row of figures, the applied voltage is progressively increased from left to right, and the results confirm that the number of deposited nanotubes increases with voltage when a surfactant-free solution is used.

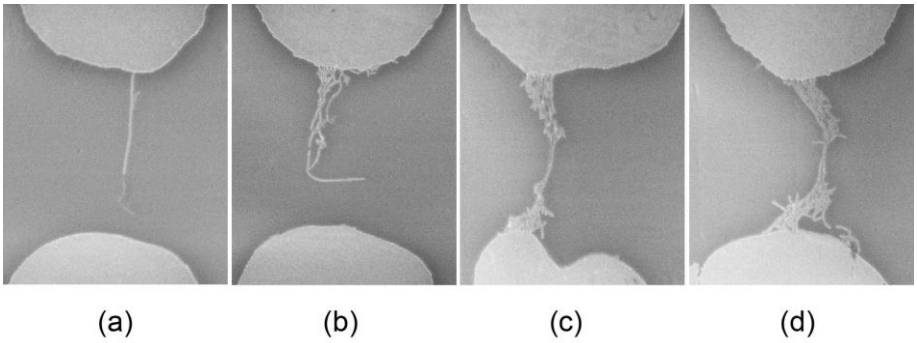


Fig. B-2. DEP results using a surfactant-free solution with a CNT concentration of 125 ng/ml. Parameters: t = 1 min, f = 500 kHz, and (a) v = 4V, (b) v = 4.8 V, (c) v = 5.6 V, (d) v = 6.2 V. The oscilloscope was in series with the setup during the experiment. The gap between the electrodes is 4 µm.

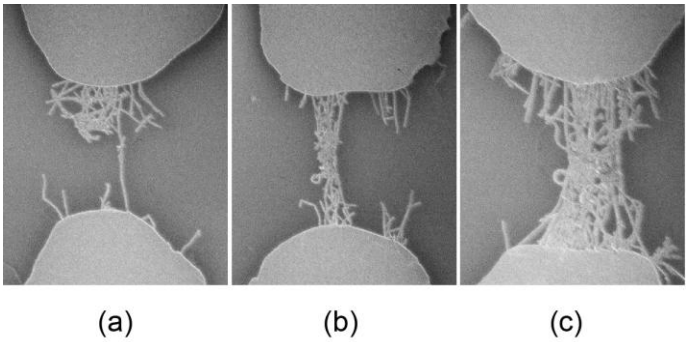


Fig. B-3. DEP results using a surfactant-free solution with a CNT concentration of 125 ng/ml. Parameters: t = 40 s, f = 1 MHz, and (a) v = 3V, (b) v = 4 V, (c) v = 5 V. The gap between the electrodes is 3 µm.

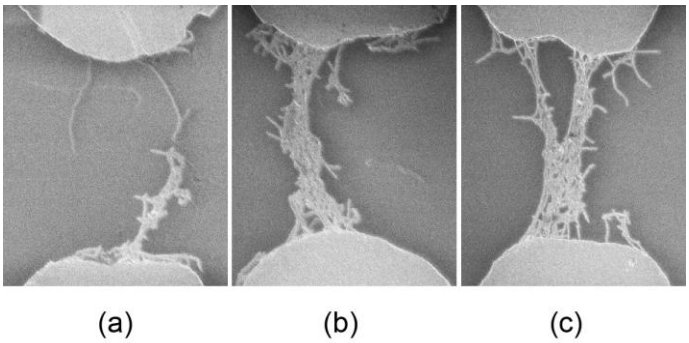


Fig. B-4. DEP results using a surfactant-free solution with a CNT concentration of 125 ng/ml. Parameters: t = 1 min, f = 500 kHz, and (a) v = 4V, (b) v = 4.8 V, (c) v = 5.6 V. The gap between the electrodes is 4 µm.

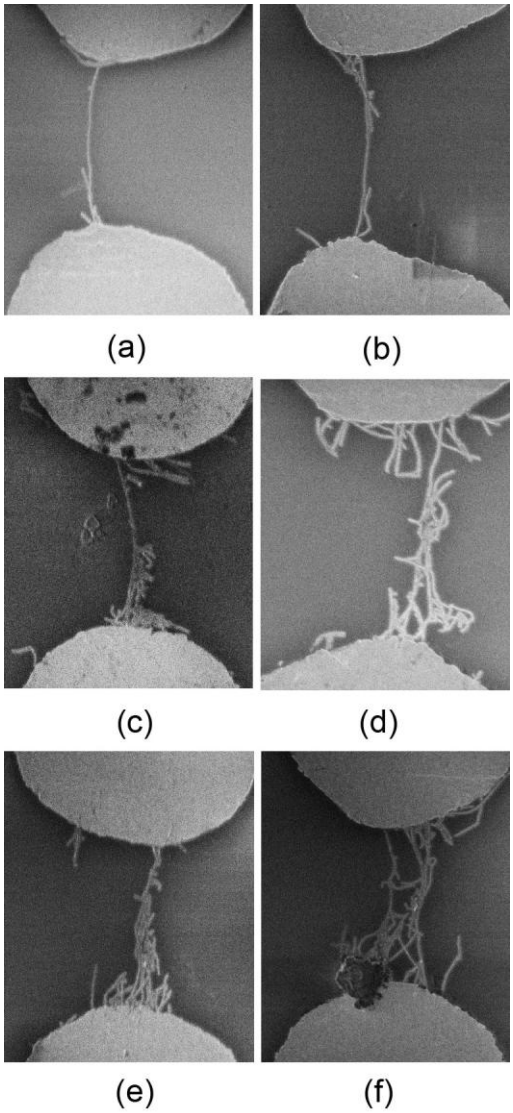


Fig. B-5. DEP results using a surfactant-free solution with a CNT concentration of 125 ng/ml. Parameters: f = 500 kHz, and (a) t = 30 s, v = 3.6 V, (b) t = 30 s, v = 4.2 V, (c) t = 60 s, v = 3.6 V, (d) t = 60 s, v = 4.2 V, (e) t = 90 s, v = 3.6 V, (f) t = 90 s, v = 4.2 V . The gap between the electrodes is 4 μm.

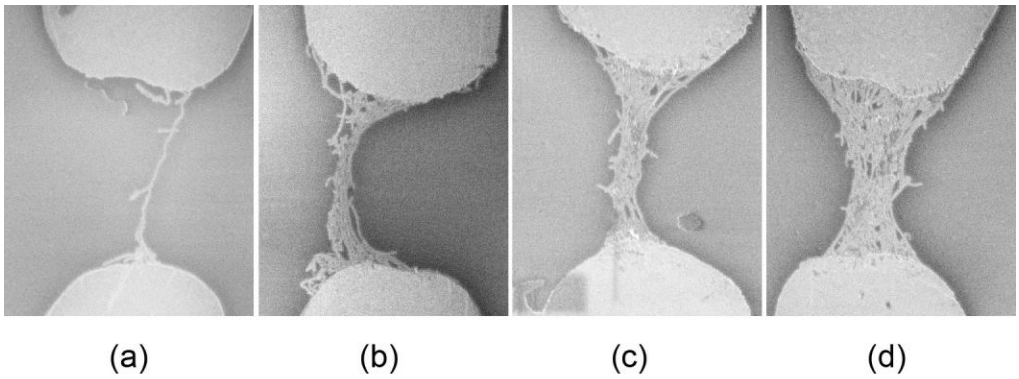


Fig. B-6. DEP results using a surfactant-free solution with a CNT concentration of 2.5 µg/ml. Parameters: t = 1 min, f = 500 kHz, and (a) v = 3.2V, (b) v = 4 V, (c) v = 4.8 V, (d) v = 5.6 V. The oscilloscope was in series with the setup during the experiment. The gap between the electrodes is 4 µm.

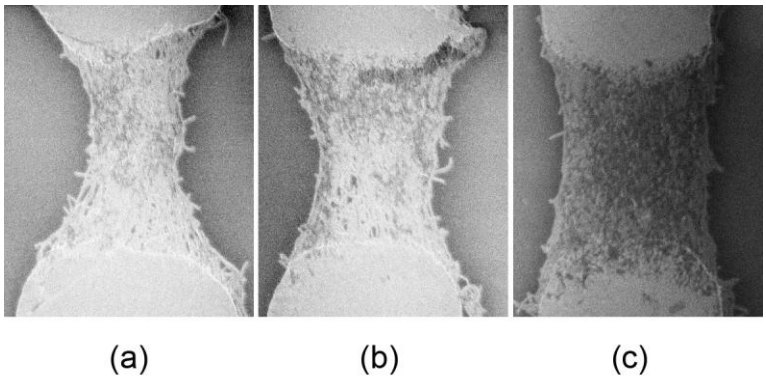


Fig. B-7. DEP results using a surfactant-free solution with a CNT concentration of 2.5 µg/ml. Parameters: t = 1 min, f = 500 kHz, and (a) v = 4V, (b) v = 4.8 V, (c) v = 5.6 V. The gap between the electrodes is 4 µm.

It is also important to note that, regardless of the type of solution used, some devices are left without any nanotubes after the process (see Fig. B-8a and d). This rules out the fluidic forces, such as surface tension, as the sole reason behind the deposition between the two electrodes. There are also devices that are entirely covered with nanotubes after the process using either surfactant-free or surfactant-containing solutions as shown in the following figure.

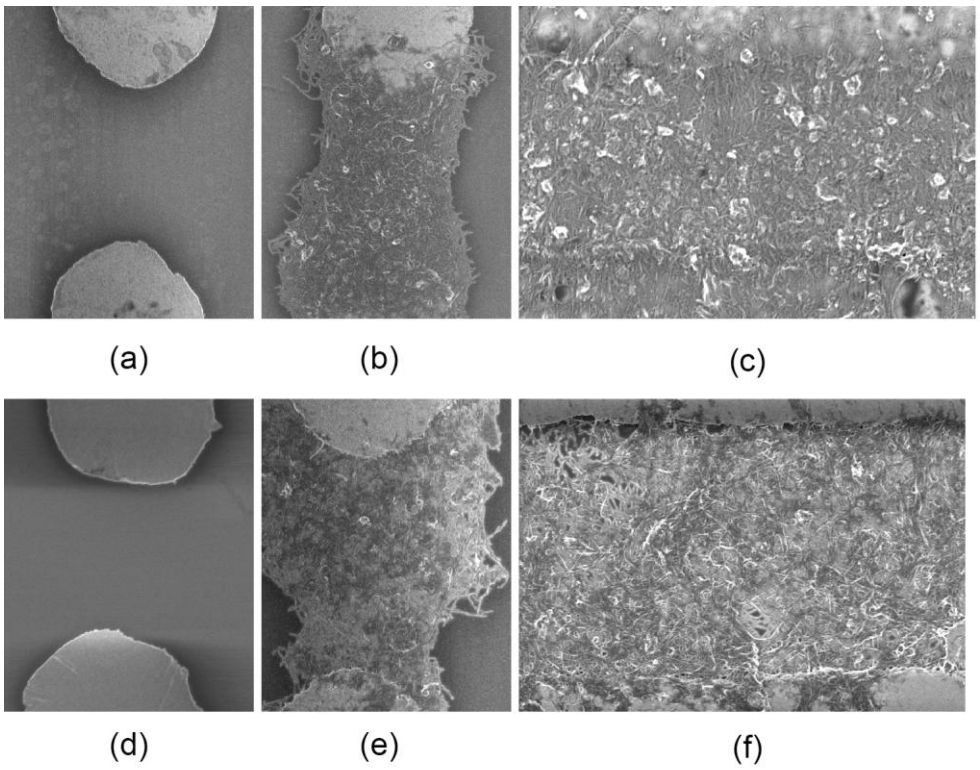


Fig. B-8. Results of experiments with surfactant-free (top row) and surfactant-containing (bottom row) solutions. (a) and (d) no nanotube deposited, (b), (c), (e), and (f) the area between the electrodes covered with nanotubes. Parameters for (b) and (e): v = 5 V, t = 1 min, f = 2 MHz. Parameters for (c) and (f): v = 5 V, t = 1 min, and f = 500 kHz.

**Image processing procedure**

In order to quantify the overall nanotube coverage, as well as the coverage near the electrodes, the following steps were performed to prepare the images of the DEP results:

1. The images were cropped to include 1 μm of the height of each electrode. Considering the length of the gap, the final image included 6 μm height of the sample, which was divided into 6 horizontal segments of equal area (Fig. B-9). The width of each image was then limited so as to have the same height-to-width ratio for all images. This ensured that the total area of all images was the same.

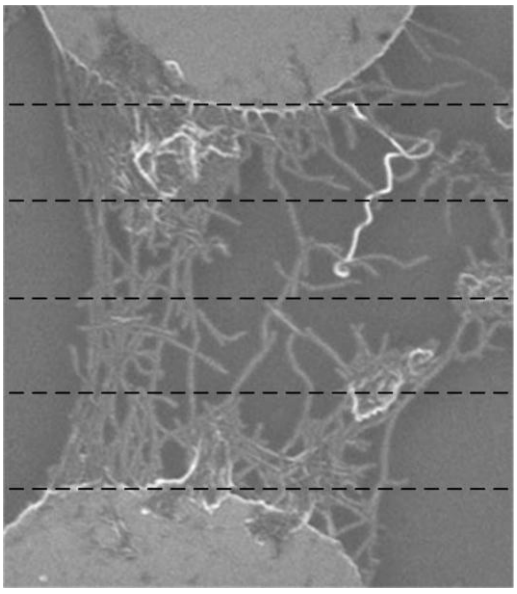

Fig. B-9. The images were cropped in order to include 1 μm of the height of each electrode in preparation for the image processing.

2. The electrodes were covered with a color similar to the substrate in order to eliminate the possibility of their being counted as nanotubes.

3. The area of coverage for each image was calculated using a procedure similar to that explained in Appendix C. Fig. B-10 shows the black-and-white images resulting from the thresholding step.

4. The two middle segments (see Fig. B-9) of each image was excluded in MATLAB, and the area covered by the nanotubes in the vicinity of the electrodes (in the remaining segments) was calculated. The ratio of the deposition close to the electrodes to the total area covered by nanotubes was thus determined.

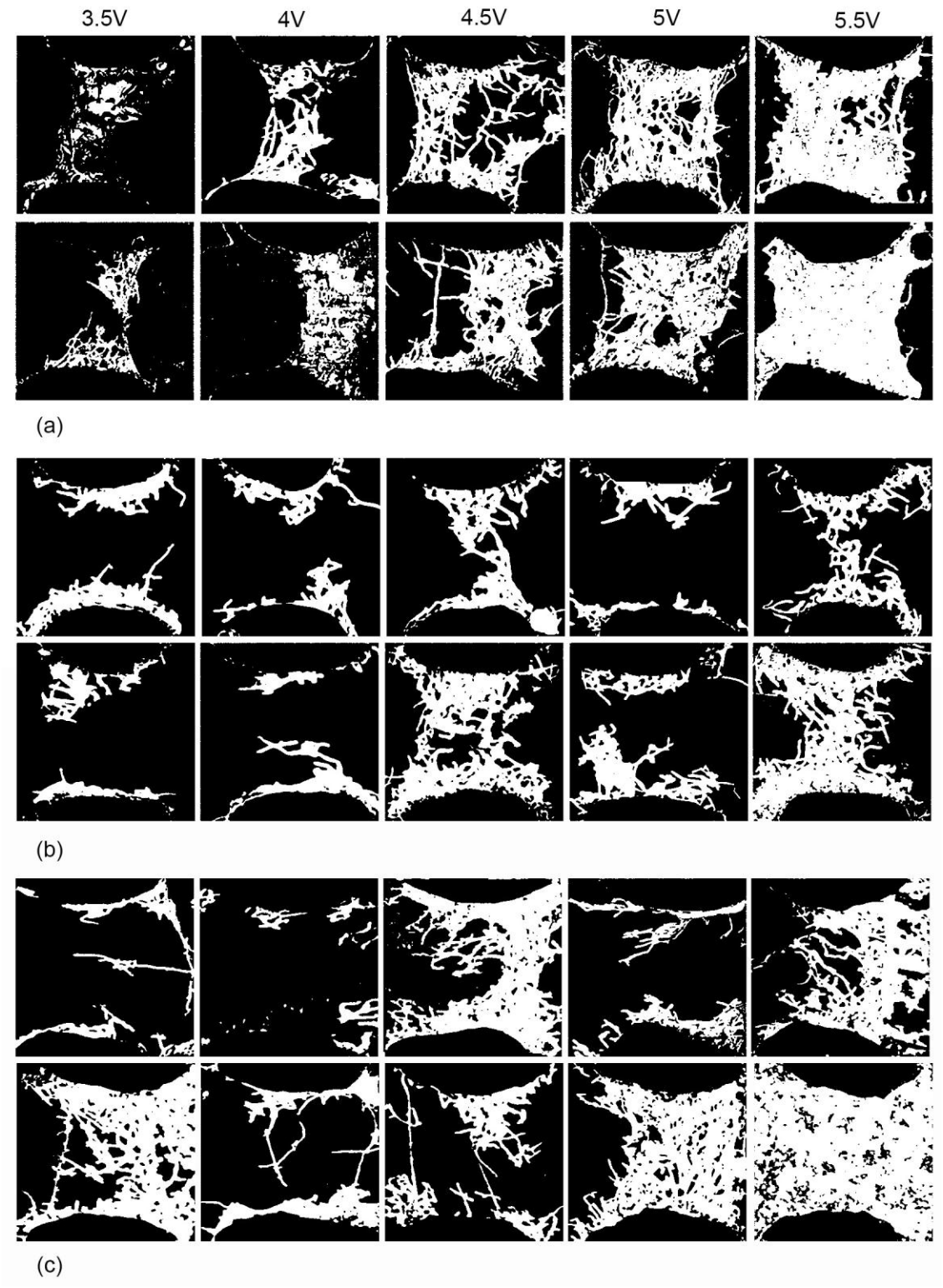


Fig. B-10. The black and white images (nanotubes are white) after image processing of the DEP results performed using (a) no surfactant, (b) 1 wt% surfactant, and (c) control solutions.

## Appendix C - Image processing procedure

The SEM images of the CNT devices presented in chapter five were used in the following procedure in order to find the ratio of the area covered by nanotubes to the entire area between the two wide electrodes (Fig. 5-2). ImageJ[5] (a public domain image processing program) and MATLAB were used for the process, according to the following algorithm:

1. Cropping the image to include only the area between the two electrodes.
2. Opening the image in ImageJ and setting the type to 32-bit.
3. Adjusting *Brightness/Contrast* (setting the Minimum and Maximum sliders in the *Brightness/Contrast* menu to cover the non-zero range of the histogram of the image).
4. Making the background even using *Process* > *Subtract Background* with a rolling ball radius of 100 pixels with the *Sliding parabloid* option checked.
5. [For samples with single nanotubes on the surface] Repeating step 4 this time with a rolling ball radius of 10 pixels (the radius of the rolling ball must be close to the size of the particles).
6. Adjusting *Brightness/Contrast*.
7. Applying the *Process* > *Smooth* filter twice to avoid singular pixels in the threshold step.
8. Using *Image* > *Adjust* > *Threshold* to convert the image to black and white by setting a threshold using the "Minimum" thresholding method. Usually a slight adjustment of the threshold for each image is necessary to improve the result.
9. Saving the image as a tiff file.

[5] http://rsb.info.nih.gov/ij/

10. Using a MATLAB code to find the ratio of the area of white pixels to the surface of the device in the saved image.

The following figure shows the initial and final, black-and-white photos.

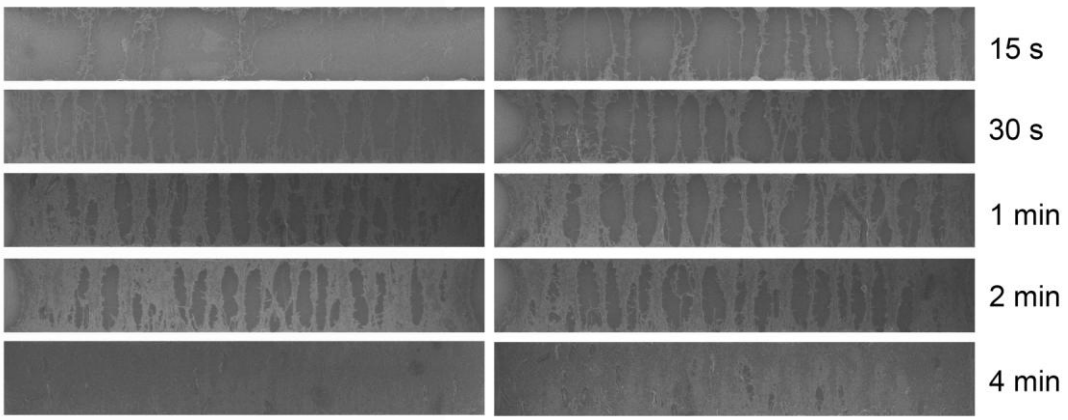


(a)

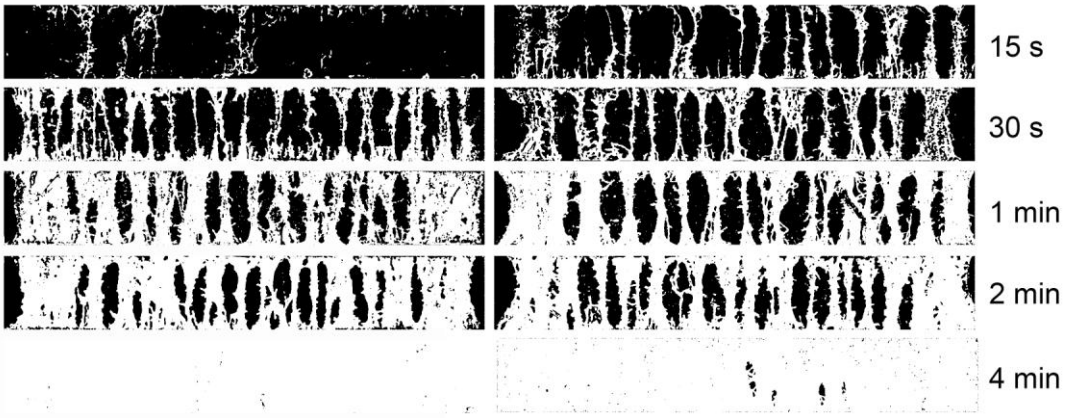


(b)

Fig.C-1. (a) Initial and (b) final, black and white images of the image processing procedure for finding the CNT-covered area between the two electrodes after the DEP experiment.

MATLAB Code:

```
clc
close all
clear all
```

```
files = dir('*.tif');
num_files = numel(files);
images = cell(1, num_files)
for k = 1:num_files
   images{k} = imread(files(k).name);
end

for i=1:num_files
   a=images{i};
   g=double(a);
   h=mat2gray(g);
   imshow(h)
   level1=0.5;
   j= im2bw(h, level1);   %,level1
   figure, imshow(j)
   [L, N]= bwlabel(j);
   D= regionprops(L, 'area');
   w=[D.Area];
   q=sum(w);
   g1=double(a);
   h1=mat2gray(g1);
   j2= im2bw(h1, 1);
   j1 = imcomplement(j2);
   [L1, N1]= bwlabel(j1);
   D1= regionprops(L1, 'area');
   w1=[D1.Area];
   q1=sum(w1);
   phi(i)=q/q1
end
```

**Appendix D - Particle tracing code**

Code for creating the velocity grids

```
%load velocityDEP and velocityETF matrices from COMSOL

%removing the negative Z velocity values
velocityDEP=real(removeZnegative(velocityDEP));
velocityETF=real(removeZnegative(velocityETF));

%creating the grid and mapping the data on it
[xx,yy,zz]=meshgrid(-8:.1:8,-10:.1:10,0:0.1:10);
uDEP=griddata3(velocityDEP(:,1),velocityDEP(:,2),velocityDEP(:,3),velocityDEP(:,4),xx,yy,zz)
;
vDEP=griddata3(velocityDEP(:,1),velocityDEP(:,2),velocityDEP(:,3),velocityDEP(:,5),xx,yy,zz)
;
wDEP=griddata3(velocityDEP(:,1),velocityDEP(:,2),velocityDEP(:,3),velocityDEP(:,6),xx,yy,zz
);

uETF=griddata3(velocityETF(:,1),velocityETF(:,2),velocityETF(:,3),velocityETF(:,4),xx,yy,zz);
vETF=griddata3(velocityETF(:,1),velocityETF(:,2),velocityETF(:,3),velocityETF(:,5),xx,yy,zz);
wETF=griddata3(velocityETF(:,1),velocityETF(:,2),velocityETF(:,3),velocityETF(:,6),xx,yy,zz);


xaxis=xx(1,:,1);
yaxis=yy(:,1,1);
zaxis=zz(1,1,:);

%Substituting NAN elements with zero
uDEP=removenan(uDEP);
vDEP=removenan(vDEP);
wDEP=removenan(wDEP);
uETF=removenan(uETF);
vETF=removenan(vETF);
wETF=removenan(wETF);

save file.mat
```

Particle tracing code:

```
clear all
%load the velocity file grids from the gridpreparation file
load CNTBridging.mat
%Drawing the CNT on the graphs
%No CNT: CNT=0, CNT half bridging: CNT=1, CNT bridging: CNT=2;
CNT=2;

%metallic or semiconducting CNTs
%the loaded DEP velocities are for metallic tubes, to convert it to 1um
%long semiconducting nanotubes with a 1nm radium the velocities should be
%multiplied by 77.1179/2.2304e5 (in case of low conductivity solution)
%metallic:1, semiconducting:0
TubeType=0;
if TubeType~=1
%     %low conductivity solution
   uDEP=77.1179/2.2304e5*uDEP;
   vDEP=77.1179/2.2304e5*vDEP;
   wDEP=77.1179/2.2304e5*wDEP;
%     %high conductivity solution
%     uDEP=0.666/4760.4*uDEP;
%     vDEP=0.666/4760.4*vDEP;
%     wDEP=0.666/4760.4*wDEP;
end

%time step
tstepdef=0.010;

%duration of the experiment in seconds
Tmax=10;

%Maximum length of each step in um
Deltamax=0.2;

%the path of deposited tubes in the gap in red in the final 3D figure
% yes:1, no:0
redline=0;

% Brownian motion
%set brownian to 1 to apply the brownian motion for each step. 0 will
%discard this motion.
brownian=1;
```

```
viscosity=0.89e-3;
len=1e-6;
rad=1e-9;
f=3*pi*viscosity*len/log(len/rad);
k=1.38e-23; %Boltzman's constant
T=293; % temperature
D=k*T/f;

%number of random points
randnum=750;
xi=8;
yi=50;
tstepsmat=cell(1,randnum);
deltastepsmat=cell(1,randnum);
tvecmat=cell(1,randnum);
xvecmat=cell(1,randnum);
yvecmat=cell(1,randnum);
zvecmat=cell(1,randnum);
uvecmat=cell(1,randnum);
vvecmat=cell(1,randnum);
wvecmat=cell(1,randnum);


tic
%making the initial positions of the random particles
parinits=rand(randnum,3);
parinits(:,1)=(parinits(:,1)-0.5)*2*8;
parinits(:,2)=(parinits(:,2)-0.5)*2*10;
parinits(:,3)=parinits(:,3)*10;

h = waitbar(0,'Please wait...');
for i=1:randnum
    xprev=parinits(i,1);
    yprev=parinits(i,2);
    zprev=parinits(i,3);
    %xprev=xi;
    %yprev=yi;
    xvec=[];
    yvec=[];
    zvec=[];
    tvec=[];
    uvec=[];
    vvec=[];
    wvec=[];
    tsteps=[];
```

```
   deltasteps=[];
   t=0;

   abort=0;
   while ((t<Tmax)&& (abort~=1))
      tstep=tstepdef;
      a=closest(xprev,xaxis);
      b=closest(yprev,yaxis);
      c=closest(zprev,zaxis);
      u=uDEP(b,a,c)+uETF(b,a,c);
      v=vDEP(b,a,c)+vETF(b,a,c);
      w=wDEP(b,a,c)+wETF(b,a,c);
      deltax=u*tstep*1e6; %deltax in um
      deltay=v*tstep*1e6; %deltay in um
      deltaz=w*tstep*1e6; %deltaz in um
      %setting the maximum displacement of particle
      if (sqrt(deltax^2+deltay^2+deltaz^2)>Deltamax)
         tstep=Deltamax*1e-
6/sqrt((uDEP(b,a,c)+uETF(b,a,c))^2+(vDEP(b,a,c)+vETF(b,a,c))^2+(wDEP(b,a,c)+wETF(b,a,c)
)^2);
         deltax=u*tstep*1e6;
         deltay=v*tstep*1e6;
         deltaz=w*tstep*1e6;
      end

      %adding the brownian motion
      if brownian==1

%  applying Brownian
         avgbrownian=sqrt(2*D*tstep)*1e6;
         deltax=deltax+normrnd(0,avgbrownian);
         deltay=deltay+normrnd(0,avgbrownian);
         deltaz=deltaz+normrnd(0,avgbrownian);
      end

      xnew=xprev+deltax;
      ynew=yprev+deltay;
      znew=zprev+deltaz;
      t=t+tstep;
      tsteps=[tsteps;tstep];
      deltasteps=[deltasteps;sqrt(deltax^2+deltay^2+deltaz^2)];
      tvec=[tvec;t];
      xvec=[xvec;xnew];
      yvec=[yvec;ynew];
      zvec=[zvec;znew];
```

```
        uvec=[uvec;u];
        vvec=[vvec;v];
        wvec=[wvec;w];
        xprev=xnew;
        yprev=ynew;
        zprev=znew;
        if ( (znew<=min(zaxis)))
            abort=1;
        end
        if (xnew>=max(xaxis))
            xprev=xprev-0.2;
        end
        if (xnew<=min(xaxis))
            xprev=xprev+0.2;
        end
        if (ynew>=max(yaxis))
            yprev=yprev-0.2;
        end
        if (ynew<=min(yaxis))
            yprev=yprev+0.2;
        end
        if (znew>=max(zaxis))
            zprev=zprev-0.2;
        end
    end
    tstepsmat{1,i}=tsteps;
    deltastepsmat{1,i}=deltasteps;
    tvecmat{1,i}=tvec;
    xvecmat{1,i}=xvec;
    yvecmat{1,i}=yvec;
    zvecmat{1,i}=zvec;
    uvecmat{1,i}=uvec;
    vvecmat{1,i}=vvec;
    wvecmat{1,i}=wvec;
    waitbar(i/randnum);
end


%3D graph of particles' paths
figure('units','inches','Position',[2 1 9 6.2]);
set(gca,'FontSize',20,'linewidth',0.75,'fontname','Arial')
xlabel('x [um]');
ylabel('y [um]');
zlabel('z [um]');
view(-70,20)
```

```
hold on
%drawing the electrodes
[xsurface,ysurface]=meshgrid(-8:16:8,-10:8:-2);
zsurface=xsurface*0;
surface(xsurface,ysurface,zsurface,'facecolor',[200 200 200]/256);
surface(-xsurface,-ysurface,zsurface,'facecolor',[200 200 200]/256);

if CNT==1
   line([0 0],[-2 0],[0 0],'LineWidth',2,'Color','black');
elseif CNT==2
   line([0 0],[-2 2],[0 0],'LineWidth',2,'Color','black');
end
for i=1:randnum
   xvec=xvecmat{1,i};
   yvec=yvecmat{1,i};
   zvec=zvecmat{1,i};
   if ((zvec(length(zvec))<0.2) && (yvec(length(yvec))>-2.5) && (yvec(length(yvec))<2.5) &&
(redline==1))
      plot3(xvec,yvec,zvec,'color','red');
   else
      plot3(xvec,yvec,zvec);
   end
end
axis([-8 8 -10 10 0 10])
% final position of the CNTs on the XY plane

figure('units','inches','Position',[3 2 8.5 5.5]);
box on
set(gca,'FontSize',20,'linewidth',0.75,'fontname','Arial')
CNTdeposited=0;
hold on
xlabel('x [um]');
ylabel('y [um]');
surface(xsurface,ysurface,zsurface,'facecolor',[220 220 220]/256);
surface(-xsurface,-ysurface,zsurface,'facecolor',[220 220 220]/256);
if CNT==1
   line([0 0],[-2 0],'LineWidth',2,'Color','black');
elseif CNT==2
   line([0 0],[-2 2],'LineWidth',2,'Color','black');
end

for i=1:randnum
   tvec=tvecmat{1,i};
   zvec=zvecmat{1,i};
   max(tvec)
```

```
      if ((max(tvec)<Tmax) && (zvec(length(zvec))<0.1))
         xvec=xvecmat{1,i};
         yvec=yvecmat{1,i};
         plot(xvec(length(xvec)),yvec(length(yvec)),'*');
         if ((yvec(length(zvec))<2.5) && (yvec(length(zvec))>-2.5))
            CNTdeposited=CNTdeposited+1;
         end
      end
end
axis([-8 8 -10 10])

CNTdeposited
depotprecent=CNTdeposited/randnum*100
toc
```

"removenan" function:

```
function[Ret]=removenan(R)
nanvector=find(isnan(R));
sizeR=size(R);
for i=1:length(nanvector)
   a=mod(nanvector(i),sizeR(1));
   b=floor(nanvector(i)/sizeR(1))+1;
   if a==0
      a=sizeR(1);
      b=b-1;
   end
   R(a,b)=0;
end
Ret=R;
```

"removeZnegative" function

```
function[Ret]=removeZnegative(R)
negVec=find(R(:,3)<0);
R(negVec,:)=[];
Ret=R;
```

"closest" function

```
function num = closest(x,R)
   vec=abs(R-x);
   vec=vec-min(vec);
   num=find(vec==0);
```